



NTNU – Trondheim
Norwegian University of
Science and Technology

Optimizing the Compression/Absorption Heat Pump System at High Temperatures

Martin Glosli Bergland

Master of Science in Mechanical Engineering

Submission date: Januar 2015

Supervisor: Trygve Magne Eikevik, EPT

Norwegian University of Science and Technology
Department of Energy and Process Engineering

EPT-M-2014-13

MASTER THESIS

for

Student Martin Bergland

Fall 2014

Optimizing the Compression/Absorption Heat Pump System at High Temperatures
*Optimalisering av kompresjons/absorpsjons varmepumpesystem ved høye temperaturer***Background**

The heat pump market has so far mainly focused on residential heat pumps for space heating and domestic hot water production. Less focus has been on heat pumps for higher temperature applications and industrial use due to high initial investment costs, competition with alternative investments, and non-mature or non-existing technologies for the applications to be served. New developments in compact high pressure components, e.g. compressors, ejectors and heat exchangers for CO₂, ammonia and hydrocarbon heat pump systems, are important drivers for change of this situation.

This master work will concentrate on the design of a high temperature hybrid heat pump for production of hot water from surplus heat. The cases for calculation will be taken from the food industry.

Objectives:**The following tasks are to be considered:**

1. Literature review of high temperature industrial heat pumps with emphasize on hybrid compression/absorptions systems
2. Develop a calculation procedure for the desuperheater, functions for the compressor efficiency and a model for the intermediate pressure in two stage model
3. Evaluate different system designs to utilize the absorption heat to achieve higher temperature than the discharge gas temperature from the compressor
4. Optimize heat exchanger design of the hybrid process to utilize the temperature glide (plate, plate and shell, shell and tube or other design)
5. Make a scientific paper of the main results for the work
6. Make proposal for further work

-- ” --

Within 14 days of receiving the written text on the master thesis, the candidate shall submit a research plan for his project to the department.

When the thesis is evaluated, emphasis is put on processing of the results, and that they are presented in tabular and/or graphic form in a clear manner, and that they are analyzed carefully.

The thesis should be formulated as a research report with summary both in English and Norwegian, conclusion, literature references, table of contents etc. During the preparation of the

text, the candidate should make an effort to produce a well-structured and easily readable report. In order to ease the evaluation of the thesis, it is important that the cross-references are correct. In the making of the report, strong emphasis should be placed on both a thorough discussion of the results and an orderly presentation.

The candidate is requested to initiate and keep close contact with his/her academic supervisor(s) throughout the working period. The candidate must follow the rules and regulations of NTNU as well as passive directions given by the Department of Energy and Process Engineering.

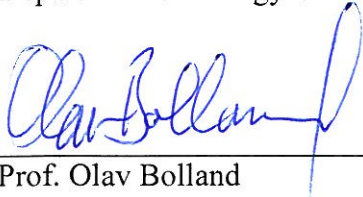
Risk assessment of the candidate's work shall be carried out according to the department's procedures. The risk assessment must be documented and included as part of the final report. Events related to the candidate's work adversely affecting the health, safety or security, must be documented and included as part of the final report. If the documentation on risk assessment represents a large number of pages, the full version is to be submitted electronically to the supervisor and an excerpt is included in the report.

Pursuant to "Regulations concerning the supplementary provisions to the technology study program/Master of Science" at NTNU §20, the Department reserves the permission to utilize all the results and data for teaching and research purposes as well as in future publications.

The final report is to be submitted digitally in DAIM. An executive summary of the thesis including title, student's name, supervisor's name, year, department name, and NTNU's logo and name, shall be submitted to the department as a separate pdf file. The final report in Word and PDF format, scientific paper and all other material and documents should be given to the academic supervisor in digital format on a DVD/CD-rom or a memory stick at the time of submission in DAIM.

- Work to be done in lab (Water power lab, Fluids engineering lab, Thermal engineering lab)
 Field work

Department of Energy and Process Engineering, August 25th 2014



Prof. Olav Bolland
Department Head



Prof Trygve M. Eikevik
Academic Supervisor
e-mail: Trygve.m.eikevik@ntnu.no

Research Advisor:
PhD Ignat Tolstorebrov

e-mails
ignat.tolstorebrov@ntnu.no

CORRECTION OF THE TASKS TO BE CONSIDERED

From the original task to be considered, one of the tasks was chosen to not be considered anyway and rather focus on the other tasks instead. The eliminated task is formed as following:

3. Evaluate different system designs to utilize the absorption heat to achieve higher temperature than the discharge gas temperature from the compressor.

. Therefore the new tasks to be considered are:

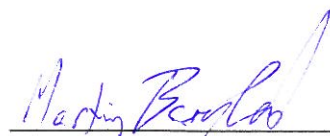
1. Literature review of high temperature industrial heat pumps with emphasize on hybrid compression/absorptions systems
2. Develop a calculation procedure for the desuperheater, functions for the compressor efficiency and a model for the intermediate pressure in two stage model
3. Optimize heat exchanger design of the hybrid process to utilize the temperature glide (plate, plate and shell, shell and tube or other design)
4. Make a scientific paper of the main results for the work
5. Make proposal for further work

These tasks are specified in agreement with the project supervisor.

Department for Energy and Process Engineering, December 18th 2014



Prof. Trygve M. Eikevik
Supervisor



Martin Glosli Bergland
Student

Preface

This project thesis is written at the Norwegian University of Science and Technology during September 2014 to January 2015. The thesis investigates optimization of compression-absorption heat pumps at high temperatures with ammonia-water as working fluid mixture.

I would like to thank Professor Trygve Magne Eikevik for being a very knowledgeable and helpful supervisor.

A special thank also goes to my co-supervisor Ignat Tolstorebrov for being available during the work.

My friend and NTNU alumni Anders Borgås have contributed to fruitful and creative discussions about the topic.

Martin Glosli Bergland

Abstract

Large amounts of low grade waste heat from industrial processes are not utilized, due to lack of heat integration equipment. Industrial processes tend to have specifications at high temperature lifts, that not are suited to be operated by conventional technology from residential heat pumps. Standard vapor compression heat pumps have undesirable high pressure ratios that are inefficient at high temperature lifts. Compression-absorption heat pumps use zeotropic working fluid mixtures that are suitable for temperatures between -10 and +160°C at system pressures below 20 bar, which make them applicable for delivering heat to high temperature processes. The advantages of the compression-absorption heat pumps, also known as the hybrid heat pump are the use of non-ozone depleting working fluid mixtures, reduced irreversibilities due to heat transfer with temperature glides, high temperature lifts, low pressure ratios and flexible capacity control.

Two separate simulation models were developed comprising a two-stage CAHP system and an absorber model. The two-stage CAHP system used waste heat water at 50°C as heat source and sink temperatures, with the objective of achieve maximum supply temperature at four different compressor discharge temperature limitations. The absorber model compared five different compact heat exchangers heating air in a cross-flow, where the main goal was to minimize the absorber height and the fan work.

The two-stage process investigated the benefits of the desuperheater, where the supply temperatures with and without the desuperheater were nearly the same. Maximum supply temperatures were obtained at 171.8°C with a COP of 2.08, when the maximum discharge temperature was set to 250°C. A correction factor was used for the intermediate pressure as $K \cdot \sqrt{P_{LP} \cdot P_{HP}}$. The optimum K-factor increased at elevating absorber pressure from 1.16 to 1.35 at absorber pressure from 17 to 47.5 bar.

Simulations from the absorber model yielded much larger mass flow rate for the air than for the mixture. The heat exchange between the air and the mixture was sensitive to the absorber height and the air mass flow rate, which resulted in large pressure drops and fan work. Finned flat tube heat exchangers gave the best results with respect to the absorber height and fan work.

There is suggested to conduct further work with other heat sink and source temperatures and also optimize the temperature lift in the two stage model. Finned flat tube heat exchangers could be further investigated in an absorber model with other dimensions and more accurate approaches for thermal resistance and fin efficiency.

Sammendrag

Store mengder spillvarme fra industrielle prosesser blir ikke utnyttet, grunnet mangel på systemer for energi- og prosessintegrasjon. Mange industrielle prosesser har spesifikasjoner med høye temperaturløft, som ikke kan opereres av teknologi benyttet i varmepumper for bygninger. Kompresjon-absorpsjons-varmepumper bruker zeotropiske arbeidsmedier som kan operere med temperaturer mellom -10 til $+160^{\circ}\text{C}$ og systemtrykk under 20 bar, hvilket gjør det mulig å levere varme til høytemperaturprosesser. Fordelene til slike varmepumper er bruk av miljøvennlig arbeidsmedier, reduserte irreversibiliteter grunnet varmeoverføring ved glidende temperaturer, høye temperaturløft, lav trykkforhold og fleksibel styring av varmeuttelse.

To separate simuleringsmodeller som omfatter henholdsvis en to-trinns kompresjon-absorpsjons-varmepumpe og en absorbermodell ble utviklet. To-trinns kompresjon-absorpsjons-varmepumpa utnyttet spillvarme ved 50°C som inngangstemperaturen for varmekilden og varmesluket med det målet om å oppnå maksimal leveransetemperatur ved fire forskjellige begrensninger på trykkgasstemperaturen. Absorbermodellen sammenlignet fem ulike kompakte varmevekslere, som varmet luft i cross-flow, der hovedmålet var å minimere absorberhøyden og vifteforbruket.

To-trinnsprosessen undersøkte fordelene med å bruke overhetingsveksler, der leveransetemperatur med og uten overhetingsveksler ga nesten de samme resultatene. Maksimal leveransetemperatur ble oppnådd ved 171.8°C med en COP på 1.16, når trykkgasstemperaturen var begrenset til 250°C . En korreksjonsfaktor ble benyttet for mellomtrykket uttrykket som $K \cdot \sqrt{P_{LP} \cdot P_{HP}}$. Optimal K-faktor økte ved økende absorbertrykk fra 1.16 til 1.35 ved absorbertrykk fra 17 til 47.5 bar.

Simuleringer fra absorbermodellen resulterte i stor forskjell mellom massestrømmen til luft og ammoniakk-vannblandingen. Varmevekslingen mellom luft og ammoniakk-vannblandingen var sensitiv for absorberhøyden og massestrømmen til luft, som medførte store trykktap og høyt vifteforbruk.

Det er foreslått å gjennomføre videre arbeid med andre inngangstemperaturer på varmekilden og varmesluket og i tillegg optimalisere temperaturløftet i to-trinns-modellen. De finnedede flate rørvarmevekslerne anbefales å undersøke nærmere i en absorbermodell med andre dimensjoner og mer nøyaktige tilnæringer for termisk resistans og finnevirkingsgrad.

Contents

Preface	i
Abstract	iii
Sammendrag	iv
Contents	v
List of Figures	vii
List of Tables	viii
Nomenclature	ix
1 Introduction	1
1.1 Background	1
1.2 Objective	2
1.3 Outline of Thesis	2
2 High temperature heat pumps	3
2.1 Closed vapor compression heat pumps	3
2.1.1 Multi-stage vapor compression heat pumps	4
2.1.2 Transcritical cycles	4
2.2 Vapor recompression cycles	5
2.3 Absorption heat pumps	5
3 Compression-Absorption Heat Pumps	7
3.1 Ammonia-Water as Working Fluid	7
3.2 The CAHP Cycle	8
3.3 Absorbers Using Ammonia-Water	12
3.4 High Temperature CAHP	14
4 Simulation Models	16
4.1 Two-stage CAHP Model	16
4.1.1 General	17
4.1.2 Thermodynamic State Properties	18
4.1.3 Compressor	19
4.1.4 Single-phase heat exchangers	20
4.1.5 Desorber and Absorber	20
4.1.6 Solution Pump and Expansion Valve	21
4.1.7 System Performance	21
4.2 Absorber Model	21
4.2.1 General	21
4.2.2 Heat exchanger functions	23
4.2.3 Thermophysical properties	25
4.2.4 Thermal resistance	25
4.2.5 Fin efficiency	27
5 Simulation Results	28
5.1 Two-stage CAHP	28

5.1.1	Simulation Scenario	29
5.1.2	Summary and Discussion	33
5.2	The Absorbers	35
5.2.1	Simulation Results	36
5.2.2	Summary and Discussion	37
6	Conclusion and Suggestions for Further Work	40
6.1	Conclusion	40
6.2	Suggestions for Further Work	41
	References	42
	Appendix	46
A	CAHP Simulation Results	47
B	Thermophysical Properties for Ammonia-Water	51
C	EES Absorber Geometry	52
D	EES Program Codes - Two-Stage CAHP	53
E	EES Program Codes - Absorbers	62
F	Scientific Paper	77

List of Figures

3.1	Temperature-concentration of an ammonia-water mixture diagram at 4 bar.	8
3.2	Schematic of the Osenbrück cycle	9
3.3	Temperature versus the cumulative heat load in desorber and absorber with an overall ammonia mass fraction of 0.73	10
3.4	Ammonia-water mixture depicted in a log P-(1/T) diagram for the CAHP cycle.	11
4.1	Schematic of the CAHP cycle.	17
4.2	Schematic of a finned tube and plate-fin heat exchanger segment. The yellow arrows indicate the flow direction for air. H, L and W stand for height, length and width. The fin pitch is expressed as p_{fin} . The plate thickness is indicated by a , while b_1 and b_2 stand for air and mixture passage width, respectively (Klein, 2014).	22
4.3	Segment and air flow arrangement.	22
4.4	Fin efficiency approaches.	27
5.1	Temperature versus the cumulative heat load in the heat sink with an circulation ratio of 1.2 and a high pressure level of 17 bar.	29
5.2	Discharge temperatures for the low and high pressure compressor stage as a function of the K-factor. The curves are represented at a circulation ratio of 1.2 and a high pressure stage at 17 bar. When both of the curves are below the dotted line, the cycle is within the limit of maximum discharge pressure for the given conditions.	29
5.3	Temperature versus the cumulative heat load in the heat sink with an circulation ratio of 0.9 and a high pressure level of 22.5 bar.	30
5.4	Discharge temperatures for the low and high pressure compressor stage as a function of the K-factor. The curves are represented at a circulation ratio of 0.9 and a high pressure stage at 22.5 bar. When both of the curves are below the dotted line, the cycle is within the limit of maximum discharge pressure for the given conditions.	30
5.5	Temperature versus the cumulative heat load in the heat sink with an circulation ratio of 0.5 and a high pressure level of 30.5 bar.	31
5.6	Discharge temperatures for the low and high pressure compressor stage as a function of the K-factor. The curves are represented at a circulation ratio of 0.5 and a high pressure stage at 30.5 bar. When both of the curves are below the dotted line, the cycle is within the limit of maximum discharge pressure for the given conditions.	31
5.7	Temperature versus the cumulative heat load in the heat sink with an circulation ratio of 0.2 and a high pressure level of 47.5 bar.	32
5.8	Discharge temperatures for the low and high pressure compressor stage as a function of the K-factor. The curves are represented at a circulation ratio of 0.5 and a high pressure stage at 30.5 bar. When both of the curves are below the dotted line, the cycle is within the limit of maximum discharge pressure for the given conditions.	32
5.9	COP versus the K-factor at the given operating conditions for the four scenario in chapter 5.1.1.1-5.1.1.4.	33
C.1	Finned tube HX (Klein,2014).	52
C.2	Plate-fin heat exchangers (Klein,2014).	52
C.3	Plain plate-fin HX (Klein,2014).	52

List of Tables

4.1	Two-stage CAHP model inputs and outputs.	18
4.2	Absorber model inputs and outputs.	23
4.3	Input and output data of the geometry EES HX function.	24
4.4	Input and output data of the heat transfer coefficient EES HX function.	24
4.5	Input and output data of the pressure drop EES HX function.	25
5.1	Parameters used for all scenario.	28
5.2	Parameters used for all absorbers.	36
5.3	Parameters used for all absorbers.	36
5.4	Simulations results for comparing the different heat exchanger types.	37
A.1	Simulations with 150°C as maximum allowable discharge temperature.	47
A.2	Simulations with 175°C as maximum allowable discharge temperature.	48
A.3	Simulations with 200°C as maximum allowable discharge temperature.	49
A.4	Simulations with 250°C as maximum allowable discharge temperature.	50
B.1	Constants for the equations of calculating the critical temperature and pressure for the ammonia-water mixture (Conde-Petit,2004).	51

Nomenclature

Latin letters

a	plate thickness	m
A_{fin}/A	fin area/total heat transfer ratio	-
(A/V)	heat transfer area/total volume	m^2/m^3
b_1	air channel width	m
b_2	mixture channel width	m
\dot{C}	capacitance rate	kW/K
c_p	specific heat capacity	$\text{kJ}/\text{kg} \cdot \text{K}$
D	diameter	m
F_{HX}	cross-flow correction factor	-
H	height	m
h	enthalpy	kJ/kg
K	correction factor for intermediate pressure	-
L	length	m
\dot{m}	mass flow rate	kg/s
P	pressure	bar
p_{fin}	fin pitch	m
P_{HX}	LMTD effectiveness	-
Pr	Prandtl number	-
q	quality	-
\dot{Q}	heat duty	kW
r	radius	m
Re	Reynolds number	-
R_{HX}	LMTD capacitance ratio	-
s	entropy	$\text{kJ}/\text{kg} \cdot \text{K}$
T	temperature	$^{\circ}\text{C}$ or K
th	thickness	m
u	internal energy	kJ/kg
u_m	mean velocity	m/s
v	specific volume	m^3/kg
\dot{V}	volumetric flow rate	m^3/s
W	width	m
\dot{W}	work	kW
x	ammonia concentration	-

Greek letters

α	heat transfer coefficient	$\text{W}/\text{m}^2 \cdot \text{K}$
ϵ	thermal efficiency	-
η	efficiency	-
λ	material conductivity	$\text{W}/\text{m} \cdot \text{K}$
ρ	density	kg/m^3

Subscripts

abs	absorber	-
avg	average	-
b	boiling point	-
C	cold	-
ch	channel	-
cf	cross-flow	-
cond	conduction	-
d	dew point	-
dc	discharge	-
des	desorber	-
dsh	desuperheater	-
ft	finned tube	-
H	hot	-
h	hydraulic	-
is	isentropic	-
liq	liquid	-
lm	log mean	-
mat	material	-
max	maximum	-
min	minimum	-
mot	motor	-
pf	plate-fin	-
s	surface	-
th	thickness	-
tot	total -	-
vap	vapor	-
vol	volumetric	-
wa	water absorber	-
wd	water desorber	-

Abbreviations

CAHP	Compression-Absorption Heat Pump	-
COP	Coefficient Of Performance	-
CR	Circulation Ratio	-
EES	Engineering Equation Solver	-
HP	High Pressure	-
HX	Heat Exchanger	-
IHX	Internal Heat Exchanger	-
LMTD	Log Mean Temperature Difference	-
LP	Low Pressure	-
MP	Intermediate Pressure	-
PR	Pressure Ratio	-
VCHP	Vapor Compression Heat Pump	-

1 Introduction

1.1 Background

There is an increase in global energy demand, with a simultaneously larger focus on inhibiting the global warming that enforces industrial production to act more energy efficient and environmentally friendly (van der Bor and Ferreira, 2013). Large amounts of low grade waste heat are not exploited, due to lack of waste heat utilization. Available low grade heat has a temperature range suited as heat sources for heat pumps in industrial processes at higher temperature levels (Chan et al., 2013).

Industrial heat pump installations have in contrast to the residential market much more complex specifications to be adapted for more unique operating conditions. These operating conditions comprise different ways of heat integration and levels of waste heat temperatures that will make a great potential for research to develop high temperature heat pumps (Jana, 2014). Unfortunately the research attention paid for industrial heat pump processes have often been neglected. Companies by now tend to focus on how to improve production processes rather than investing in energy efficiency. Increasing energy prices is an incentive that makes integration of heat pumps even more economically profitable than it is at the moment. When the temperature levels of the waste heat are determined by the process conditions and process equipment design are already set for the existing plant, implementing of heat pump might be a barrier. Therefore there is a need to find possibilities to integrate heat pumps technology into standard process machinery, to make it practically and economically feasible (Jakobs et al., 2010).

Political restrictions such as the Kyoto Protocol and F-gas directive are forcing refrigerant manufacturers to produce refrigerants that not will increase global warming or the ozone layer depletion. Natural refrigerants are therefore very a promising choice in heat pumps. That requires an increased focus on the further development on complementary heat pump technology for natural refrigerants (Calm, 2008).

Systems which are able to deliver both heating and cooling are economical desirable. This implies that industrial heat pumps must operate with high temperature lifts from heat source to heat sink to fulfil the task of heating and cooling at the same time. Standard vapor compression heat pumps have undesirable high pressure ratios under such temperature lifts, which results in higher compressor work versus COP and that requires expensive heat pump components. A combination of ammonia/water as working fluid is well suited for such operations, with temperatures between -10 to $+160^{\circ}\text{C}$ and system pressures below 20 bar. The natural refrigerant mixture of ammonia/water is at that way able to reach such temperature lifts by phase changes through an absorber and desorber (Nordtvedt, 2005). Hybrid heat pumps utilize these properties.

Energy efficiency for high temperature heat pumps can be enhanced by reducing the irreversibilities of the components, especially for the compressors and heat exchangers. Improvements in the operation and the development of components are crucial to make high temperature heat pumps more efficient and profitable. High temperature heat pumps with natural refrigerants and suited components are important in industrial processes to meet the requirements for cost efficient and sustainable operations.

1.2 Objective

The objective of this master thesis is to evaluate a compression-absorption heat pump cycle for high temperatures, using waste heat as heat source. Ammonia-water will be used as working fluid mixture. A two-stage CAHP simulation model will be developed with the main goal to maximize the supply temperature in four scenario with different compressor discharge temperature limitations. The thermodynamic benefits of a desuperheater, plus functions for intermediate pressure and compressor efficiencies are also to be considered.

An absorber model will also be developed, in order find to different types of heat exchangers. The absorber comprises an ammonia-water mixture heating air in cross-flow from 90°C. The most suited absorber is evaluated from the criteria of required absorber length and fan power input.

Highlights from the thesis will end an a scientific paper.

1.3 Outline of Thesis

Chapter 2 presents a short overview of the current technologies for different high temperature heat pump applications.

Chapter 3 contains a literature review of the ammonia-water,compression-absorption heat pump and heat exchangers used for absorption. A little explanation of the ammonia-water mixture and CAHP fundamentals are also included.

Chapter 4 explains the setup for the two simulation models. A two-stage compression-absorption heat pump and a comparison of different heat exchanger designs for an absorber.

Chapter 5 presents the results from the simulations with an evaluating discussion.

Chapter 6 comprises the conclusion and suggestions for further work.

2 High temperature heat pumps

High temperature heat pump applications in industry are referred to as heat pumping systems that are able to deliver heat above 80°C (Stene, 1993). Heat demand, availability of waste heat and type of available energy are all factors to determine the proper heat pump application. The major types of industrial heat pumps are:

- Closed vapor compression heat pumps (VCHP)
- Vapor recompression cycles
- Absorption heat pumps

The compression-absorption heat pump will be discussed later in chapter 3.

2.1 Closed vapor compression heat pumps

The simplest closed vapor compression cycle consists of four main components, namely an evaporator, compressor, condenser and an expansion valve. A working fluid is circulating within the closed cycle (Stene, 2001). The working fluid absorbs heat under isothermal conditions from an external heat source in the evaporator, before entering the compressor and undergoes a compression to the high pressure level. After the compression, the working fluid enters the condenser for an isothermal heat rejection to an external heat sink followed by an isenthalpic expansion back to the low pressure stage of the cycle.

Vapor compression heat pumps are basically developed for heat sink temperatures below 50°C. One of the keys for high temperature vapor compression cycles is therefore the development of working fluids with favourable thermodynamic and environmental properties (Zhou et al., 2012). In order to fulfil the environmental concerns, natural refrigerants are considered as the most promising working fluids. Hydrocarbons, carbon dioxide, ammonia and water are the most significant natural refrigerants (Bolaaji and Huan, 2013).

Ammonia has high volumetric heat capacity that requires smaller compressor volume compared to other working fluids. Low expansion losses yields high theoretical COP. However, high saturation pressure at low condenser temperatures is a limitation at high temperature operation. Condensation at 78.5°C requires a saturation pressure of 40 bar. High discharge temperatures is another challenge with respect to lubricant solubility, which requires cooling at high temperature lifts (Stene, 1993).

In contradiction to ammonia, water has low saturation pressure up to 200°C ($p_{sat} < 15.5$ bar). The critical pressure of 221.2 bar and temperature at 374.2°C are very high by taking other refrigerants into consideration. Water has many favourable properties at high temperature operations. Good heat transfer properties are provided by high heat capacity and vaporization heat. Even at higher temperatures, water is thermal stable and chemical inert. It is also a very environmentally benign working fluid with no ozone depletion and global warming potential. In addition, water is neither toxic, flammable nor explosive. Furthermore, water is cheap and available everywhere (Yuan and Blaise, 1988). On the other hand, low volumetric heat capacity is a major disadvantage in closed vapor compression cycles. The low volumetric heat capacity is caused by low evaporation pressure and vapor density. A temperature lift from 50 to 150°C requires compressor inlet and outlet pressures of 0.1 and 4-5 bar respectively, hence a pressure ratio between

50-60. However, centrifugal compressors are able to handle sub-atmospheric pressures and high pressure ratios and still operate at decent efficiencies (Pearson, 2012; Stene, 1993).

Many of the short-chained hydrocarbons have several working fluids with favourable properties for high temperature heat pump cycles. A drawback with hydrocarbons is their safety requirements due to flammability. Nevertheless, by taking safety precautions for gas detection, ventilation and emergency lightning, hydrocarbons can safely be operated for high temperature heat pump cycles (Pearson, 2012).

2.1.1 Multi-stage vapor compression heat pumps

Large temperature lifts and high pressure ratio induces reduced compressor efficiencies, expansion losses, plus high discharge temperatures that entail lubricant decomposition. These problems can be reduced by dividing the compression and expansion into several stages, hence multi-stage heat pumps systems (Stene, 2001). Multi-stage vapor compression heat pumps are classified as compound or cascade systems. Compound systems consists of two or more compressor stages connected in series, where one working fluid is circulating through the entire cycle. In order to cool the discharge temperature, the compound system is equipped with an intermediate pressure receiver with full or partly intercooling between the compressor stages. Cascade systems comprises two independently operated single-stage heat pump cycles, a lower temperature unit and one for higher temperature operations. The condenser in the low temperature unit works as an evaporator for the high temperature cycle with indirect heat exchange. This heat exchange results in extra temperature losses, but makes it possible to utilize different refrigerants suited to the different temperature levels (Chua et al., 2010). Stavset et al. (2014) reported an analysis of a cascaded high temperature heat pump cycle by using hydrocarbons. Propane was used in the bottom cycle and butane/isobutane in the top cycle for heating water from 95 to 115°C, with good performance results.

2.1.2 Transcritical cycles

In transcritical cycles, the working fluids rejects heat above the critical point at constant pressure and gliding temperatures. Under supercritical conditions the refrigerant is neither gas nor liquid and the temperature is independent of the pressure. Instead of employing a condenser, transcritical cycles applies gas coolers, in order to obtain supercritical heat rejection. Carbon dioxide has a very low critical temperature (31.1°C) that makes it suited for transcritical operations. High working pressure leads to beneficial characteristics in terms of high volumetric heat capacity, smaller compressor volume and pipe dimensions. However, the great difference between the high and low pressure side induces large expansion losses. On the other hand, the throttling losses could be compensated by implementation of an ejector (Austin and Sumathy, 2011). The theoretical COP is relatively low, but the actual system efficiency could be considerably higher due to the low pressure ratio excellent transport properties of CO_2 . Transcritical heat pumps are most suited at high temperature glides and can deliver heat up to 120°C and are used in district heating, domestic hot water production, plus industrial process water. The transcritical heating is most efficient when the heat sink is heated from 10 to at least 80-90°C. Many industrial processes produce waste heat above or close to the crit-

ical temperature for CO_2 , which makes the implementation of transcritical heat pumps unfavourable (Kim et al., 2004; Pearson, 2012).

2.2 Vapor recompression cycles

Vapor recompression systems utilize high pressure waste vapor, in order to supply heat to another process stream. This waste vapor acts both as a waste heat and working fluid. In process where the waste vapor is re-used directly are classified as open systems. Indirect condensation in heat exchangers are called closed systems. Vapor recompression cycles can either be mechanically or thermally driven, hence classified as mechanical vapor recompression (MVR) and thermal vapor recompression (TVR), where MVR is the most common of the two cycles (Laue, 2006).

Drying is the largest application area for high temperature heat pumps. Estimates evaluate that drying constitute to 15-25 % of the total industrial energy demand in developed countries with a corresponding poor energy utilization. Food production, wood drying and construction materials manufacturing are examples of branches that apply high temperature drying. In addition to waste vapor utilization from other processes is a practical way to exploit heat, water is an attractive and highly available working fluid. It has sufficiently high critical temperature to provide efficient condensation. The condensing pressure of water at $180^\circ C$ is approximately 10 bar, which is relatively low and will decrease the equipment manufacturing costs (Tolstorebrov et al., 2014). The most common MVR cycles have heat source temperatures from 70 to $80^\circ C$ and deliver heat between 110 and $150^\circ C$. Some systems are even able to deliver heat up to $200^\circ C$. COP for MVR-systems is typically between 10 to 30, which is much higher than closed vapor compression cycles. Investment cost will also be lower for MVR cycle, due to a simpler configuration with fewer components (Laue, 2006).

TVR systems are not as prevalent as MVR. In spite of low investment and maintenance cost the system efficiency in general low, especially at increasing temperature lifts, the TVR cycle will have a significant decrease in COP. Such cycles are best suited in small scale systems and when there is a large difference between fuel and electricity prices (Leonardo Energy, 2007; Stene, 1993).

2.3 Absorption heat pumps

Absorption are thermally driven heat pumps classified as either type I or type II. Both types are configured with the same main components as the VCHP, except from the compressor, which is replaced with an absorption circuit. The absorption circuit comprises a solution pump, absorber and a desorber. The condensation and evaporation in such systems occur at gliding temperatures, hence zeotropic working fluid pairs. $H_2O/LiBr$ and NH_3/H_2O are the most prevalent working pairs. Type I is also referred to as a heat amplifier, because the heat pumping process is heat increasing. This type I heat pumps absorb heat from a high and low temperature heat source for rejecting heat to an intermediate temperature heat sink. Supply temperatures are achievable at around $100^\circ C$ with a COP of 1.4-1.6 for type I heat pumps. Type II is referred to as a heat transformer, due to its temperature increasing heat pump process. This type absorbs heat from from two intermediate temperature heat sources, in order to reject heat at a higher temperature level. COP for a type II are approx at 0.45-0.50 with a delivering

temperature slightly above 100°C (Stene, 1993). One of the largest barriers for implementation of absorption heat pumps tends to be large capital costs and are therefore best suited in small scale systems, where price difference is smaller. The price relation between oil/gas firing and electricity is a crucial factor, if absorption heat pumps could be competitive compared to compression heat pumps. Access to cheap waste heat will be vital for investing in absorption heat pumps(Nordtvedt, 2013).

3 Compression-Absorption Heat Pumps

By the use of zeotropic working fluids, the CAHP absorbs and releases heat at gliding temperatures, which results in lower irreversibilities. Flexible capacity, high achievable working temperatures and environmentally benign working fluids are some of the characteristics about the compression-absorption heat pump.

3.1 Ammonia-Water as Working Fluid

Ordinary single component working fluids have constant saturation temperatures at a given pressure. In binary working fluids, the saturation temperature is not only determined by the pressure, but also by the mixture composition. The most volatile of the two components is classified as the refrigerant, while the other one is referred to as the absorbent. The refrigerant evaporates/condensates more quickly, which yields changes in concentration and thus saturation temperature for the mixture. Evaporation of the refrigerant causes higher concentration of the absorbent, that leads to increased saturation temperature and reduced vapor pressure of the remaining mixture. This phenomenon called boiling point elevation is a colligative property, which means composition dependent (Atkins and de Paula, 2006). For NH_3/H_2O mixtures, ammonia works as the refrigerant and water constitutes the absorbent. The advantages of boiling point elevation for ammonia-water will be discussed more thoroughly later in this chapter.

Temperature-concentration diagrams are useful to show the behaviour of condensation/evaporation of binary mixtures at a given pressure. Figure 3.1 depicts a temperature-concentration diagram for ammonia-water at 4 bar. A concentration of 0.0 equals pure water, while $x = 1.0$ corresponds to pure ammonia. Pure water has a saturation temperature at 143.6°C at 4 bar, compared to pure ammonia at -1.9°C . The boiling point line indicates where the first vapor bubble is formed from subcooled liquid for a given concentration during heating. In the same manner, the dew point line shows the temperature at which the first liquid droplet is formed from superheated vapor when the mixture is cooled at a specified concentration (Alefeld and Radermacher, 1994). An evaporation process for the ammonia-water mixture at 4 bar is described in figure 3.1:

- The process starts with a 50 weight-% concentration of ammonia at 10°C as subcooled liquid in point 1.
- When adding heat to the mixture, the temperature increases until it reaches the boiling point at point 2_b at 33.5°C for the given concentration. At this temperature the first vapor bubble starts to form and the ammonia concentration, which is in thermal equilibrium with the surrounding liquid is 99.6 weight-%, depicted at point 2_d .
- By adding more heat, more of the mixture evaporates and reaches 94.3°C at point 3. If all the vapor remains in contact with the liquid, the mixture is in two-phase. The ammonia concentration of the vapor is then 82.6 weight-%, denoted by point 3_d and the concentration of the liquid is 18.7 weight-% indicated by point 3_b .
- When adding even more heat, the evaporation is completed at 121.9°C indicated by point 4_d . The vapor has the same ammonia concentration as the initial subcooled liquid at point 1. The concentration of the last droplet to evaporate is 7.7 weight-% denoted by point 4_b .

- Further heating results in superheated vapor. Point 5 indicates superheated vapor at 150°C.

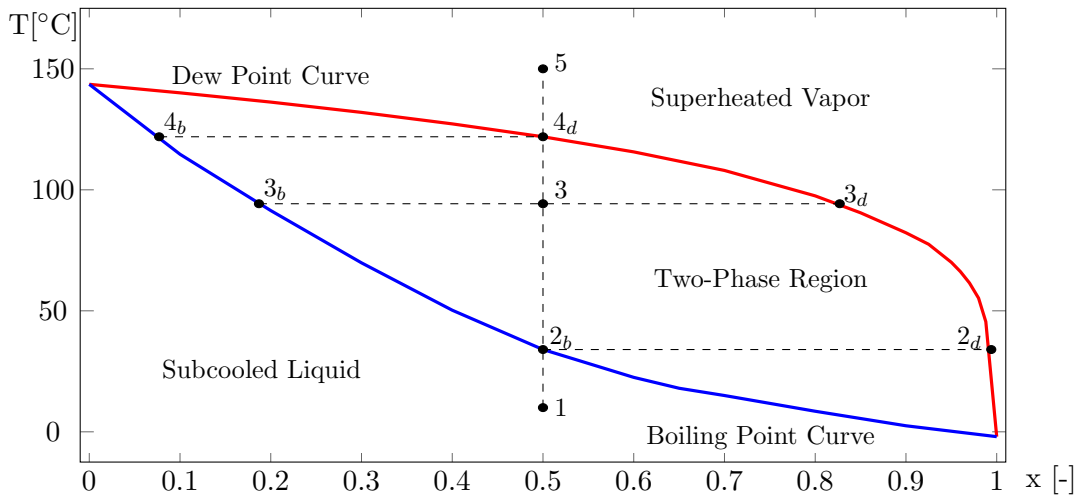


Figure 3.1: Temperature-concentration of an ammonia-water mixture diagram at 4 bar.

Ideal heat pump cycles with single component refrigerants are considered as Carnot cycles with isothermal heat rejection and absorption. As previously noted, binary working fluids are heat exchanging at gliding temperatures, where an ideal cycle is considered as a Lorentz cycle. Such cycles, the working fluid have a better temperature match with heat source/sink, that theoretically will give a smaller entropy production than ideal Carnot cycles (Radermacher and Hwang, 2005).

3.2 The CAHP Cycle

The simplest type of compression-absorption heat pump cycle is the Osenbrück cycle, indicated in figure 3.2. The cycle is based on the vapor compression cycle principles that employ a binary working fluid mixture and a liquid solution circuit. At the outlet of the desorber there is a two-phase mixture consisting of saturated liquid and saturated vapor which are in thermodynamic equilibrium. The saturated vapor enters the compressor for a pressure increase (1-2). Simultaneously, the saturated liquid with a low ammonia concentration (weak solution) achieves its pressure increase from the solution pump (3-4). High pressure weak solution increases the temperature through the solution heat exchanger(4-5). Thereafter, the weak solution absorbs the vapor in the absorber resulting in heat rejection to an external heat sink and a solution with high ammonia concentration (strong solution). During the vapor absorption, the heat rejection takes place at gliding temperatures and with a gradually higher ammonia concentration of the solution (2/5-6). In the subsequent step, the strong solution is cooled down by the weak solution in the solution heat exchanger(6-7), followed by an expansion to the low pressure level (7-8). To conclude the cycle, heat absorption from a heat source is made in the desorber, where the ammonia solution concentration becomes gradually lower and vapor is formed(8-1/3). This desorption occurs at gliding temperatures(Nordtvedt, 2005).

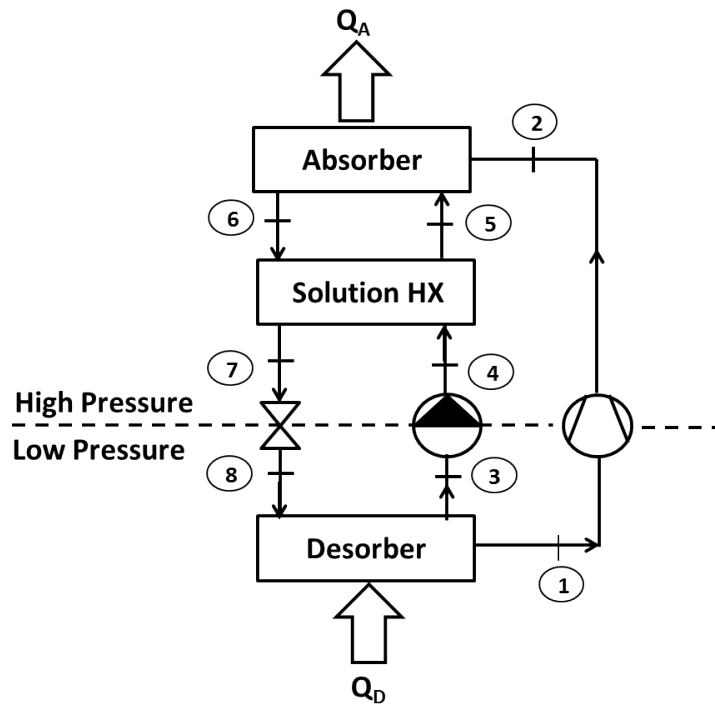


Figure 3.2: Schematic of the Osenbrück cycle

The principles of an compression-absorption cycle was first described in 1895 as the Osenbrück cycle. In the fifties some theoretical publications of using ammonia-water mixtures were reported. Little research of the subject has been made until the eighties. At that time the hybrid heat pump and the use of natural working fluids became more interesting, due to a larger focus on energy savings and environmentally friendly operations (Itard, 1998).

Stokar and Trepp (1987) compared a CAHP cycle with a conventional compression heat pump. An oil-free, one-stage compressor was used with spine tube heat exchangers as the absorber and the desorber. Ammonia-water was selected as working fluid mixture due to high latent heat, which resulted in reduced losses in the solution circuit. Another reason for the choice of ammonia-water was also because of good heat and mass transfer properties, which affected the design of the absorber and the desorber. The CAHP showed two major advantages over the VCHP. The advantage was the ability of a wide range capacity control due to simple adjustments of the mixture composition. The second was the substantially higher heating coefficient of performance because of the temperature glide in the absorber and desorber. Test plant experiments achieved a $COP_{heating}$ of 4.3 for the hybrid system and 3.3 for the conventional heat pump. The heating coefficient of performance for the CAHP was a calculated value, since the isentropic compressor efficiency and electric motor efficiency were assumed to be 70% and 85% respectively. The oil-free compressor was not designed for the heat pump application and it actually achieved lower efficiencies.

Itard and Machielsen (1994) used ammonia-water in their study to show that binary working fluids has non-linear temperature profiles, which are strongly dependant on their composition. The observation concluded that the LMTD method for modelling heat exchangers was not applicable. Small temperature differences between the streams or

large temperature glides can lead to infeasible temperature profiles. Figure 3.3 illustrate how the temperature profiles can behave under certain conditions in an absorber and a desorber of the CAHP cycle. In a desorber the cold stream of NH_3/H_2O absorbing heat will have the smallest temperature difference known as the pinch point at either the inlet, outlet or both sides of the heat exchanger. On the other hand, if a hot stream of ammonia-water rejecting heat to a heat sink in an absorber and the pinch point takes place at the inlet or outlet, infeasible temperature profiles might occur if the absorber capacity and heat sink mass flow are not adjusted to this concern. Figure 3.3 gives an example for both a feasible and infeasible heat exchange.

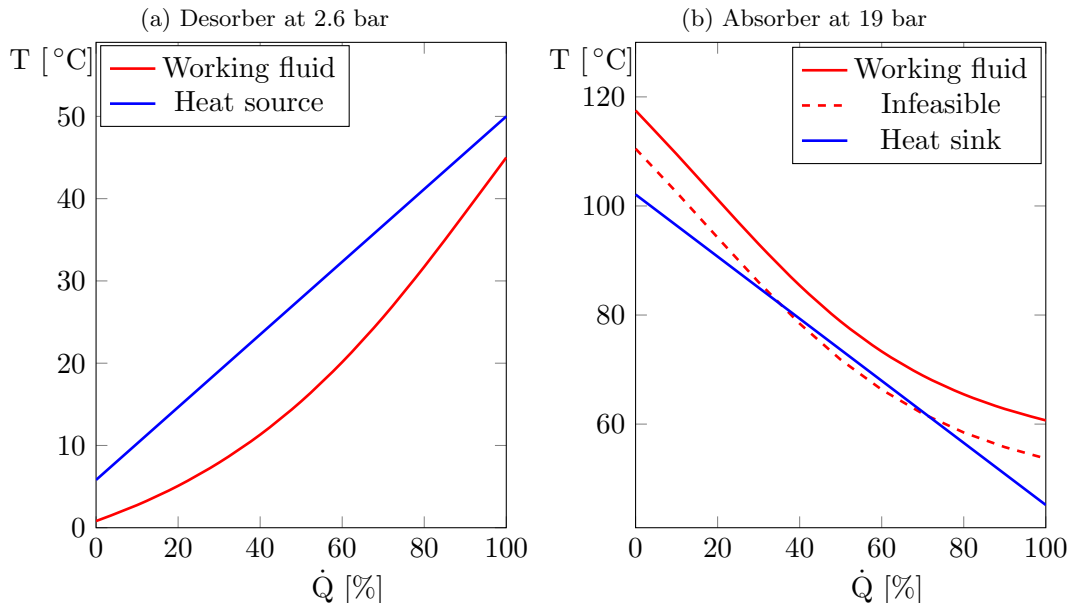


Figure 3.3: Temperature versus the cumulative heat load in desorber and absorber with an overall ammonia mass fraction of 0.73

Hultén and Berntsson (1999,2002) reported a comparison study for the CAHP. In contrast to earlier comparison studies, this study compared the hybrid heat pump to a VCHP with a more relevant industrial design, including indirect economizer coupling, suction gas heat exchanger, sub-cooler and surface enhancements in the evaporator and condenser. Isobutane was used as working fluid in the VCHP and ammonia-water in the CAHP. The absorber and desorber were modelled as vertical falling-film tube-and-shell heat exchangers. The comparison was performed for various heating applications and with specified investment evaluations. Hultén and Berntsson listed the main advantages of the CAHP as:

- Small swept volume to the compressor.
- High heat transfer coefficients (depending on the operating conditions and components).
- Non-ozone-depleting working fluid.
- An extra degree of freedom, due to variable composition. This enhances the flexibility of the heat pump installation, such that it easily can be adapted to different temperature levels and capacities.

- High working temperatures can be achieved (at least 150°C).
- Decrease in system irreversibility can be provided by fitting the absorber glide to the temperature glides of the heat source and heat sink.

The main drawbacks were described as:

- No gain in economizer coupling.
- Leakage will change the composition and the operating conditions.
- Ammonia is hazardous and flammable (but still well known).

Both heat pump systems achieved the same COP when the heat sink and heat source glides were 10 K. The CAHP was evaluated to have a 12 % better heating coefficient of performance than the VCHP, when the same temperature glides were increased to 20 K. At even higher temperature lifts and temperature levels, the hybrid heat pump was reported to be relatively worse than the VCHP. The study indicated that both cycles remained at an equal performance level, when economics was taken into consideration.

In conventional vapor compression heat pump systems, the condensing pressure exceeds the design pressure of standard refrigeration components, when temperatures approach 100°C. Pure ammonia with a condensing temperature at 100°C has a saturation pressure of 62.6 bar. However, the effect of the saturation pressure reduction can be exploited by mixing the ammonia with water. A 90 weight-% ammonia-water solution reduces the same condensing temperature to 54 bar, while 50 weight-% gives a saturation pressure of 22.4 bar. Figure 3.4 shows how changes in saturation temperatures can be varied at fixed pressure levels and varying solution concentrations. The numbers indicated in the refer to the cycle state points in figure 3.4. Temperature glides and levels will also be easily adjusted by altering the composition, which favourable at changing heat sink and source temperatures (Nordtvedt, 2005).

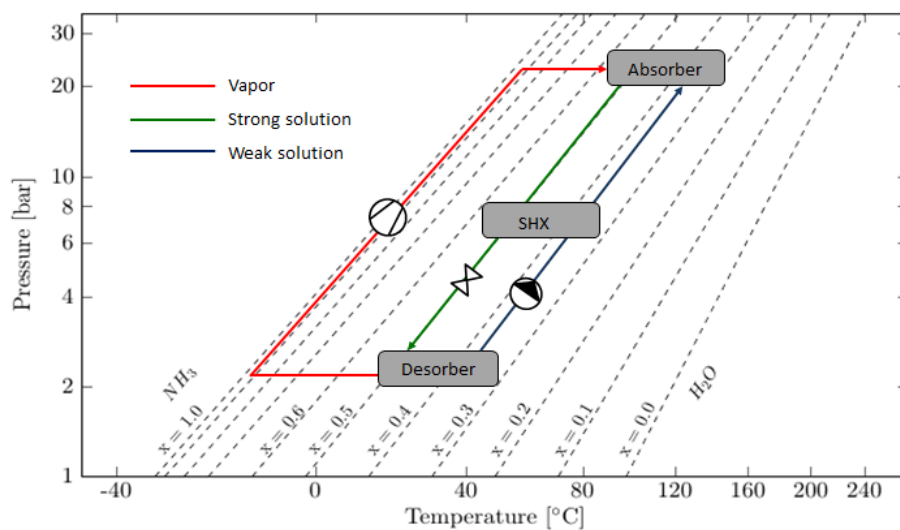


Figure 3.4: Ammonia-water mixture depicted in a log P -($1/T$) diagram for the CAHP cycle.

3.3 Absorbers Using Ammonia-Water

The performance of the absorber has a critical impact on the overall system efficiency and costs in compression absorption heat pump systems (Killion and Garimella, 2001). As previously noted, evaporation and condensation of ammonia-water comprises complex heat and mass transfer processes, which has led to incomplete understanding of the thermodynamics and numerous errors in the literature. Therefore, absorption processes requires an understanding of the thermodynamics of fluid mixtures, phase equilibria, plus heat and mass transfer (Vuddagiri and Eubank, 1998). Two absorption modes are recommended to enhance the heat and mass transfer, namely the falling film absorption and the bubble absorption mode. Thin falling film heat transfer mode gives relatively high heat transfer coefficients and is stable during operation. On the other hand, the falling film mode have difficulties regarding wettability and require good liquid distributors at the inlet of the liquid flow. Bubble type heat transfer provides high heat transfer coefficients, in addition to good wettability and mixing between the liquid and the vapor (Kang et al., 2002). However, the bubble vapor mode requires vapor distribution and a pressure difference on the vapor side to transport the vapor bubble through the pool of liquid. This problem is not prevalent in ammonia-water systems, due to sufficient system pressure, but the pressure drop should still be considered carefully. In general, vapor distribution is easier to achieve than liquid distribution (Lee et al., 2002a).

Kang et al. (2000) carried out a parametric heat and mass transfer analysis for an ammonia-water mixture for two different absorption modes; falling film and bubble modes. A plate heat exchanger was used to design the two absorption modes. They found that the local absorption rate was always higher in the bubble mode due to larger mass transfer area, a better mixing and higher heat transfer coefficients. This resulted in about 50% smaller size of the heat exchanger area for the bubble mode compared to the falling film type. The results also stated that the heat transfer coefficient had a more significant impact on the heat exchanger size in the falling film mode compared to the bubble mode, while the mass transfer coefficient has a more significant effect in the bubble mode than the falling film mode. Lee et al. (2002a,b) carried out an experimental analysis of an ammonia-water absorption process for the falling film and bubble modes in a plate-type heat exchanger. The experiments were made to investigate how the solution flow rate and gas flow rate influenced the absorber performance. An increased solution flow rate resulted in a small increase of mass transfer and more heat was generated. The heat transfer coefficient was significantly affected at low solution flow rates, especially for the falling film mode, but became less important at higher solution flow rates. The heat transfer performance yielded good heat transfer performance for the bubble mode, but unchanged or even worse for the falling film mode at increasing gas flow rates. Their results showed that the bubble modes were superior to the falling film modes for heat and mass transfer on a general basis.

Fernández-Seara et al. (2005) performed an analysis of the mass and heat transfer processes during the absorption of ammonia-water in a co-current vertical shell and tube absorber. Water was used as absorber cooling medium. They later continued their work with an analysis of an air-cooled ammonia-water vertical tubular absorber (Fernández-Seara et al., 2007). The co-current absorption model took into account that the absorption process was distinguished by changing flow regimes. Churn flow took place at the absorber inlet, followed by slug flow at the intermediate stage and bubbly flow at the end of the absorption process. They observed that the absorption process

slowed down through the process, due to gradually decreased heat and mass transfer. Consequently, the required tube length increased from the first to the last tube row, in order to complete the absorption process. The sizing of the absorber should therefore be based on the required absorption length of the last tube row. An optimum tube row pitch was found, where higher pitch values caused a significant increase in the absorber length and pitch values below entailed larger absorber length difference between the tube rows. Moreover, Fernández-Seara et al. (2007) found that there was an optimum tube diameter that minimized the absorber length and that the optimum diameter changed slightly for each row. The fin spacing also played an important role on the absorber sizing and should be reduced as much as possible. As the air velocity decreased, the absorber length increased and appeared to be crucial at low air velocities, which should be taken into account to select fans for the absorber.

Jung et al. (2014) studied the thermal characteristics of plate type ammonia-water bubble absorbers for compression-absorption heat pump applications. The effects of absorber internal pressure, ammonia weak solution concentration and absorber geometric dimensions on the absorber capacity and system COP were investigated. Three different heat exchanger designs and ammonia weak solution concentrations were experimentally tested. The absorber capacity increased with increasing absorber pressure for all cases. This pattern can be explained by an increasing absorption rate at higher pressures. The absorption latent heat also increases with increasing saturation pressure. This pattern can be explained by an increasing absorption rate at higher pressures. The absorption latent heat also increased with increasing saturation pressure and decreasing ammonia solution concentration. Therefore, a decreasing ammonia weak solution resulted in higher absorber capacity. From the comparisons of these effects, the absorber pressure had a larger impact on the absorber capacity than the ammonia weak solution concentration. The COP showed the same trend as the absorber capacity for the different cases. Aspect ratios of plate length over plate distance (L/D) and plate width over plate distance (W/D) were used for the three different heat exchanger designs. They concluded that the heat transfer coefficient of the solution side increased with the increasing aspect ratio (L/D), while the aspect ratio (W/D) did not give any significant effects. The experimental correlation for the Nusselt number was obtained with an error band of $\pm 20\%$ for ammonia-water bubble absorption process in plate heat exchangers. Compared to the experimental correlations from Cerezo et al. (2010), the correlations had too large deviations, since their experiments were tested at other operating conditions. Therefore, it is recommended that the two different experimental correlations should only be adopted for each operating conditions with valid ranges of Re and Pr .

Besides higher efficiency demands, there is a growing need for product miniaturization in the industrial sector. Mini-channel exchangers have turned up as a promising for these requirements, due to their ability to reduce costs and increase the efficiency for similar capacities as compared to the macro-channel exchangers. This type of heat exchangers are a relatively new technology and not many papers have been published on this topic. However, hydrodynamic instabilities are reported to have a profound effect on the heat and mass transfer coefficient during absorption in mini-channel exchangers (Nefs et al., 2014).

Nefs et al. (2014) performed an investigation of a prototype multi-tube mini-channel exchanger with the geometry of a shell and tube heat exchanger without baffles. Ammonia-water was at the shell side, while the water flowed counter-currently at the tube side in the absorber. A mathematical model was developed and compared with experimental

results. The pressure drop and the overall characteristics of the ammonia-water were studied. The presence of hydrodynamic instabilities were reported to increase the pressure drop and decrease the heat transfer coefficient. These effects were not taken into account in the mathematical model and thus caused a large disagreement between the model and the experiments. Consequently, the pressure drop was under predicted and the heat transfer coefficient was over predicted in the model.

3.4 High Temperature CAHP

Brunin et al. (1997) studied the possible working domains for compression-absorption heat pumps using ammonia-water. A prototype of CAHP was made and tested in a laboratory. The cycle was calculated with a set of different average concentration of the rich and weak solution, with a 0.10kg/kg difference between the two solution for all the tests. In order to find the pinch point of the the absorber and desorber, the minimum temperature difference was assumed to be at the outlet for both of the heat exchangers. Linear variation in saturation temperature was another simplification they made. Delivering water up to 120°C with a strong solution ammonia concentration of 0.35kg/kg solution, where the system efficiencies comparable to vapor compression heat pumps. The knowledge of CAHP was limited at that time, which made it uncompetitive with other systems, according to economic and reliability concerns.

Rane et al. (1993) investigated a two-stage compression heat pump with solution circuit using ammonia-water. A low temperature desorber and a high temperature absorber comprised the heat source and sink, respectively. The heat pump was configured as a cascade system with only one compressor stage, where a low temperature absorber delivered heat to a high temperature desorber. In order to optimize the heat pump, four different system configurations comprising a rectifier, desuperheater and a bleed line were tested in simulation models. The system with a desuperheater and a bleed line obtained the best performance results. Rane and Radermacher (1993) continued their work experimentally, where temperature lifts above 100 K and absorber temperatures of more than 100°C were achieved with a COP of 1.04. Compared to a single stage ammonia vapor compression cycle, the heat pump developed by Rane and Radermacher (1993) measured one third of the pressure ratio and twice as high cooling COP.

Zhou and Radermacher (1997) compared three different CAHP cycles using ammonia-water. A single-stage and two-stage vapor compression cycle with a solution circuit and the third system, which was a combination of the others, namely a vapor compression heat pump with a solution circuit and a desorber/absorber heat exchange (DAHX cycle) were all experimentally tested. Test results from the experiments indicated highest COP for the one-stage cycle, while the two-stage cycle yielded the highest temperature lifts. The two-stage cycle was the most beneficial for high temperature lifts, due to the possibilities for individual adjustments of the absorber pressure and the solution concentration. This was not possible for the DAHX system, where the absorber pressure decreased with decreasing solution concentration. Therefore it was difficult for the DAHX system to increase the pressure and the solution concentration simultaneously to achieve high temperature lifts.

Sveine et al. (1998) designed and developed a two-stage CAHP with ammonia-water as working fluid pair. In addition to standard components, two solution heat exchangers and a desuperheater were used in the model. The process was limited to the maximum

compressor discharge temperature of 160°C. From the simulations, a COP of 3.8 was achieved at heat sink and source temperatures at 53 and 117°C, respectively. The solution heat exchanger between the compressor stages had a considerable impact on the COP. Reduction in discharge temperatures and heating of the strong solution were positive consequences from that specific solution heat exchanger. Nordtvedt (2005) used the work from Sveine et al. (1998) to further develop the CAHP for laboratory testing. The tests measured a COP of 2.47 when heating water from 50 to 93° and simultaneously cooling water from 50 to 17°.

Costs of compression-absorption heat pumps are most often related to operating costs, without taking overall costs into account. Jensen et al. (2014a) evaluated the CAHP based on technical and economic constraints. They compared the CAHP to the best possible vapor compression heat pump using natural working fluids. Temperature lifts were restricted by a compressor discharge temperature of 180°C, due to thermal stability of the oil lubrication and in order to reduce wear by thermal stress. Heat sink temperatures up to 140°C was only achieved by the compression-absorption heat pump in the simulations. The CAHP delivered higher heat supply temperatures and temperature lifts than the conventional VCHP. However, the compression-absorption cycle requires larger heat transfer area compared to a pure ammonia vapor compression heat pump. Even after inclusion of the lifetime costs at the operating points where both systems were applicable, the CAHP required overall costs between 5 and 30% lower than VCHP. In spite of lower costs, Jensen et al. concluded that the vapor compression cycle could still be preferred at small cost differences. This argument was based on the simplicity of the VCHP, plus the broader range of suppliers and contractors.

In order to investigate the possibilities for delivering heat supply temperatures above 100°C in a CAHP cycle using ammonia-water, Jensen et al. (2014b) carried out a one-stage numerical model. Ammonia mass fraction of the rich solution and circulation ratio were constrained parameters at heat supply temperatures of 100, 125, 150, and 175°C. Standard refrigeration components were applicable at heat supply temperatures of 100°C. High pressure ammonia components increased the attainable supply temperatures to 125°C. The set of possible for standard refrigeration and high pressure ammonia components were mainly constrained by the high pressure and compressor discharge temperature. Heat supply temperatures of 150 and 175°C were only feasible using transcritical CO_2 components modified to sustain discharge temperatures up to 250°C. The use of such components assumed that ammonia-water were compatible for transcritical CO_2 components. At circulation ratios below 0.5 and rich ammonia solution mass fractions between 0.2-0.8, a set of combinations entailed a considerably increase in pressure ratio. Consequently, the reduction in COP and the increase of compressor discharge temperature resulted in recommended operating conditions outside those ranges. Jensen et al. suggested to further investigate the use of two-stage compression and oil cooled compressors that will reduce the compressor discharge pressure.

4 Simulation Models

In order to optimize the compression-absorption heat pump system at higher temperatures, two simulation models are carried out. Among the models a two-stage CAHP process heating water with different limitations for maximum allowable discharge temperatures. The other model, an absorber used for heating air in cross-flow with ammonia-water. Five different heat exchanger designs were tested. Calculation of the two models are computed in Engineering Equation Solver (EES) with an external procedure for the thermodynamic properties of the ammonia-water mixture (Klein, 2014; Ibrahim and Klein, 1993). EES codes for both of the models are given in Appendix D and E.

4.1 Two-stage CAHP Model

A schematic of the hybrid heat pump cycle is illustrated in figure 4.1. The CAHP cycle consists of a desorber, liquid/vapor separator, a two-stage compressor, two solution heat exchangers, a desuperheater, an absorber, a high pressure liquid receiver, an expansion valve and a solution pump. Heat absorption from the heat source is achieved in the desorber, where mainly ammonia is desorbed from a strong ammonia-water solution, resulting in a weak ammonia-water solution and vapor are entering the liquid/vapor separator. From there, the vapor is fed into the compressor and compressed in two stages to a high pressure level and sent to the desuperheater and then the absorber. The weak solution is raised to the high pressure level by a solution pump. Right before the absorber, the weak solution and the vapor are mixed. In the absorber, the weak solution absorbs the vapor and rejects heat to the heat sink, hence a strong ammonia-water solution entering the high pressure liquid receiver. Further, the strong solution is cooled by the weak solution in the solution heat exchanger #1 and then expanded to the low pressure stage. At the intermediate pressure stage the superheated vapor is cooled down by the weak solution in heat exchanger #2.

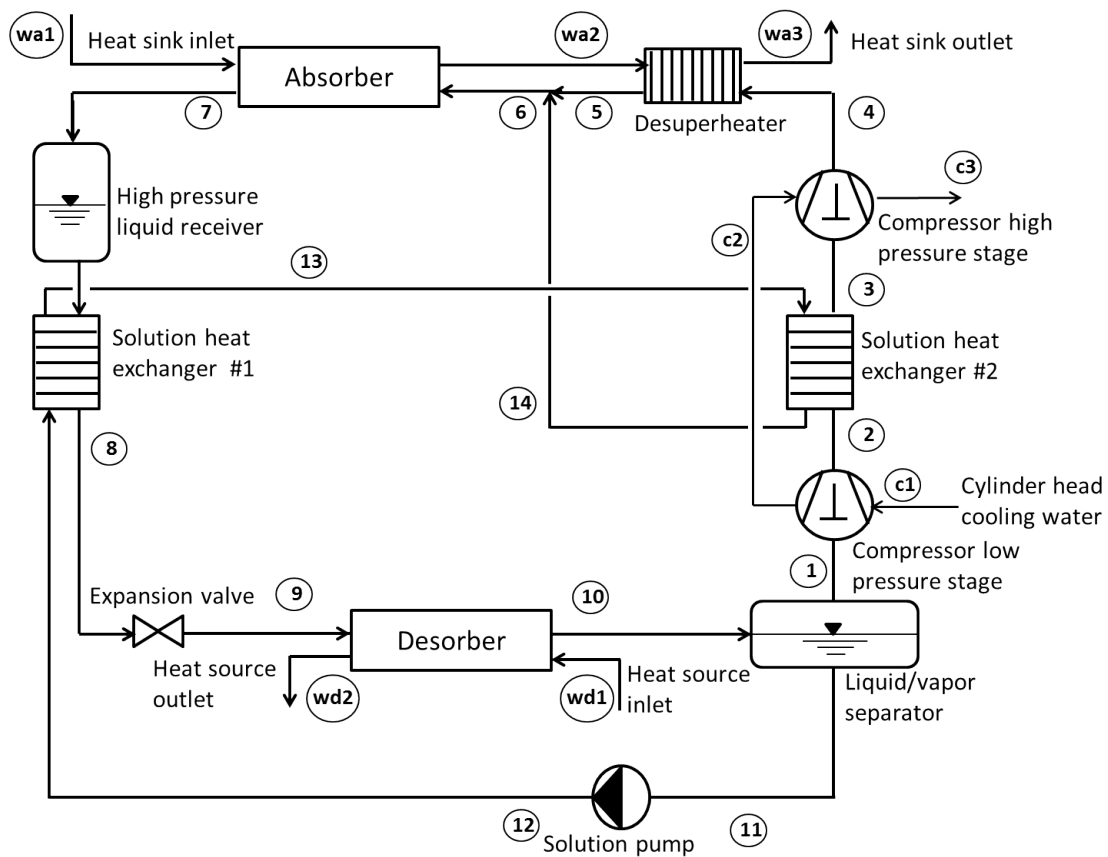


Figure 4.1: Schematic of the CAHP cycle.

4.1.1 General

The simulation tool is based on fundamental thermodynamics including energy and mass balances and heat transfer relations. In order to achieve thermodynamic parameters of the hybrid heat pump, the following assumptions were set:

1. Heat losses to the surroundings are negligible.
2. Frictional pressure drops in the system are negligible.
3. The fluid flows are counter-current in all of the heat exchangers.
4. The strong solution leaving the absorber is saturated.
5. The mixing of the vapor and weak solution at the absorber inlet is adiabatic.
6. The vapor at the compressor inlet is in thermodynamic equilibrium with liquid in the liquid/vapor separator.
7. The solution pump efficiency is 100%.

Table 4.1: Two-stage CAHP model inputs and outputs.

Inputs	Outputs
Absorber pressure	Intermediate pressure
Desorber pressure	Vapor and liquid mass flow rate
CR	Strong solution ammonia concentration
Correction factor	Overall strong solution flow rate
Thermal efficiency of internal heat exchangers	Heat sink outlet temperature
Minimum temperature difference in desorber and absorber	Thermodynamic state points
Heat sink performance	System performance

Equation (4.1) expresses the energy balance for the heat exchangers, while (4.2) is for the compressor and solution pump. Overall mass balance and ammonia mass balance are calculated by the use of equation (4.3) and (4.4), respectively. The ratio between the weak solution and vapor flow, the circulation ratio (CR) is given in equation (4.5). Ammonia concentration in the strong solution, ZZ is calculated from equation (4.6).

$$\sum(\dot{m} \cdot h)_{in} - \sum(\dot{m} \cdot h)_{out} = 0 \quad (4.1)$$

$$\sum(\dot{m} \cdot h)_{in} + \dot{W} - \sum(\dot{m} \cdot h)_{out} = 0 \quad (4.2)$$

$$\sum(\dot{m})_{in} - \sum(\dot{m})_{out} = 0 \quad (4.3)$$

$$\sum(\dot{m} \cdot x)_{in} - \sum(\dot{m} \cdot x)_{out} = 0 \quad (4.4)$$

$$CR = \frac{\dot{m}_{liq}}{\dot{m}_{vap}} \quad (4.5)$$

$$ZZ = \frac{\dot{m}_{vap} \cdot x_{vap} + \dot{m}_{liq} \cdot x_{liq}}{\dot{m}_{tot}} \quad (4.6)$$

4.1.2 Thermodynamic State Properties

In order to calculate the thermodynamic state point properties of the cycle, a procedure called NH3H2O from the external library developed by Ibrahim and Klein (1993) is applied in EES. That procedure can return eight thermodynamic properties for ammonia-water mixtures from three known input parameters. The procedure is called from EES by the statement:

```
CALL NH3H2O(Code;ln1;ln2;ln3:T,P,x,h,s,u,v,q)
```

The parameters to the left of the colon are inputs to the NH₃H₂O procedure and the other eight values are outputs calculated from the procedure. These outputs operate in SI units where:

- T = Temperature [K] (position 1)
- P = Pressure [bar] (position 2)
- x = Ammonia mass fraction [kg ammonia/kg mixture] (position 3)
- h = Enthalpy [kJ/kg] (position 4)
- s = Entropy [kJ/kg·K] (position 5)
- u = Internal energy [kJ/kg] (position 6)
- v = Specific volume [m³/kg] (position 7)
- q = Vapor quality [kg vapor/kg mixture] (position 8)

The ln1, ln2 and ln3 are referring to the known properties and the Code to the numbered position of the latter properties in the CALL procedure. If the temperature, pressure and quality are known, the Code will be 128. Water is used as heat sink and heat source fluid and has an in-built function in EES, which makes it simpler than ammonia-water to determine its thermodynamic state properties.

4.1.3 Compressor

The compressor to be used is an oil-lubricated to-stage reciprocating type, where the cylinder heads are water-cooled. According to the setup Nordtvedt (2005) made, the models for reciprocating type, the models used for isentropic and volumetric efficiency were taken from some data fitted polynomial functions. The functions were correlated to the pressure ratio across the compressor, while the motor efficiency (η_{mot}) is set to 0.9. Isentropic efficiency and volumetric efficiency for each compressor stage are given by equation (4.7) and (4.8), respectively. In accordance with assumption 6 in chapter 4.1.1 the vapor at the compressor inlet is assumed to be in thermodynamic equilibrium with the liquid in the liquid/vapor separator. Equation (4.9) calculates the compressor inlet conditions, found from the heat source inlet temperature (T_{wd1}) and the minimum temperature difference at the desorber outlet ($\Delta T_{des,out}$). Intermediate pressure P_{MP} can be determined with respect to the maximum allowable discharge temperature (Koelet et al., 1992). In order to find the optimal intermediate pressure at the given operating conditions, P_{MP} is expressed with a correction factor K (K-factor) calculated in equation (4.10). The mass flow rate at the compressor inlet is given in equation (4.11) by the CR and strong solution mass flow rate. Water cooling of the compressor cylinder heads \dot{Q}_{head} is assumed to be 5% of the shaft power. The low pressure specific shaft work ($h_2 - h_1$) is given in equation (4.12), where the enthalpy difference for the high pressure stage is made by the same method.

$$\eta_{is} = 0.9051 - 0.0422 \cdot PR \quad (4.7)$$

$$\eta_{vol} = 1.0539 - 0.0788 \cdot PR \quad (4.8)$$

$$T_{10} = T_{wd1} - \Delta T_{des,out} = T_1 = T_{11} \quad (4.9)$$

$$P_{MP} = K \sqrt{P_{LP} \cdot P_{HP}} \quad \text{where} \quad K \geq 1 \quad (4.10)$$

$$\dot{m}_1 = \frac{\dot{m}_{tot}}{1 + CR} \quad (4.11)$$

$$h_2 - h_1 = \frac{h_{2,is} - h_1}{\eta_{is}} - \frac{\dot{Q}_{head,LP}}{\dot{m}_2} \quad \text{where} \quad \frac{\dot{Q}_{head,LP}}{\dot{m}_2} = 0.05 \cdot (h_2 - h_1) \quad (4.12)$$

4.1.4 Single-phase heat exchangers

The flow direction in the single-phase heat exchangers are counter-current. Capacitance rate \dot{C} is given in equation (4.13). EES does not provide the specific heat capacity c_p for the ammonia-water, hence it is predicted as $c_p = \Delta h / \Delta T$. The heat transfer for the solution heat exchangers are calculated from equation (4.14), (4.15) and (4.16) (Incropera et al., 2006).

$$\dot{C} = \dot{m} \cdot c_p \quad (4.13)$$

$$\varepsilon = \frac{\dot{Q}}{\dot{Q}_{max}} \quad (4.14)$$

$$\dot{Q}_{max} = \dot{C}_{min} \cdot (T_{H,in} - T_{C,in}) \quad (4.15)$$

$$\dot{Q} = \varepsilon \cdot \dot{C}_{min} \cdot (T_{H,in} - T_{C,in}) \quad (4.16)$$

4.1.5 Desorber and Absorber

Desorber Pinch points are set to occur at the inlet and outlet of the desorber. Minimum temperature difference ($\Delta T_{des,in} = \Delta T_{des,out}$) is set to 5 K. This means that the temperature glide of the ammonia-water mixture and the heat source will be equal and calculated according to equation (4.17) The heat source fluid mass flow rate will then be adjusted to the specified temperature glide the desorber, since no infeasible temperature profiles can occur inside that heat exchanger.

$$T_{10} - T_9 = T_{wd,1} - T_{wd,2} \quad (4.17)$$

Absorber In order to obtain feasible temperature profiles through the entire absorber, a minimum allowable temperature difference is specified between the heat sink fluid and ammonia-water mixture. The pinch point occurs somewhere inside the absorber, which makes it more difficult to predict the heat sink outlet temperature. Therefore, the absorber heat load is divided into 50 segments, where the energy balance calculation is made from equation 4.1 and employed at each segment. The heat sink mass flow rate is thus calculated from the requirement of minimum temperature difference through the entire absorber.

4.1.6 Solution Pump and Expansion Valve

Solution pump The pressure lift from the solution pump is assumed to be isentropic.

Expansion valve At the expansion valve outlet, the liquid is in thermodynamic equilibrium with the vapor created in the expansion process.

4.1.7 System Performance

COP, heating performances and required input power are found from equation (4.18) to (4.22).

$$COP = \frac{\dot{Q}_{abs} + \dot{Q}_{dsh}}{\dot{W}_{mot} + \dot{W}_{pump}} \quad (4.18)$$

$$\dot{Q}_{abs} = \dot{m}_{tot} \cdot \Delta h_{6-7} \quad (4.19)$$

$$\dot{Q}_{dsh} = \dot{m}_{vap} \cdot \Delta h_{4-5} \quad (4.20)$$

$$\dot{W}_{mot} = \frac{\dot{m}_{vap} \cdot (\Delta h_{2-1} + \Delta h_{4-3})}{\eta_{mot}} \quad (4.21)$$

$$\dot{W}_{pump} = \dot{m}_{liq} \cdot \Delta h_{12-11} \quad (4.22)$$

4.2 Absorber Model

4.2.1 General

The absorber model is adapted from the available compact heat exchanger library in EES and consists of 10 segments, where each segment are equally dimensioned. The heat exchangers are grouped in two categories as finned tube and plate-fin heat exchangers. Figure 4.2 shows the two heat exchanger categories, while figure 4.3 depicts how the segments are stacked. The output properties in one segment are the input properties in the next segment. Input and output are listed in table 4.2.

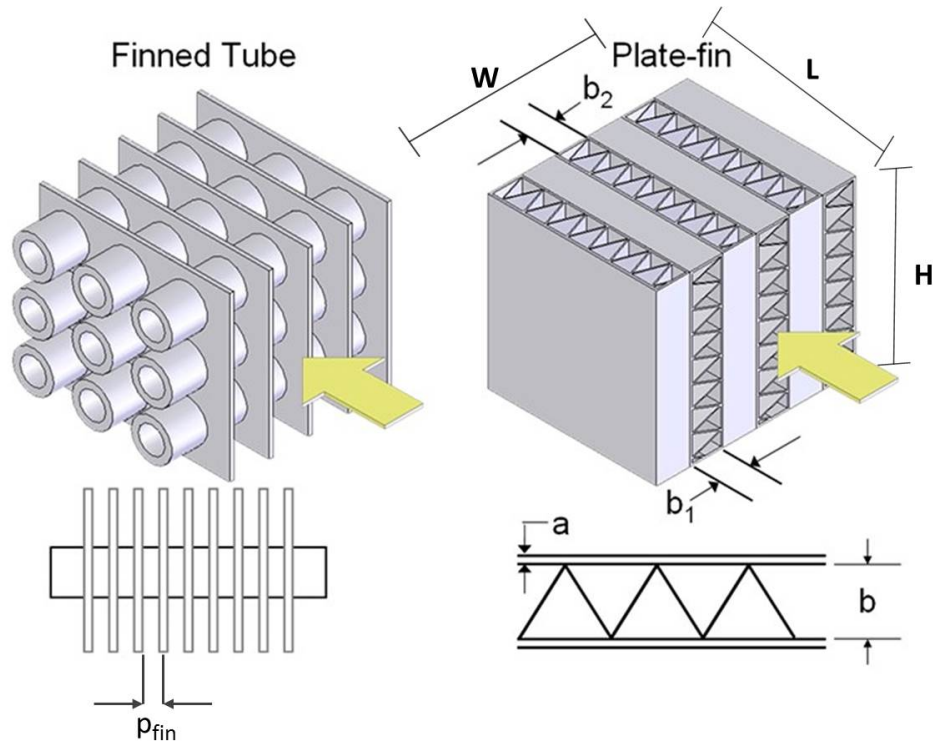


Figure 4.2: Schematic of a finned tube and plate-fin heat exchanger segment. The yellow arrows indicate the flow direction for air. H , L and W stand for height, length and width. The fin pitch is expressed as p_{fin} . The plate thickness is indicated by a , while b_1 and b_2 stand for air and mixture passage width, respectively (Klein, 2014).

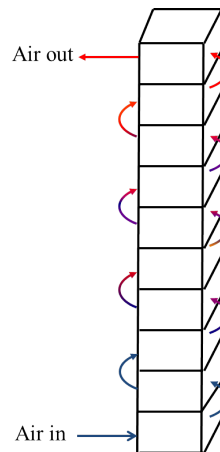


Figure 4.3: Segment and air flow arrangement.

Table 4.2: Absorber model inputs and outputs.

Inputs	Outputs
heat exchanger type	Heat exchanger properties
Mixture inlet properties	Mixture outlet properties
Air inlet properties	Air outlet properties
Absorber duty	Actual heat transferred

The simulation process is modelled as following:

1. Mixture and air inlet temperatures are set.
2. Mixture and air outlet temperatures are guessed.
3. In the initial iteration set, the temperature decrease for the mixture and increase for the air are equal for all 10 segments.
4. A new mixture and air temperature are mixture and air temperature are calculated in all 10 segments with the calculated properties.
5. Each iteration calculates the properties through all the 10 segments.
6. Heat transfer coefficients, actual heat transfer and temperature difference in all 10 segments are calculated using the mean temperature of the initial and calculated temperature in the previous iteration.
7. The simulation process executes 10 iterations, where the input temperature in each segment is the value of the input and calculated temperature in the previous segment.

The EES codes for the simulation process are given in Appendix E.

4.2.2 Heat exchanger functions

Cross-flow correction All the heat exchanger types are configured for cross-flow, such that a correction factor (F_{HX}) to calculate LMTD is required. The LMTD effectiveness (P_{HX}) and LMTD capacitance ratio (R_{HX}) are calculated according to equation (4.23) and (4.24). EES has a function that calculates F_{HX} by using P_{HX} , R_{HX} and flow type as inputs. The corrected LMTD is thus found from equation (4.25), where $\Delta T_{lm,cf}$ is the uncorrected LMTD for cross-flow (Nellis and Klein, 2009).

$$P_{HX} = \frac{T_{C,out} - T_{C,in}}{T_{H,in} - T_{C,in}} \quad (4.23)$$

$$R_{HX} = \frac{\dot{C}_C}{\dot{C}_H} = \frac{T_{H,in} - T_{H,out}}{T_{C,out} - T_{C,in}} \quad (4.24)$$

$$\Delta T_{lm} = F_{HX} \cdot \Delta T_{lm,cf} \quad (4.25)$$

Other functions EES has functions for calculating the heat exchanger geometry, air heat transfer coefficient and pressure drop. The heat exchanger types are given in the EES compact heat exchanger library. Input and output variables for geometry, air heat transfer coefficient and pressure drop are listed in table (4.3) to (4.5).

Table 4.3: Input and output data of the geometry EES HX function.

Inputs		Outputs	
Variable	Comment	Variable	Comment
HX type		D_o [m] **	The outside diamter of the tube
a [m] *	Plate thickness	fin_{pitch} [m^{-1}]	Number of fins per meter
b_2 [m] *	Thickness of passages through which the second fluid passes	D_h [m]	Hydraulic diameter
		fin_{thk} [m]	thickness of fins
		σ [-]	Minimum free flow area/frontal area
		(A/V) [m^2/m^3]	Heat transfer area/total volume
		$A_{fin}\backslash A$	Fin area/total area
		b_1 [m]	Thickness of the air flow passages

Table 4.4: Input and output data of the heat transfer coefficient EES HX function.

Inputs		Outputs	
Variable	Comment	Variable	Comment
HX type		α_{air} [$W/m^2 \cdot K$]	Heat transfer coefficient of air
a [m] *	Plate thickness		
b_2 [m] *	Thickness of passages through which the second fluid passes		
\dot{m} [kg/s]	Air mass flow rate in the HX		
A_{fr} [m^2]	Frontal area of the HX		
Fluid	Air for these simulations		
P [bar]	Inlet pressure		
T_{avg} [K]	Average temperature between air and mixture		

Table 4.5: Input and output data of the pressure drop EES HX function.

Inputs		Outputs	
Variable	Comment	Variable	Comment
HX type		ΔP [Pa]	Air pressure drop
a [m] *	Plate thickness		
b_2 [m] *	Thickness of passages through which the second fluid passes		
\dot{m} [kg/s]	Air mass flow rate in the HX		
A_{fr} [m ²]	Frontal area of the HX		
L [m]	Length of the HX in flow direction		
Fluid	Air for these simulations		
T_{in} [K]	Fluid inlet temperature		
T_{out} [K]	Fluid outlet temperature		
P [bar]	Inlet pressure		

* Applies only to plate-fin heat exchangers.

** Applies only to finned circular tubes.

4.2.3 Thermophysical properties

EES does not provide any calculation procedure for the ammonia-water viscosity or liquid mixture conductivity. Therefore, those calculations are made from the equations of Conde-Petit (2004). The calculation procedures are found in Appendix B.

4.2.4 Thermal resistance

Total thermal resistance and conductance The total thermal resistance and conductance are calculated according to equation (4.26) and (4.27). Fouling resistance is neglected from the total thermal resistance. The heat duty in equation (4.28) is used to correct the outlet temperatures for the mixture and the air in each segment.

$$R_{tot} = R_{in} + R_{cond} + R_{out} \quad (4.26)$$

$$UA = \frac{1}{R_{tot}} \quad (4.27)$$

$$\dot{Q} = UA \cdot \Delta T_{lm} \quad (4.28)$$

Thermal resistance between mixture and mixture-side surface The average mixture density (ρ_{avg}) changes along the absorber and depends on the vapor quality, saturated liquid density (ρ_{liq}) and the saturated vapor density (ρ_{vap}) at the given pressure and temperature. The calculation of (ρ_{avg}) is shown in equation (4.29). Assuming constant mixture mass flow rate, the mean ammonia-water (u_m) velocity is computed as in equation (4.30). In order to simplify the ammonia-water calculations, the other thermophysical properties are computed with the mixture liquid properties. Hence, the Reynolds number (Re_D), Prandtl number and the heat transfer coefficient (α_{mix})

are calculated using equation (4.31) to (4.33). Dittus - Boelter equation is applied for the heat transfer coefficient, which assumes constant conditions through each segment. Moreover, the thermal resistance between the mixture and the channel wall is computed according to equation(4.34) (Incropera et al., 2007).

$$\rho_{avg} = \rho_{liq} \cdot (1 - q) + \rho_{vap} \cdot q \quad (4.29)$$

$$u_m = \frac{4 \cdot \dot{m}}{\rho_{avg} \cdot \pi D_h^2} \quad (4.30)$$

$$Re_D = \frac{\rho_{liq} \cdot u_m \cdot D_h}{\mu_{liq}} \quad (4.31)$$

$$Pr = \frac{c_p \cdot \mu_{liq}}{\lambda_{liq}} \quad (4.32)$$

$$\alpha_{mix} = 0.023 \cdot Re_D^{0.8} \cdot Pr^{0.4} \cdot \frac{\lambda_{liq}}{D_h} \quad (4.33)$$

$$R_{in} = \frac{1}{\alpha_{mix} \cdot \pi \cdot D_h \cdot L} \quad (4.34)$$

Thermal resistance between air and air-side surface Total heat transfer area (A_{tot}) and air heat transfer coefficient (α_{air}) are found from the EES functions for geometry and heat transfer coefficient explained in chapter 4.2.2. The overall surface efficiency ($\eta_{sur,overall}$) calculations are given in chapter 4.2.5. Hence, the thermal resistance between the air and air-side surface (R_{out}) is calculated in equation (4.35).

$$R_{out} = \frac{1}{\eta_{sur,overall} \cdot \alpha_{air} \cdot A_{tot}} \quad (4.35)$$

Conduction resistance in the mixture channel wall The two types of heat exchangers have different calculation methods for the conduction resistance. Equation (4.36) is used for thre finned tube heat exchanger, while equation (4.37) calculates the plate-fin type conduction resistance. λ_{mat} is the conductivity found from an EES function, based on the heat exchanger material and average mixture temperature. The conduction area which applies for the plate-fin heat exchangers is approximated according to equation (4.38), where $N_{ch,mix}$ represents the number of mixture channels per segment.

$$R_{cond,ft} = \frac{\ln\left(\frac{D_{out}}{D_h}\right)}{2 \cdot \lambda_{mat} \cdot \pi \cdot L_{tube}} \quad (4.36)$$

$$R_{cond,pf} = \frac{th_{plate}}{\lambda_{mat} \cdot A_{cond}} \quad (4.37)$$

$$A_{cond} = 2 \cdot H \cdot L \cdot (N_{ch,mix} - 1) \quad (4.38)$$

4.2.5 Fin efficiency

An annular fin approach was used to estimate the fin efficiency (η_{fin}) the fin efficiency for the finned tube heat exchangers. In order to estimate the plate-fin heat exchangers fin efficiency a straight-base rectangular fin approach was used. The two approaches are calculated from functions in EES. Figure 4.4 depict the two fin efficiency approaches. The EES annular rectangular fin function requires the effective radius ($r_{effective}$), in order to calculate the fin efficiency. $r_{effective}$ is calculated according to equation (4.39). Moreover, the straight-base fin efficiency function is calculated with L_{fin} . For simplifications, L_{fin} is calculated according to equation (4.40). The overall surface efficiency is given in equation (4.41), where $(A_{fin} \setminus A)$ is found from the EES geometry function (Nellis and Klein, 2009).

$$r_{effective} = \sqrt{\frac{A_{s,fin,tot} \cdot p_{fin}}{2 \cdot \pi \cdot L_{tube}} + \frac{D_{out}^2}{4}} \quad (4.39)$$

$$L_{fin} \approx 2 \cdot b_1 \quad (4.40)$$

$$\eta_{sur,overall} = 1 - (A_{fin} \setminus A) \cdot (1 - \eta_{fin}) \quad (4.41)$$

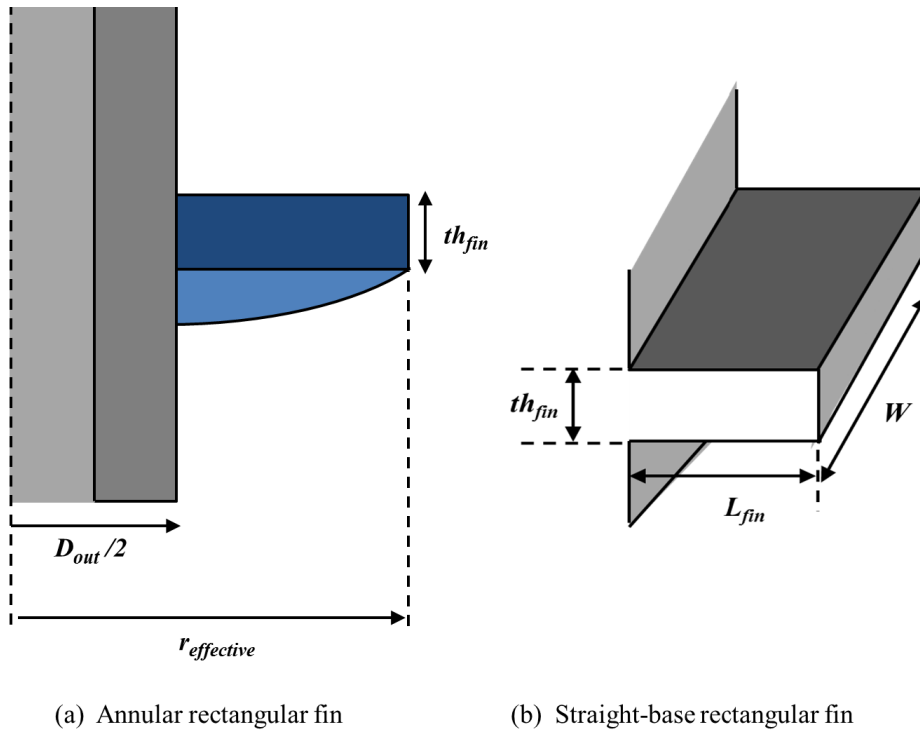


Figure 4.4: Fin efficiency approaches.

5 Simulation Results

5.1 Two-stage CAHP

The main objectives of the two-stage compression-absorption heat pump simulations are to obtain maximum allowable supply temperatures at different limitations of maximum allowable compressor discharge temperatures. In order to achieve this goal, optimal levels for intermediate and high pressure, circulation ratio and the suitability of the desuperheater are evaluated. Inlet heat sink and source temperatures are set to 50°C for all the simulations. The maximum allowable compressor discharge temperature is the limiting factor for high supply temperatures. Therefore, the simulations are carried out in four scenario with maximum allowable discharge temperatures of 150, 175, 200 and 250°C. The low pressure level is set to 2.6 bar, which corresponds to a water content of approximately 2% in the compressor vapor. This pressure level is fixed in all the simulations, in order to reduce the degrees of freedom and optimization variables. The suitability of the desuperheater in the cycle is tested by comparing the simulations at optimal operating conditions with and without the latter heat exchanger. Two different approaches were used for the desuperheater. In method #1, the vapor was cooled down to the weak solution temperature and down to saturated vapor by approach #2. Results presented for each scenario are the best according to the optimization, while several other results are also given in Appendix A.

Table 5.1: Parameters used for all scenario.

Parameter	Value
Q_{sink} heat sink duty [kW]	100
η_{motor} compressor motor [-]	0.9
$\epsilon_{IH\#1}$ thermal efficiency IHX#1 [-]	0.8
$\epsilon_{IH\#2}$ thermal efficiency IHX#2 [-]	0.75
$T_{sink,in}$ inlet heat sink temperature [°C]	50
$T_{source,in}$ inlet heat source temperature [°C]	50
P_{LP} Desorber pressure [bar]	2.6

5.1.1 Simulation Scenario

5.1.1.1 Discharge temperature limitation of 150°C

A maximum allowable compressor discharge temperature of 150°C resulted in an optimal circulation ratio of 1.2, which corresponds to a strong ammonia concentration of 64 weight-%. The high pressure level was then simulated at 17 bar. Consequently, the optimal intermediate pressure was found at 7.71 bar with a corresponding K-factor of 1.16, plus a high and low pressure ratio of 2.2 and 2.97, respectively. Moreover, the relation between the K-factor and the discharge compressor temperature for the high and low compressor stage are depicted in figure 5.1. The mixture was cooled down from 109.5 to 65.5°C, while the heat sink water was heated to 103.3°C, when the desuperheater was decoupled. On the other hand, the heat sink water was heated to 103°C, for both of the approaches for the desuperheater. Figure 5.2 shows the temperature curves for the mixture and the heat sink, both with and without the desuperheater. The simulation yielded a COP of 3.85.

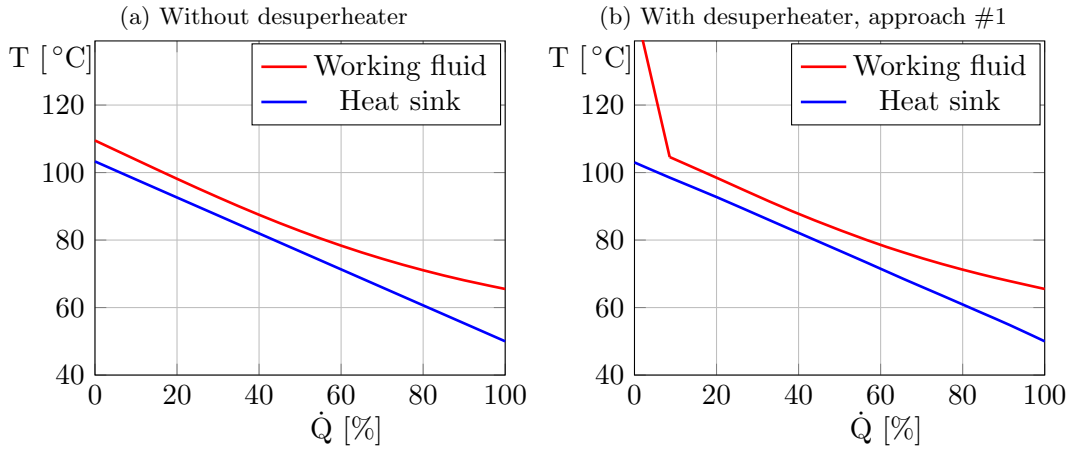


Figure 5.1: Temperature versus the cumulative heat load in the heat sink with an circulation ratio of 1.2 and a high pressure level of 17 bar.

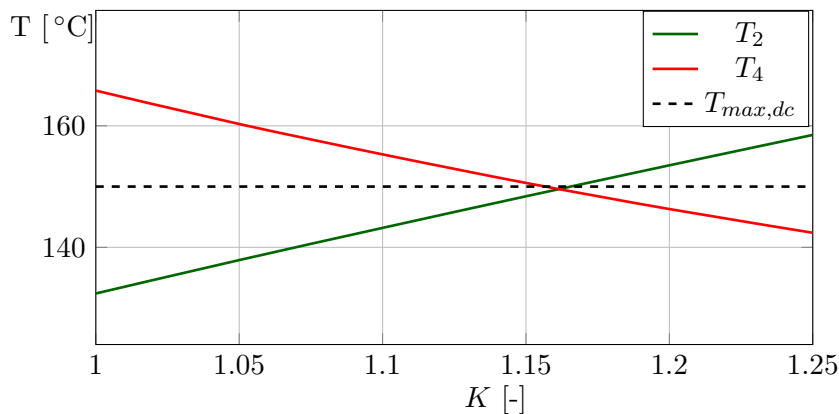


Figure 5.2: Discharge temperatures for the low and high pressure compressor stage as a function of the K-factor. The curves are represented at a circulation ratio of 1.2 and a high pressure stage at 17 bar. When both of the curves are below the dotted line, the cycle is within the limit of maximum discharge pressure for the given conditions.

5.1.1.2 Discharge temperature limitation of 175°C

A maximum allowable compressor discharge temperature of 175°C resulted in an optimal circulation ratio of 0.9, which corresponds to a strong ammonia concentration of 68 weight-%. The high pressure level was then simulated at 22.5 bar. Consequently, the optimal intermediate pressure was found at 9.41 bar with a corresponding K-factor of 1.23, plus a high and low pressure ratio of 2.39 and 3.62, respectively. Moreover, the relation between the K-factor and the discharge compressor temperature for the high and low compressor stage are depicted in figure 5.3. The mixture was cooled down from 124.5 to 72.6°C, while the heat sink water was heated to 119.5°C, when the desuperheater was decoupled. On the other hand, the use of desuperheater cooling approach #1 and #2 yielded supply temperatures of 119.7 and 119.8°C, respectively. Figure 5.4 shows the temperature curves for the mixture and the heat sink, both with and without the desuperheater. The simulation yielded a COP of 3.20.

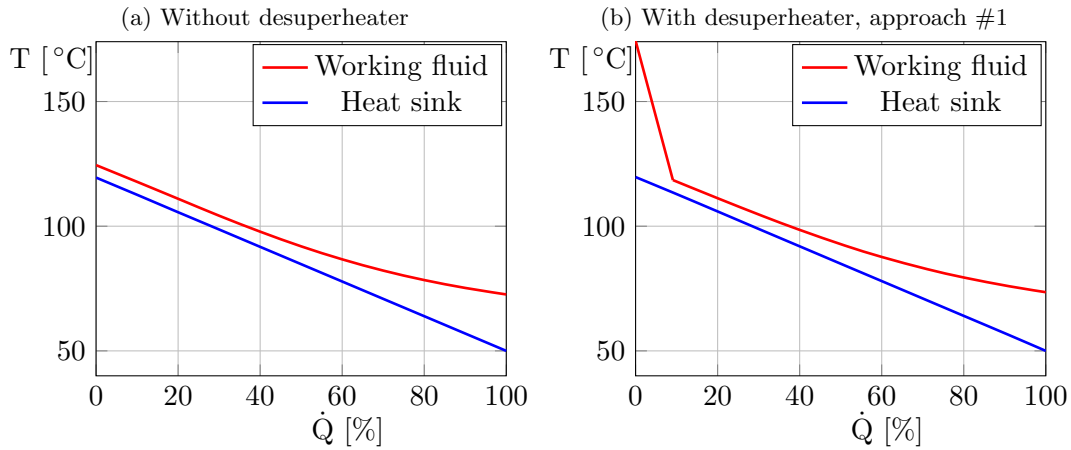


Figure 5.3: Temperature versus the cumulative heat load in the heat sink with an circulation ratio of 0.9 and a high pressure level of 22.5 bar.

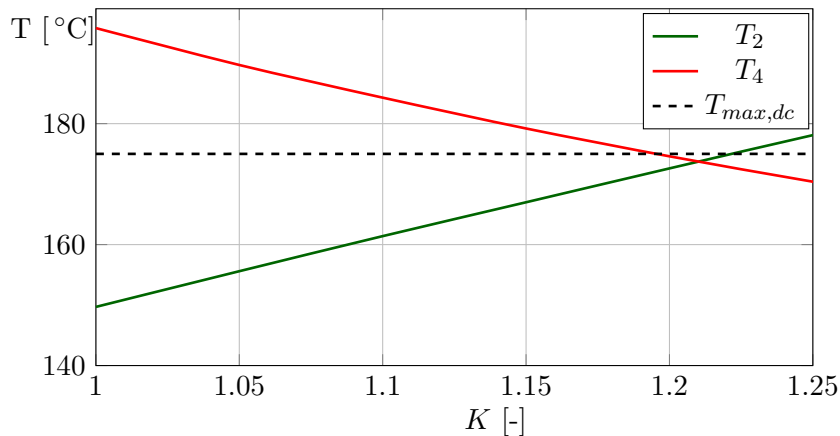


Figure 5.4: Discharge temperatures for the low and high pressure compressor stage as a function of the K-factor. The curves are represented at a circulation ratio of 0.9 and a high pressure stage at 22.5 bar. When both of the curves are below the dotted line, the cycle is within the limit of maximum discharge pressure for the given conditions.

5.1.1.3 Discharge temperature limitation of 200°C

A maximum allowable compressor discharge temperature of 200°C resulted in an optimal circulation ratio of 0.5, which corresponds to a strong ammonia concentration of 77 weight-%. The high pressure level was then simulated at 30.5 bar. Consequently, the optimal intermediate pressure was found at 11.22 bar with a corresponding K-factor of 1.26, plus a high and low pressure ratio of 2.72 and 4.32, respectively. Moreover, the relation between the K-factor and the discharge compressor temperature for the high and low compressor stage are depicted in figure 5.5. The mixture was cooled down from 144.6 to 78.7°C, while the heat sink water was heated to 136.4°C, when the desuperheater was decoupled. On the other hand, the heat sink water was heated to 136.8°C, for both of the approaches for the desuperheater. Figure 5.6 shows the temperature curves for the mixture and the heat sink, both with and without the desuperheater. The simulation yielded a COP of 2.66.

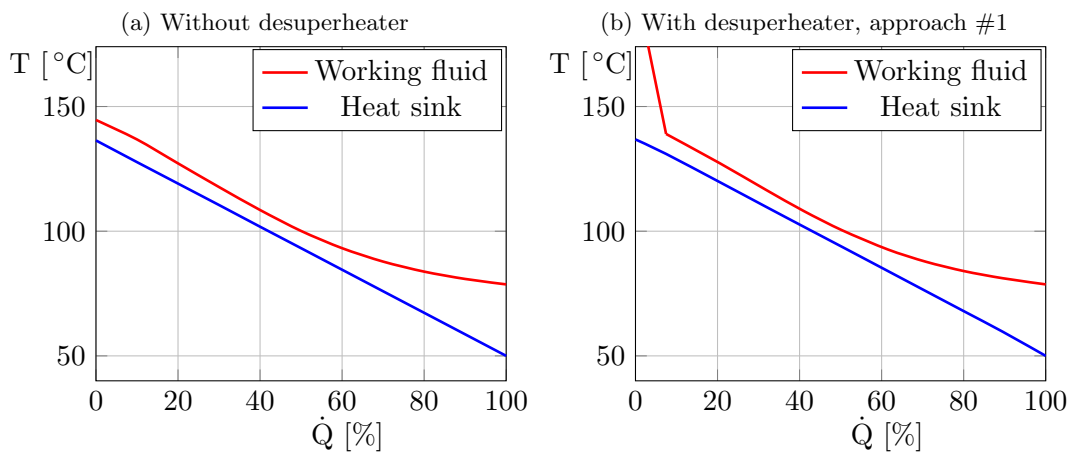


Figure 5.5: Temperature versus the cumulative heat load in the heat sink with an circulation ratio of 0.5 and a high pressure level of 30.5 bar.

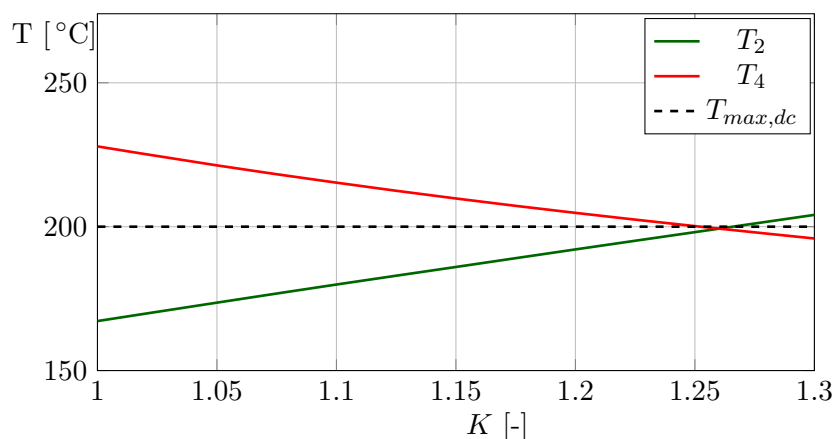


Figure 5.6: Discharge temperatures for the low and high pressure compressor stage as a function of the K-factor. The curves are represented at a circulation ratio of 0.5 and a high pressure stage at 30.5 bar. When both of the curves are below the dotted line, the cycle is within the limit of maximum discharge pressure for the given conditions.

5.1.1.4 Discharge temperature limitation of 250°C

A maximum allowable compressor discharge temperature of 250°C resulted in an optimal circulation ratio of 0.2, which corresponds to a strong ammonia concentration of 88 weight-%. The high pressure level was then simulated at 47.5 bar. Consequently, the optimal intermediate pressure was found at 15.0 bar with a corresponding K-factor of 1.35, plus a high and low pressure ratio of 3.17 and 5.77, respectively. Moreover, the relation between the K-factor and the discharge compressor temperature for the high and low compressor stage are depicted in figure 5.7. The mixture was cooled down from 213.2 to 93.4°C, while the heat sink water was heated to 169.1°C, when the desuperheater was decoupled. On the other hand, the use of desuperheater cooling approach #1 and #2 yielded supply temperatures of 169.6 and 171.8°C, respectively. Figure 5.8 shows the temperature curves for the mixture and the heat sink, both with and without the desuperheater. The simulation yielded a COP of 2.08.

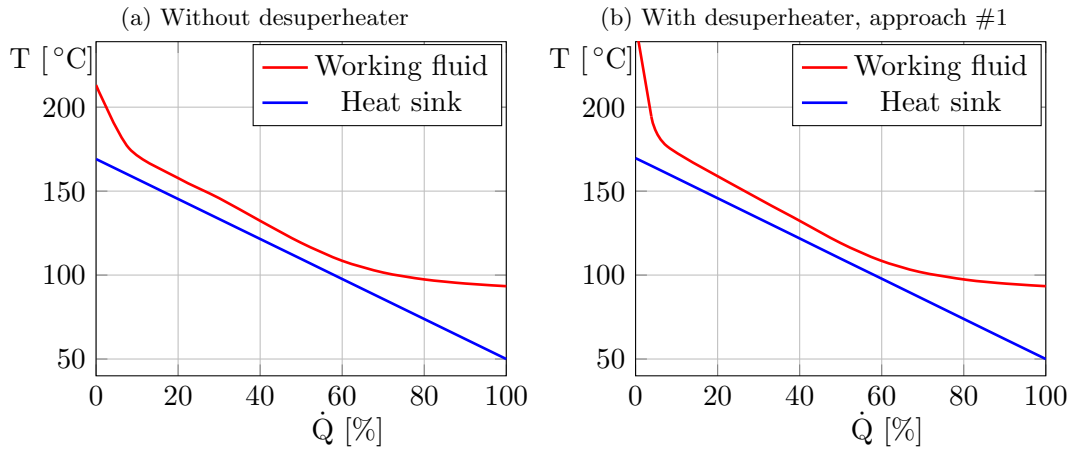


Figure 5.7: Temperature versus the cumulative heat load in the heat sink with an circulation ratio of 0.2 and a high pressure level of 47.5 bar.

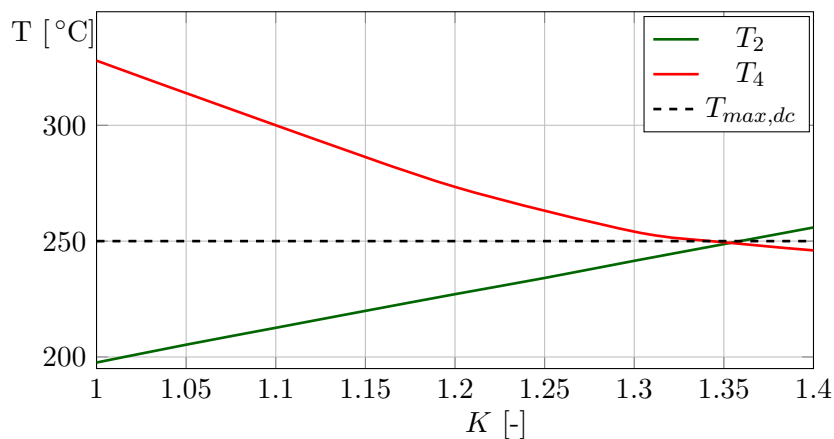


Figure 5.8: Discharge temperatures for the low and high pressure compressor stage as a function of the K-factor. The curves are represented at a circulation ratio of 0.5 and a high pressure stage at 30.5 bar. When both of the curves are below the dotted line, the cycle is within the limit of maximum discharge pressure for the given conditions.

5.1.1.5 COP vs K-factor

Figure 5.9 shows the relation between COP and the K-factor under the given operating conditions for the scenario described in 5.1.1.1-5.1.1.4. For scenario three first scenario, the difference in COP between a K-factor of 1 and the K-factor at maximum COP varied from 0.16-0.26%. On the other hand, for the fourth scenario, that difference in COP was 2.5%, where a K-factor of K equals a COP of 2.045, while maximum COP of 2.096 corresponds to a K-factor of 1.23. In order to stay within the limits of maximum discharge temperature, the K-factor could not be determined by maximum COP for the respective scenario.

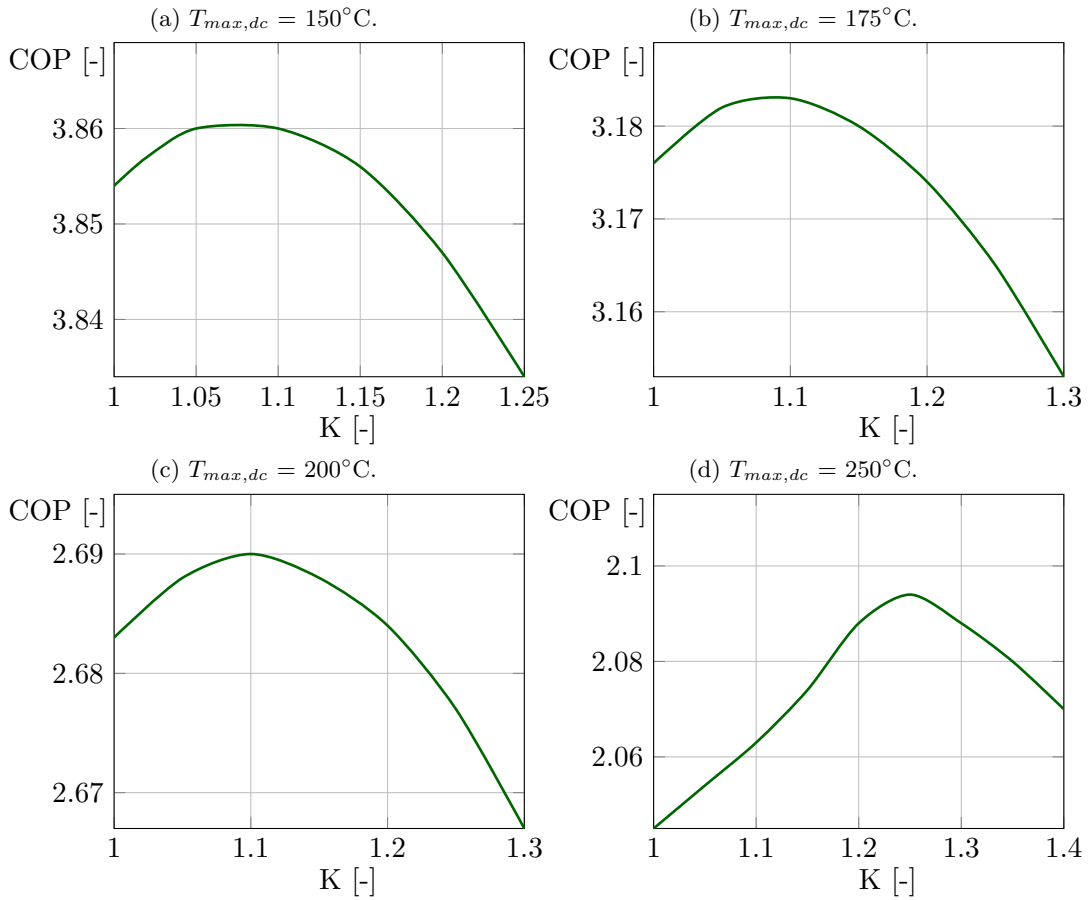


Figure 5.9: COP versus the K-factor at the given operating conditions for the four scenario in chapter 5.1.1.1-5.1.1.4.

5.1.2 Summary and Discussion

Comparing the scenario In order to summarize the simulations listed in table A.1 to A.4, increasing the maximum allowable discharge temperature from 150 to 250°C gave the following results:

- Increasing absorber pressure
- Increasing K-factor
- Increasing supply temperatures

- Increasing required compressor volume at the low pressure stage
- Decreasing required compressor volume the the high pressure stage
- Decreasing COP
- Decreasing circulation ratio
- Decreasing compressor efficiencies
- Approximately unchanged vapor mass flow rate, but decreasing total mixture mass flow rate
- Approximately no increase for the supply temperature by the use of desuperheater

Optimizing the scenario In order to achieve maximum supply temperature, the absorber pressure, circulation ratio and the K-factor were optimized for each scenario. By making these variables deviate from the optimum results, the outcomes would either end with a lower supply temperature or exceed the maximum allowable discharge temperature. Simulation #22 and #24 are examples where the maximum allowable discharge temperatures are exceeded as a consequence of too high absorber pressure and low circulation ratio.

K-factor Elevating K-factor decreased the low pressure stage discharge temperature, simultaneously as it reduced the high pressure discharge temperature, due to higher intermediate pressure. The difference in COP did not substantially vary. According to figure 5.9, the variation in COP were near to 0% for the three first scenario, while the simulations showed a difference of 2.5% from maximum COP at a K-factor of 1.23, compared to a K-factor of 1.0. However, with that small variations in COP at alternating K-factor, there is not recommended to determine the K-factor at maximum coefficient of performance. The K-factor should be determined in order to adjust the discharge temperature when other variables are already set. Figure 5.2, 5.4, 5.6 and 5.8 depict the allowable K-factor when the lower and higher pressure levels, plus the circulation ratio are known. The figures show that the discharge temperature will exceed the maximum allowable temperature at either the lower or higher compressor stage. A decrease in the absorber pressure could allow a wider range of the K-factor for each scenario, synchronously as the supply temperature would become lower.

Mass flow rates The total mixture mass flow rate is determined by the heat sink duty of 100 kW and the mixture enthalpy difference, hence the mixture mass flow rate became smaller at higher supply temperatures. At the maximum the mixture mass flow rate was simulated to 0.131 kg/s, which was almost twice as the minimum of 0.069 kg/s. Moreover, the vapor mass flow rate was almost constant during the simulations according to equation (4.11). In addition, also the heat sink and source mass flow rate decreased at increasing supply temperatures. As the heat sink mass flow rate is determined by the 5 K minimum temperature difference and the fixed heat duty, resulted in the decreased mass flow rate during from scenario #1 to #4.

Compressor volume Equal heat sink duty and equal inlet pressure at the low pressure inlet contributed to approximately unchanged vapor mass flow rate for all the scenario.

Unchanged specific volume at the lower compressor stage yielded constant theoretic compressor volume at that stage. However, the volumetric efficiency resulted in a variation of the required swept volume from 154 m³/h in scenario #1 to 203 m³/h in scenario #4 at the low pressure stage. At the higher compressor stage, the specific volume decreased at increasing pressure. Therefore, the increasing intermediate pressure entailed a lower required swept volume. An intermediate pressure at 15 bar required a swept volume of 42 m³/h at the high pressure stage, compared to a P_{MP} of 7.71 bar and a required swept volume of 55 m³/h.

Desuperheater As earlier noted, two different methods were used when the vapor was cooled in the desuperheater. Cooling method #1 where the vapor was cooled down to weak solution temperature, while cooling method #2 was cooled to saturated vapor. Both of the methods gave the same supply temperature for the first three scenario. The supply temperatures were approximately the same as the simulations without the use of desuperheater. In the scenario with lower discharge temperature limitations, both of the methods resulted in almost the same heat duty. Both of the methods yielded the same supply temperature in scenario #3, even if the difference between the desuperheater heat duty for the two methods was large. However, there was a difference in the cooling methods for scenario #4, where the supply temperatures were simulated to 169.6 and 171.8°C for method #1 and #2, respectively. The heat duty of the desuperheaters were then found at 3.9 kW for method #1 and 23.3 kW for method #2. Hence, the supply temperature increased if the desuperheater performed a significant heat duty. In comparison, the largest supply temperature without desuperheater was computed to 169.1°C.

Absorber pressure At increasing P_{HP} , the heat sink outlet temperatures increased as well. The optimum circulation ratio decreased at elevated absorber pressures. This can be explained from the decreasing mixture mass flow rate and the nearly constant vapor mass flow rate. Since the vapor mass flow rate remains approximately constant, the liquid mixture flow rate decreases simultaneously with the total mass flow rate, hence a decrease in the optimum CR. The required compressor input power increases at higher absorber pressures for two reasons. First reason is due increased compressor work at higher pressure lifts. The other reason is caused by decreasing isentropic efficiency at elevating pressure ratio. At a P_{HP} of 17 bar the mean isentropic efficiency for the two compressor stages is 0.80, compared to 0.72 at an absorber pressure of 47.5. As mentioned in foregoing paragraphs, an absorber pressure elevation entails increasing optimum K-factor and decreasing COP.

5.2 The Absorbers

The main objective of the absorber simulations is to find the best suited heat exchanger in order to obtain minimum absorber length and minimize the required fan power. The process comprises a cross-flow absorber heating air from 90°C to a guessed temperature of 125 °C, while cooling ammonia-water from 150°C to a guessed temperature of 100°C. Guessed absorber duty is to 50 kW. Five different compact heat exchangers from the EES heat exchanger library comprise the simulation scenario for the absorbers. Geometry for the heat exchangers are constrained by the EES library constraints, which are given

in Appendix C. The heat exchanger types in the simulations are a finned circular tube, finned flat tube, louvered plate-fin, wavy plate-fin and plain plate-fin. The heat exchanger type and EES model name are listed in table 5.3. According to figure 4.2, the width and length are equal for all the heat exchanger simulations. In order to obtain complete absorption and feasible outlet temperatures, the average air velocity and absorber length are adapted to each heat exchanger.

Table 5.2: Parameters used for all absorbers.

Parameter	Value
Q_{abs} absorber duty [kW]	50
P_{HP} absorber pressure [bar]	25
$T_{mix,in}$ mixture inlet temperature [°C]	150
$T_{air,in}$ air inlet temperature [°C]	90
ZZ overall mixture ammonia concentration [-]	0.5238
\dot{m}_{mix} mixture mass flow rate [kg/s]	0.0639
a plate thickness [m]*	0.003
b_2 mixture channel width [m]*	$b_1/4$
L length of segment [m]	0.1
W width of segment [m]	0.8
Material	Stainless steel AISI304

* Applies only for plate-fin heat exchangers.

Table 5.3: Parameters used for all absorbers.

HX number	HX type	Model name
# 1	Finned circular tube	s8.0-3/8T
# 2	Finned flat tube	s9.68-087
# 3	Louvered plate-fin	s38-606
# 4	Wavy plate-fin	s1144-38W
# 5	Plain plate-fin	s1027T

5.2.1 Simulation Results

Table 5.4 shows some important parameters from the simulation result for comparing the five heat exchangers. Geometric parameters as hydraulic diameter and fin pitch are constrained by the EES library design constraints.

Table 5.4: Simulations results for comparing the different heat exchanger types.

HX number	#1	#2	#3	#4	#5
Minimum free flow area/frontal area [-]	0.534	0.697	0.426	0.511	0.541
Minimum free flow area/frontal area [-]	0.913	0.795	0.640	0.847	0.863
Heat transfer area/ total volume [m^2/m^3]	587	751	383	632	565
Total heat transfer area [m^2]	9.4	14.4	5.5	8.1	19.0
Conduction area [m^2]	-	-	1.05	1.28	2.77
Frontal free area [m^2]	0.085	0.134	0.061	0.065	0.182
Hydraulic diameter [m]	0.0062	0.0036	0.0045	0.0032	0.0038
Total absorber height [m]	2.0	2.5	1.8	1.6	4.2
Fin pitch per meter [m^{-1}]	315	381	239	450	404
Pressure drop [kPa]	4.28	1.56	35.8	41.4	1.32
Required fan power input [kW]	14.6	8.7	140	162	5.3
Mean air velocity [m/s]	10	10	16	15	5.5
Mean mixture velocity [m/s]	0.093	0.105	0.421	1.09	0.928
Avg mixture heat transfer coefficient [$W/m^2 \cdot K$]	1017	1129	3479	8065	6877
Avg air heat transfer coefficient [$W/m^2 \cdot K$]	155	71.0	335	402	71.4
Mixture mass flow rate per channel/tube [kg/s]	0.00051	0.00059	0.0011	0.0016	0.0019
Air mass flow rate [kg/s]	0.794	1.30	0.91	0.90	0.93
Air/mixture mass flow rate ratio [-]	12.4	20.3	14.3	14.0	14.5
Mixture outlet temperature [$^{\circ}C$]	107.2	93.9	91.3	94.7	91.3
Air outlet temperature [$^{\circ}C$]	142.5	131.4	147.8	146.7	146.7
R_{cond} [K/W]	$1.9 \cdot 10^{-4}$	$1.9 \cdot 10^{-4}$	$1.7 \cdot 10^{-4}$	$1.4 \cdot 10^{-4}$	$6.6 \cdot 10^{-5}$
R_{in} [K/W]	$2.0 \cdot 10^{-3}$	$1.8 \cdot 10^{-3}$	$2.0 \cdot 10^{-3}$	$1.9 \cdot 10^{-3}$	$8.5 \cdot 10^{-4}$
R_{out} [K/W]	$1.8 \cdot 10^{-3}$	$1.2 \cdot 10^{-3}$	$1.2 \cdot 10^{-3}$	$1.4 \cdot 10^{-3}$	$2.4 \cdot 10^{-3}$
R_{tot} [K/W]	$4.0 \cdot 10^{-3}$	$3.1 \cdot 10^{-3}$	$3.4 \cdot 10^{-3}$	$3.4 \cdot 10^{-3}$	$3.3 \cdot 10^{-3}$
Number of mixture channels [-]	-	-	57	41	34
Number of tubes [-]	124	108	-	-	-

5.2.2 Summary and Discussion

According to the simulations, there was a large difference between the air and mixture mass flow rate, due to a corresponding difference in the specific heat capacity. The air mass flow rate demand was between 12 to 20 times higher than the mixture mass flow rate. There were only small variations in the total thermal resistance from $3.33 - 4.03 \cdot 10^{-3}$ K/W. The large pressure drops and required fan power input for some of the heat exchangers up to 162 kW are very special for the simulations. The results from the simulations and comparison of the five absorbers can be summarized as:

- There was a trade-off between required fan power and absorber height.
- Required fan power had a large influence on the process performance.

- The difference between air and mixture mass flow rate was large.
- The heat exchangers were sensitive to the relation between absorber and air mass flow rate to make a feasible heat exchange.
- Finned flat tube heat exchanger was the most preferable.

The heat exchange between the mixture and air was very sensitive to absorber height and the air mass flow rate. If the absorber height was too large, the mixture becomes subcooled and the mixture outlet temperature would be lower than the inlet air temperature and thus infeasible heat exchange. In addition, the heat exchange depended on a certain air mass flow rate, which required a high mean air velocity. This is why some of the heat exchangers required a high mean air velocity.

The finned tube heat exchangers had a large number of tubes, resulting in a lower mixture heat transfer coefficient, compared to the plate-fin heat exchangers. A smaller frontal area (A_{fr}) provides a smaller air heat transfer coefficient for type #2 than #1. The pressure drop for type #2 was significantly lower than for the circular finned tube heat type. The flat finned heat exchanger also had a lower outer thermal resistance, due to higher heat transfer area and smaller air heat transfer coefficient. An advantage of using type #1 was the short absorber height, but still the flat finned tube heat exchanger had a substantially lower required fan power which made it preferable over the circular finned tube heat exchanger.

Compared to the finned tube heat exchanger, the plate-fin heat exchangers had smaller numbers of mixture channels, which lead to higher mixture heat transfer coefficients. Minimum free flow area - frontal area ratio (σ) were low for heat exchanger #3 and #4, which entail the large air velocity demand. The large air velocity also resulted in substantially high required fan power input and pressure drops. As earlier noted, the high values of required fan power was caused by the sensitivity of fluctuations in the absorber height and air mass flow rate. A required fan power of 140 and 162 kW was three times the absorber heat duty and exclude the usefulness of those heat exchanger types. On the other hand, the plain plate-fin was promising with respect to a required fan power of 5,3 kW. A disadvantage of type #5 is the large absorber height. A little decrease in the absorber height entailed a large increase for the mean air velocity and the fan power input.

The high mean air velocity for some of the heat exchangers were not fully realistic. One reason might be an error in the simulation model. Moreover, the ratio between the absorber width and length is very high in order to reduce the pressure drop. However, there are methods that could reduce the air velocity without changing the frontal area. First, by increasing the tube spacing for the finned tube heat exchangers and the channel opening the plate-fin types. This will increase the free frontal area, reduce the air velocity and keep the air mass flow rate unchanged. As earlier noted, the functions for the EES are constrained to the in-built geometry and changing that for each heat exchanger requires a more complex setup. Second method, reduce the air inlet temperature. That reduces the air mass flow rate, but simultaneously increases the absorber temperature losses. Considering the large required fan power, reducing the air inlet temperature could still be a better alternative.

Finned flat tube heat exchangers would be more interesting to investigate for future work, due to its beneficial characteristics of absorber height and pressure drop. A more accurate approach for the conduction resistance and fin efficiency could be more favourable, since

it was based on circular tubes and not flat tubes in model. The heat exchanger could be modelled with other dimensions, in order to reduce the air velocity.

6 Conclusion and Suggestions for Further Work

6.1 Conclusion

The main results from the two-stage CAHP simulations are:

- A maximum discharge temperature of 150°C resulted in a COP of 3.85, absorber pressure at 17 bar, supply temperature of 103.3°C and a K-factor of 1.16. At a maximum discharge temperature of 250°C resulted in a COP of 2.08, absorber pressure of 47.5 bar, supply temperature of 171.8°C and a K-factor of 1.35.
- The K-factor increases at elevating absorber pressure and has negligible impact on the COP within the relevant simulation range. Optimum K-factor was found at 1.16 and 1.35 at absorber pressures of 17 and 47.5 bar, respectively.
- At a heat sink duty of 100 kW, the mixture mass flow rate varied from 0.131 to 0.069 kg/s with an almost constant vapor mass flow rate. The mixture mass flow rate, plus the heat sink and heat source mass flow rate decreased at increasing supply temperature.
- The volumetric efficiency entailed higher swept compressor volume at increasing pressure ratio at the low pressure stage. On the other hand, the swept volume at the high pressure stage decreased at increasing pressure, due to a decreasing specific volume of the compressor inlet gas.
- Cooling the discharge gas down to saturated vapor yielded a slightly higher supply temperature than cooling down to the weak solution temperature by the use of a desuperheater. The supply temperatures with the use of a desuperheater were approximately the same as the supply temperatures without the desuperheater.
- Increasing P_{HP} resulted in increasing supply temperatures. The optimum circulation ratio decreased at elevated absorber pressures, due to a decrease in the mixture mass flow rate and the nearly constant vapor mass flow rate. Elevated absorber pressure resulted in decreased COP.

The main results from the absorber simulations are:

- There was a large difference between the air and mixture mass flow rate, due to a corresponding difference in the specific capacity. The simulations resulted in an air mass flow rate between 12 to 20 higher than the mixture mass flow rate.
- The heat exchange between the air and the mixture was very sensitive to the absorber height and the air mass flow rate. A too large absorber height could cause subcooled mixture outlet temperatures below the air inlet temperature and thus infeasible heat exchange.
- Required fan power input had a large impact on the process. Large demands for air velocity resulted in large pressure drop and required fan power input, due to the sensitivity to the absorber height and the air mass flow rate. It is difficult to determine if the high air mass flow rates are real or if there are any errors in the simulation model.
- Finned flat tube heat exchangers was found to be the most preferable type of the simulated heat exchangers, due to its low pressure drops and absorber height. An

absorber duty of 50 kW yielded an absorber height of 2.5 m and a required fan power input of 8.7 kW.

6.2 Suggestions for Further Work

Based on the work carried out in this thesis, the following aspects are suggested to be investigated in future work:

- If there are requirements for simultaneously heat and cooling, optimization for temperature lifts could be favourable in the two-stage model.
- Investigate the conditions with other sink and source inlet temperatures in the two-stage model.
- Develop models for the internal heat exchangers in the two-stage model.
- Investigation of the flat finned tube heat exchanger modelled with other dimensions in the absorber model.
- More accurate approach of the conduction resistance and the fin efficiency for the flat tube heat exchanger in the absorber model.
- An absorber model with lower air inlet temperatures.

References

- Alefeld, G. and Radermacher, R. (1993) *Heat Conversion Systems*. Boca Raton, Florida: CRC Press
- Atkins, P. and de Paula, J. (2006) *Physical Chemistry*. 8th edition. Oxford: University Press.
- Austin, B. T and Sumathy, K. (2011) "Transcritical carbon dioxide heat pump systems: A review", *Renewable and Sustainable Energy Reviews*, vol.15, pp. 4013-4029.
- Brunin et al. (1997) "Comparison of the working domains of some compression heat pumps and a compression-absorption heat pump", *International journal of refrigeration*, vol. 20, no. 5, pp.308-318.
- Bolaji, B.O. and Huan, Z. (2013) "Ozone depletion and global warming: Case for the use of natural - a review", *Renewable and Sustainable Energy Reviews*, vol. 18, pp.49-54.
- Calm, J.M. (2008) "The next generation of refrigerants- Historical review, considerations, and outlook", *International journal of refrigeration*, vol.31, pp.1123-1133.
- Cerezo et al. (2010) "Comparison of numerical and experimental performance criteria of an ammoniawater bubble absorber using plate heat exchangers", *International Journal of Heat and Mass Transfer* 53, vol.31, pp.1123-1133.
- Chan, C.W., Ling-Chin, J. and Roskilly, A.P. (2013) "Reprint of: A review of chemical heat pumps, thermodynamic cycles and thermal energy storage technologies for low grade heat utilization", *Applied thermal Engineering*, vol.53, issue 2, pp.160-176.
- Chua et al. (2010) "Advances in heat pump systems: A review", *Applied thermal Engineering*, vol.87, pp. 3611-3624.
- Conde-Petit, D.M.R. (2004) "Thermophysical properties of $NH_3 + H_2O$ solution for the industrial design of absorption refrigeration equipment". Zürich: M. Conde Engineering
- Fernández-Seara et al. (2005) "Ammonia-water absorption in vertical tubular absorbers" *International Journal of Thermal Sciences*, vol. 44, pp.277-288.
- Fernández-Seara et al. (2007) "Analysis of an air cooled ammonia-water vertical tubular absorber" *International Journal of Thermal Sciences*, vol. 46, pp.93-103.
- Hultén, M. and Berntsson, T. (1999) "The compression/absorption cycle - influence of some major parameters on COP and a comparison with the compression cycle", *International Journal of Refrigeration*, vol. 22, pp.91-106.
- Hultén, M. and Berntsson, T. (2002) "The compression/absorption cycle - conceptual design improvements and comparisons with the compression cycle", *International Journal of Refrigeration*, vol. 25, pp.487-497.
- Ibrahim, C.M. and Klein, S.A. (1993) "Thermodynamic Properties of Ammonia-Water Mixtures", *ASHRAE Trans*, vol. 21, no.2, pp. 1495.
- Itard, L.C.M. (1998) "Wet compression-resorption heat pump cycle: thermodynamic analysis and design", dissertation, TU Delft.

- Itard, L.C.M. and Machielsen, C.H.M. (1994) "Considerations when modelling compression/resorption heat pumps", *International Journal of Refrigeration*, vol. 17, issue 7, pp.453-460.
- Jakobs, R., Cibis, D., Laue, H. (2010) "Status and outlook: Industrial Heat Pumps", in Purdue e-Pubs (edi.), *International Refrigeration and Air Conditioning Conference*, Karlsruhe and Breuberg, Germany, July 12-15, 2010.
- Jana, A.K. (2014) "Advances in heat pump assisted distillation column: A review", *Energy Conversion and Management*, vol.77, pp.287-297.
- Jensen et al. (2014a) "Technical and economic working domains of industrial heat pumps: Part 2 - Ammonia-water hybrid absorption-compression heat pumps", unpublished paper presented on the 11th IIR Gustav Lorentzen Conference on Natural refrigerants, Hanzhou, China.
- Jensen et al. (2014b) "Investigation of ammonia/water hybrid absorption/compression heat pumps for heat supply temperatures above 100 °C", unpublished presented paper on the International Sorption Heat Pump Conference, Washington, USA.
- Jung et al. (2014) "Thermal performance estimation of ammonia-water plate bubble absorbers for compression/absorption hybrid heat pump application", *Energy*, vol. 75, pp.371-378.
- Kang et al. (2000a) "Analytical investigation of two different absorption modes: falling film and bubble types", *International Journal of Refrigeration*, vol. 23, pp.430-443.
- Killion, J.D. and Garimella, S. (2001) "A critical review of models of coupled heat and mass transfer in falling-film absorption", *International Journal of Refrigeration*, vol. 24, pp.755-797.
- Kim et al. (2004) "Fundamental process and system design issues in CO₂ vapor compression systems", *Progress in Energy and Combustion Science*, vol. 30, pp. 119-174.
- Klein, S.A. (2014) "Engineering Equation Solver", Professional version 9.605, F-Chart Software, Madison, WI53744, USA.
- Koelet, P.C., Pieter and Gray (1992) "Industrial Refrigeration". Palgrave Macmillan.
- Laue, H.J. (2006) "Heat pumps", *Renewable energy*, Springer Berlin Heidelberg.
- Lee et al. (2002a) "Comparison of heat and mass transfer in falling film and bubble absorbers of ammonia-water", *Experimental Heat Transfer*, vol. 15, pp. 191-205.
- Lee et al. (2002b) "Experimental analysis of bubble mode in a plate-type absorber" *Chemical Engineering Science*, vol. 57, pp. 1923-1929.
- Leonardo Energy (2007) "Industrial heat pumps", *Power quality and utilization guide*.
- Nefs et al. (2014) "Experimental validation of a mini-channel multi-tube ammonia-water absorption/desorption model", unpublished presented paper on the 11th IIR Gustav Lorentzen Conference on Natural Refrigerants, Hanzhou, China.
- Nellis, G. and Klein, S. (2009) *Heat Transfer*. New York: Cambridge University Press.
- Nordtvedt, S.R. (2013) "Norsk deltagelse i IEA Heat Pump Programme Annex 34 - sluttrappport", Kjeller: Institutt for energiteknikk.

- Nordtvedt, S.R. (2005) "Experimental and theoretical study of a compression/absorption heat pump with ammonia/water as working fluid" Ph.D dissertation, Norwegian University of Science and Technology.
- Pearson, A. (2012) "High temperature heat pumps with natural refrigerants", *IEA Heat Pump Centre Newsletter*, vol.30, no.1, pp.33-35.
- Radermacher, R. and Hwang, Y. (2005) "Vapor Compression Heat Pumps with Refrigerant Mixtures". Boca Raton, Florida: CRC Press.
- Rane et al. (1993) "Performance enhancement of a two-stage vapour compression heat pump with solution circuits by eliminating the rectifier", *International Journal of Refrigeration*, volume 16, issue 4, pp. 247-257.
- Rane, M.V. and Radermacher, R. (1993) "Feasibility study of a two-stage vapour compression heat pump with ammonia-water solution circuits: experimental results", *International Journal of Refrigeration*, volume 16, issue 4, pp. 258-264.
- RnLib (2013) Thermodynamic and Transport Properties of Refrigerants and Refrigerant Mixtures.
- Stavset et al. (2014) "Analysis of high temperature heat pumps applying natural working fluids", unpublished presented paper on the 11th IIR Gustav Lorentzen Conference on Natural Refrigerants, Hanzhou, China.
- Stene, J. (2001) "Varmepumper - Grunleggende Varmepumpeteknikk", Trondheim: SINTEF Energiforskning AS.
- Stene, J. (1993) "Varmepumper - Industrielle anvendelser", Trondheim: NTH - SINTEF Kuldeteknikk.
- Stokar, M. and Trepp, C. (1987) "Compression heat pump with solution circuit Part 1: design and experimental results", *International Journal of Refrigeration*, vol. 10, issue 7, pp.87-96.
- Sveine et al. (1998) "Design of high temperature absorption/compression heat pump". *Natural working fluids*, IIR Gustav Lorentzen Conference on Natural Refrigerants, Oslo, Norway.
- Tolstorebrov et al. (2014) "Energy efficiency by vapor compression superheated steam drying systems", unpublished paper presented on the 11th IIR Gustav Lorentzen Conference on Natural Refrigerants, Hanzhou, China.
- van der Bor, D.M. and Infante Ferreira C.A. (2013) "Quick selection of industrial heat pump types including the impact of thermodynamic losses", *Energy*, vol. 53, pp.312-322.
- Vuddagiri, S.R. and Eubank, P.T. (1998) "Condensation of Mixed Vapor and Thermodynamics", *AIChE Journal*, vol. 44, no.11, pp.2526-2541.
- Yuan, Q.S. and Blaise, J.C "Water - a working fluid for CFC replacement", *International journal of refrigeration*, vol.11, no.4, pp.243-247.
- Zhou, Q. and Radermacher, R. (1997) "Development of a vapor compression cycle with a solution circuit and desorber/absorber heat exchange", *International Journal of Refrigeration*, vol. 20, no. 2, pp. 85-95.

Zhou, G. et al. (2012) "Review Status on High Temperature Heat Pumps" *Applied Mechanics and Materials*, vol.170-173, pp. 2550-2553.

CAHP Simulation Results

Table A.1: Simulations with 150°C as maximum allowable discharge temperature.

Simulation #	#1	#2	#3	#4	#5	#6
P_{HP} [bar]	17	17	17	18	16.5	17
P_{MP} [bar]	7.71	7.71	7.71	7.73	7.73	7.18
PR_{LP} [-]	2.97	2.97	2.97	2.97	2.97	2.76
PR_{HP} [-]	2.20	2.20	2.20	2.33	2.14	2.37
K [-]	1.16	1.16	1.16	1.13	1.18	1.08
CR [-]	1.2	1.2	1.2	0.8	1.4	0.9
ZZ [-]	0.64	0.64	0.64	0.70	0.61	0.68
$\dot{m}_{mix,tot}$ [kg]	0.131	0.131	0.131	0.107	0.143	0.113
\dot{m}_{source} [kg]	0.535	0.535	0.535	0.441	0.586	0.466
\dot{m}_{sink} [kg]	0.45	0.45	0.45	0.505	0.463	0.52
\dot{Q}_{abs} [kW]	100	91.4	90.5	100	100	100
\dot{Q}_{dsh} [kW]	0	8.6	9.5	0	0	0
\dot{Q}_{des} [kW]	76.6	76.6	76.6	76.0	76.9	76.9
$\dot{Q}_{ihx\#1}$ [kW]	5.1	5.1	5.1	2.7	6.4	2.9
$\dot{Q}_{ihx\#2}$ [kW]	10.9	10.9	10.9	11.9	10.7	10.7
COP [-]	3.85	3.85	3.85	3.75	3.91	3.90
\dot{W}_{LP} [kW]	13.6	13.6	13.6	13.6	13.6	12.5
\dot{W}_{HP} [kW]	9.7	9.7	9.7	10.3	9.3	10.5
\dot{W}_{pump} [kW]	0.12	0.12	0.12	0.09	0.13	0.09
$\eta_{is,LP}$ [-]	0.78	0.78	0.78	0.78	0.78	0.78
$\eta_{is,HP}$ [-]	0.81	0.81	0.81	0.81	0.81	0.81
$\eta_{vol,LP}$ [-]	0.82	0.82	0.82	0.82	0.82	0.82
$\eta_{vol,HP}$ [-]	0.88	0.88	0.88	0.87	0.89	0.88
q_6 [-]	0.455	0.424	0.421	0.579	0.410	0.541
v_3 [m^3/kg]	0.209	0.209	0.209	0.205	0.210	0.22
T_2 [°C]	149.4	149.4	149.4	149.7	149.7	141.1
T_4 [°C]	149.8	149.8	149.8	149.1	149.0	149.3
T_5 [°C]	149.8	95.7	90.1	149.1	149.0	149.3
T_6 [°C]	109.5	104.6	104.1	113.8	107.7	110.5
T_7 [°C]	65.5	65.5	65.5	61.2	67.2	60.6
T_9 [°C]	10.8	10.8	10.8	3.8	13.6	5.5
T_{14} [°C]	95.7	95.7	95.7	113	91.4	102.1
$T_{sink,abs,out}$ [°C]	103.3	98.5	98	97.2	101.6	95.9
$T_{sink,dsh,out}$ [°C]	-	103.0	103.0	-	-	-
$T_{source,out}$ [°C]	15.8	15.8	15.8	8.8	18.6	10.5

Table A.2: Simulations with 175°C as maximum allowable discharge temperature.

Simulation #	#7	#8	#9	#10	#11	#12
P_{HP} [bar]	22.5	22.5	22.5	23	22	22.5
P_{MP} [bar]	9.41	9.41	9.41	9.43	9.38	9.33
PR_{LP} [-]	3.62	3.62	3.62	3.63	3.61	3.59
PR_{HP} [-]	2.39	2.39	2.39	2.44	2.35	2.41
K [-]	1.23	1.23	1.23	1.22	1.24	1.22
CR [-]	0.9	0.95	0.95	0.85	1.1	0.85
ZZ [-]	0.68	0.68	0.68	0.69	0.65	0.69
$\dot{m}_{mix,tot}$ [kg]	0.112	0.115	0.115	0.110	0.124	0.110
\dot{m}_{source} [kg]	0.450	0.461	0.461	0.437	0.451	0.438
\dot{m}_{sink} [kg]	0.342	0.341	0.341	0.345	0.348	0.351
\dot{Q}_{abs} [kW]	100	91.0	87.6	100	100	100
\dot{Q}_{dsh} [kW]	0	9.0	12.4	0	0	0
\dot{Q}_{des} [kW]	71.9	71.9	71.9	71.6	72.1	72.0
$\dot{Q}_{ihx\#1}$ [kW]	5.1	5.6	5.6	4.9	6.8	4.7
$\dot{Q}_{ihx\#2}$ [kW]	13.0	12.8	12.8	12.4	12.4	13.1
COP [-]	3.20	3.20	3.20	3.17	3.23	3.21
\dot{W}_{LP} [kW]	16.9	16.9	16.9	16.9	16.8	16.7
\dot{W}_{HP} [kW]	11.1	11.1	11.1	11.4	11.0	11.2
\dot{W}_{pump} [kW]	0.12	0.12	0.12	0.12	0.15	0.12
$\eta_{is,LP}$ [-]	0.75	0.75	0.75	0.75	0.75	0.75
$\eta_{is,HP}$ [-]	0.80	0.80	0.80	0.80	0.80	0.80
$\eta_{vol,LP}$ [-]	0.77	0.77	0.77	0.77	0.77	0.77
$\eta_{vol,HP}$ [-]	0.87	0.87	0.87	0.87	0.87	0.87
q_6 [-]	0.555	0.486	0.486	0.573	0.491	0.572
v_3 [m^3/kg]	0.176	0.176	0.176	0.182	0.179	0.177
T_2 [°C]	174.4	174.4	174.4	174.8	174	173.3
T_4 [°C]	172.1	173.6	173.6	174.4	174	171.4
T_5 [°C]	172.1	118	98	174.4	174	171.4
T_6 [°C]	124.5	118.5	116.2	125.9	122.5	124.8
T_7 [°C]	72.6	73.5	73.5	72.7	75.1	71.7
T_9 [°C]	6.7	7.7	7.7	5.8	10.3	5.7
T_{14} [°C]	120.8	118	118	124	111.3	123.2
$T_{sink,abs,out}$ [°C]	119.5	113.5	111.2	118.9	117.5	117.8
$T_{sink,dsh,out}$ [°C]	-	119.7	119.8	-	-	-
$T_{source,out}$ [°C]	11.7	12.7	10.8	10.8	15.3	10.7

Table A.3: Simulations with 200°C as maximum allowable discharge temperature.

Simulation #	#13	#14	#15	#16	#17	#18
P_{HP} [bar]	30.5	30.5	30.5	31	30	30.5
P_{MP} [bar]	11.2	11.2	11.2	11.2	11.2	11.0
PR_{LP} [-]	4.32	4.32	4.32	4.32	4.31	4.25
PR_{HP} [-]	2.72	2.72	2.72	2.76	2.68	2.76
K [-]	1.26	1.26	1.26	1.25	1.27	1.24
CR [-]	0.5	0.5	0.5	0.4	0.6	0.45
ZZ [-]	0.77	0.77	0.77	0.80	0.75	0.79
$\dot{m}_{mix,tot}$ [kg]	0.088	0.088	0.088	0.082	0.094	0.085
\dot{m}_{source} [kg]	0.345	0.345	0.345	0.325	0.365	0.336
\dot{m}_{sink} [kg]	0.275	0.273	0.273	0.278	0.281	0.283
\dot{Q}_{abs} [kW]	100	93.2	84.2	100	100	100
\dot{Q}_{dsh} [kW]	0	6.8	15.8	0	0	0
\dot{Q}_{des} [kW]	66.3	66.3	66.3	66.1	66.6	66.4
$\dot{Q}_{ihx\#1}$ [kW]	3.5	3.5	3.5	2.7	4.3	3.0
$\dot{Q}_{ihx\#2}$ [kW]	15.3	15.3	15.3	15.6	15.0	15.2
COP [-]	2.68	2.68	2.68	2.65	2.69	2.68
\dot{W}_{LP} [kW]	20.3	20.3	20.3	20.3	20.2	19.9
\dot{W}_{HP} [kW]	13.3	13.3	13.3	13.6	13.1	13.6
\dot{W}_{pump} [kW]	0.095	0.095	0.095	0.077	0.11	0.086
$\eta_{is,LP}$ [-]	0.72	0.72	0.72	0.72	0.72	0.73
$\eta_{is,HP}$ [-]	0.79	0.79	0.79	0.76	0.79	0.79
$\eta_{vol,LP}$ [-]	0.71	0.71	0.71	0.71	0.71	0.72
$\eta_{vol,HP}$ [-]	0.84	0.84	0.84	0.84	0.84	0.84
q_6 [-]	0.760	0.723	0.675	0.826	0.702	0.790
v_3 [m^3/kg]	0.151	0.151	0.151	0.150	0.152	0.153
T_2 [°C]	199.3	199.3	199.3	199.3	199.3	196.9
T_4 [°C]	199.3	199.3	199.3	198.9	199.6	199.2
T_5 [°C]	199.3	157.8	107	198.9	199.6	199.2
T_6 [°C]	144.6	139	131	146.8	142.6	145.2
T_7 [°C]	78.7	78.7	78.7	77.3	80	77.6
T_9 [°C]	-1.0	-1.0	-1.0	-3.5	1.4	-2.3
T_{14} [°C]	157.8	157.8	157.8	166.9	151.3	160.9
$T_{sink,abs,out}$ [°C]	136.4	131	123.3	135.3	134.5	133.9
$T_{sink,dsh,out}$ [°C]	-	136.8	136.8	-	-	-
$T_{source,out}$ [°C]	4.0	4.0	4.0	1.5	6.4	2.7

Table A.4: Simulations with 250°C as maximum allowable discharge temperature.

Simulation #	#19	#20	#21	#22	#23	#24
P_{HP} [bar]	47.5	47.5	47.5	48	47	47.5
P_{MP} [bar]	15.0	15.0	15.0	15.1	15.0	14.8
PR_{LP} [-]	5.77	5.77	5.77	5.80	5.78	5.69
PR_{HP} [-]	3.17	3.17	3.17	3.18	3.13	3.21
K [-]	1.35	1.35	1.35	1.35	1.36	1.33
CR [-]	0.2	0.2	0.2	0.2	0.25	0.15
ZZ [-]	0.88	0.88	0.88	0.88	0.86	0.90
$\dot{m}_{mix,tot}$ [kg]	0.069	0.069	0.069	0.069	0.071	0.065
\dot{m}_{source} [kg]	0.104	0.104	0.104	0.103	0.104	0.102
\dot{m}_{sink} [kg]	0.198	0.197	0.193	0.188	0.199	0.197
\dot{Q}_{abs} [kW]	100	96.1	76.7	100	100	100
\dot{Q}_{dsh} [kW]	0	3.9	23.3	0	0	0
\dot{Q}_{des} [kW]	56.7	56.7	56.7	56.5	56.9	56.0
$\dot{Q}_{ihx\#1}$ [kW]	1.9	1.9	1.9	2.0	2.5	1.4
$\dot{Q}_{ihx\#2}$ [kW]	18.8	18.8	18.8	18.8	18.7	14.5
COP [-]	2.08	2.08	2.08	2.07	2.09	2.05
\dot{W}_{LP} [kW]	26.7	26.7	26.7	26.8	26.7	26.0
\dot{W}_{HP} [kW]	16.6	16.6	16.6	16.7	16.4	18.0
\dot{W}_{pump} [kW]	0.060	0.059	0.059	0.060	0.073	0.044
$\eta_{is,LP}$ [-]	0.66	0.66	0.66	0.66	0.66	0.67
$\eta_{is,HP}$ [-]	0.77	0.77	0.77	0.77	0.77	0.77
$\eta_{vol,LP}$ [-]	0.60	0.60	0.60	0.60	0.60	0.60
$\eta_{vol,HP}$ [-]	0.80	0.80	0.80	0.80	0.80	0.80
q_6 [-]	1	1	0.902	1	1	1
v_3 [m^3/kg]	0.121	0.121	0.121	0.120	0.121	0.131
T_2 [°C]	248.7	248.7	248.7	249.7	249.1	245.8
T_4 [°C]	249.5	249.5	249.5	251.3	249.3	281.9
T_5 [°C]	249.5	225.9	121.2	251.3	249.3	281.9
T_6 [°C]	213.2	194.5	154	215.1	184.3	251.2
T_7 [°C]	93.4	93.4	93.4	93.9	94.2	92.0
T_9 [°C]	-7.6	-7.6	-7.6	7.6	-6.3	-8.9
T_{14} [°C]	225.9	225.9	225.9	226.5	216.4	227.2
$T_{sink,abs,out}$ [°C]	169.1	165.1	144	175.3	168.5	169.8
$T_{sink,dsh,out}$ [°C]	-	169.6	171.8	-	-	-
$T_{source,out}$ [°C]	-2.6	-2.6	-2.6	-2.6	-1.3	-4.9

Thermophysical Properties for Ammonia-Water

Critical temperature and pressure Critical ammonia-water mixture temperature and pressure are calculated from equation (B.1) and (B.2), where the constants are given in table (A.1).

$$T_{crit,mix} = \sum_{i=0}^4 a_i x^i \quad (B.1)$$

$$P_{crit,mix} = \sum_{i=0}^4 b_i x^i \quad (B.2)$$

Table B.1: Constants for the equations of calculating the critical temperature and pressure for the ammonia-water mixture (Conde-Petit,2004).

i	a_i	b_i
0	647.14	220.64
1	-199.822 371	-37.923 795
2	109.035 522	36.424 739
3	-239.626 271	-41.851 597
4	88.689 691	-63.805 617

Thermal conductivity Saturation pressure of each component is calculated from the temperature of each component obtained in equation (B.3) to (B.5). The thermal conductivity of the liquid mixture (β_{liq}) is computed using equation (B.6), where the (β_{liq}) is based on the given temperature and pressure.

$$\theta_{mix} = \frac{T}{T_{crit,mix}} \quad (B.3)$$

$$T_{x,NH_3} = \theta \cdot 405.4 \quad (B.4)$$

$$T_{x,H_2O} = \theta \cdot 674.14 \quad (B.5)$$

$$\beta_{sol} = x \cdot \beta_{NH_3} + (1 - x) \cdot \beta_{H_2O} \quad (B.6)$$

Viscosity Viscosity of each component is calculated using the same temperature and pressure as for (β_{liq}). The viscosity of the liquid mixture is found from equation (B.7) to (B.9).

$$\mu_{mix} = \exp[x \cdot \ln(\mu_{NH_3}) + (1 - x) \cdot \ln(\mu_{H_2O}) + \Delta\mu_{T,x}] \quad (B.7)$$

$$\Delta\mu_{T,x} = [0.534 - 0.815 \cdot \frac{T}{674.14}] \cdot F \quad (B.8)$$

$$F = 6.38 \cdot (1 - x)^{1.125x} \cdot (1 - e^{-0.585x(1-x)^{0.18}}) \cdot (\mu_{NH_3}^{0.5} \cdot \mu_{H_2O}^{0.5}) \quad (B.9)$$

C EES Absorber Geometry

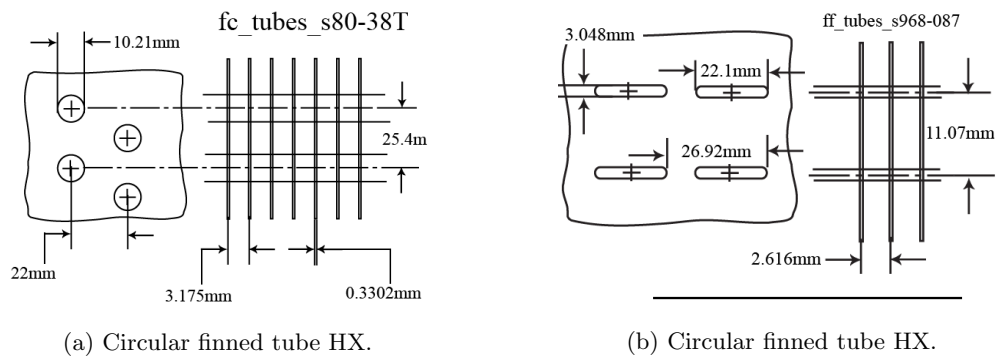


Figure C.1: Finned tube HX (Klein,2014).

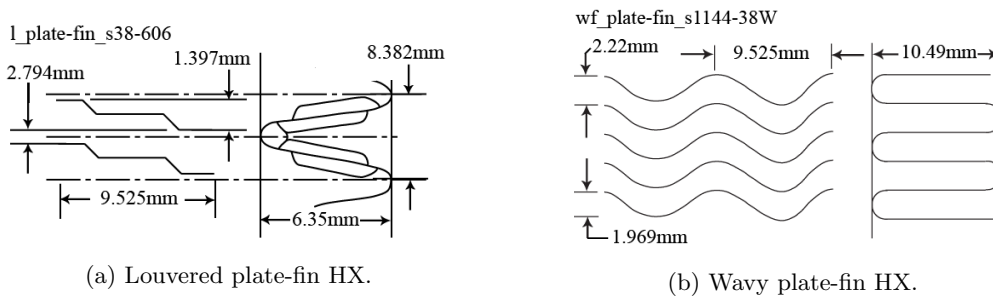


Figure C.2: Plate-fin heat exchangers (Klein,2014).

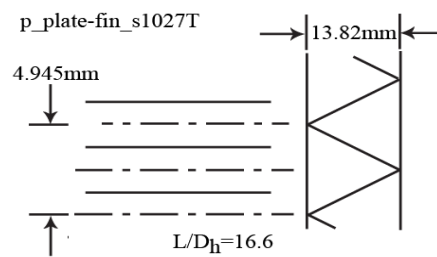


Figure C.3: Plain plate-fin HX (Klein,2014).

EES Program Codes - Two-Stage CAHP

\$UnitSystem SI K bar kJ mass rad

"Before reading this script, it would be easier to start to read at {INPUT PARAMETERS} .

Afterwards, the reader can go back and read the {FUNCTIONS}. This is recommended since the functions first in the script only because of syntax reasons."

{FUNCTIONS}

```
function tk(T)
    tk:= T - 273,15                                {Coverts from K to C}
end

procedure ihx1(T;K;P;O;Z;X;M;N;E:C1;C2)
    qihx:= 0
    if(T<K) then goto 10
    i:= 1
    CALL NH3H2O(123;T;P;Z:T[i];P[i];x[i];h[i];s[i];u[i];v[i];q[i]) {T=T[7] = , P=P_HP, Z-Ammonia concentration in the vapour}
    i:= i + 1
    CALL NH3H2O(123;K;P;Z:T[i];P[i];x[i];h[i];s[i];u[i];v[i];q[i]) {K=T[8] = , P=P_HP, Z=ZZ, for state 8}
    qh:= (h[1] - h[2]) * M                          {qh- ideal heat exchange from 7-8. M-Mixed solution flow rate}
    i:= i + 1
    CALL NH3H2O(123;T;O;X:T[i];P[i];x[i];h[i];s[i];u[i];v[i];q[i]) {T=T[13] = , O=P_HP, X=Ammonia concentration in the weak solution}
    i:= i + 1
    CALL NH3H2O(123;K;O;X:T[i];P[i];x[i];h[i];s[i];u[i];v[i];q[i]) {K=T[12] = , O=P_HP, X=Ammonia concentration in the weak solution}
    qc:= (h[3] - h[4]) * N                          {qc- ideal heat exchange from 13-12. N-Liquid flow rate}
    qmax:= min(qh;qc)                               {ideal heat exchange in IHX1}
    qihx = qmax * E                                {actual heat exchange in IHX1, E=Thermal efficiency IHX 1}

10: C1:= h[1] - (qihx / M)                          {Return value for h[8]}
    C2:= h[4] + (qihx / N)                          {Return value for h[13]}
end

procedure ihx2(T;K;P;O;Z;X;M;N;E:C1;C2)

    i:= 1
    CALL NH3H2O(123;T;P;Z:T[i];P[i];x[i];h[i];s[i];u[i];v[i];q[i]) {T=T[2] = , P=P_MP, Z-Ammonia concentration in the vapour}
    i:= i + 1
    CALL NH3H2O(123;K;P;Z:T[i];P[i];x[i];h[i];s[i];u[i];v[i];q[i]) {K=T[2] = , P=P_MP, Z=x_vap, for state 3}
    qh:= (h[1] - h[2]) * M                          {qh- ideal heat exchange from 2-3. M-Vapor flow rate}
    i:= i + 1
    CALL NH3H2O(123;T;O;X:T[i];P[i];x[i];h[i];s[i];u[i];v[i];q[i]) {T=T[14] = , P=P_HP, X=x_liq, for state 14}
    i:= i + 1
    CALL NH3H2O(123;K;O;X:T[i];P[i];x[i];h[i];s[i];u[i];v[i];q[i]) {K=T[13] = , P=P_HP, X=x_liq, for state 13}
    qc:= (h[3] - h[4]) * N                          {qc- ideal heat exchange from 14-13. N-Liquid flow rate}
    qmax:= min(qh;qc)                               {ideal heat exchange in SHX2}
    qihx = qmax * E                                {actual heat exchange in SHX2, E=epsilon_ihx2}

    C1:= h[1] - (qihx / M)                          {Return value for h[3]}
```


K = 1,16

eta_motor = 0,9 [-] {Motor efficiency of the compressor}
 epsilon_ihx1 = 0,8 [-] {Thermal efficiency IHX 1}
 epsilon_ihx2 = 0,75 [-] {Thermal efficiency IHX 2}
 F\$ = 'Water'

P_dwater = 3 {Heat source pressure}
 P_ewater = 3 {Heat sink pressure}

{OTHER PARAMETERS}

T_1 = T_wd1 - DELTAT_min {Desorber outlet temperature}
 DELTAT_lift = T_cod - T_dwater2
 P_MP = K*sqrt(P_LP * P_HP) {Intermediate pressure}
 PR_LP = P_MP / P_LP {Compressor pressure ratio}
 PR_HP = P_HP / P_MP
 x_liq = x[11] {Ammonia concentration in the weak solution}
 ZZ = (m_lr*x_liq + m_vr*x_vap) / m_ar {Overall ammonia concentration}
 x_vap = x[1] {Ammonia concentration in the vapour to the compressor}

eta_isen_1 = 0,9051 - 0,0422*PR_LP {Isentropic compressor efficiency}
 eta_isen_2 = 0,9051 - 0,0422*PR_HP {Isentropic compressor efficiency}
 eta_is_mean = (eta_isen_1 + eta_isen_2) / 2
 eta_vol_LP = 1,0539 - 0,0788*PR_LP {Volumetric compressor efficiency}
 eta_vol_HP = 1,0539 - 0,0788*PR_HP {Volumetric compressor efficiency}

\$IfNot Parametric Table

CR = 1,2 {Circulation ratio}
 \$Endif
 m_dot_mix = Q_absorber / DELTAh_absorber {Mixed solution flow rate}
 m_dot_vap = m_dot_mix / (1 + CR) {Vapor flow rate}
 m_dot_liq = m_dot_mix - m_dot_vap {Liquid flow rate}
 Q_absorber = Q_sink - Q_desuperheater {Heat load in the absorber}
 Q_sink = 100
 Q_ihx1 = (h[7] - h[8]) * m_dot_mix
 Q_ihx2 = (h[2] - h[3]) * m_dot_vap

{CYCLE DATA (Array [1]-[14])}

{---- 1 ----}

CALL NH3H2O(128;T_1;P_LP;1:T[1];P[1];x[1];h[1];s[1];u[1];v[1];q[1])

{---- 2 ----}

CALL NH3H2O(235;P_MP;x_vap;s[1]:T_2s;P_2s;x_2s;h_2s;s_2s;u_2s;v_2s;q_2s)

$h_2 = (1,05 \cdot h[1] + ((h_{2s} - h[1]) / \eta_{isen_1})) / 1,05$ {Enthalpy at state 2 included compressor cooling}

CALL NH3H2O(234;P_MP;x_vap;h_2:T[2];P[2];x[2];h[2];s[2];u[2];v[2];q[2])

{---- 3 ----}

CALL ihx2(T[2];T[13];P_MP;P_HP;x_vap;x_liq;m_vr;m_lr;epsilon_ihx2:h_3;h_14) {Calling the ihx2 procedure to get return values for h[3], h[14] and heat exchanged in IHX2}

CALL NH3H2O(234;P_MP;x_vap;h_3:T[3];P[3];x[3];h[3];s[3];u[3];v[3];q[3])

{---- 4 ----}

CALL NH3H2O(235;P_HP;x_vap;s[3]:T_4s;P_4s;x_4s;h_4s;s_4s;u_4s;v_4s;q_4s)

$h_4 = (1,05 \cdot h[3] + ((h_{4s} - h[3]) / \eta_{isen_2})) / 1,05$ {Enthalpy at state 4 included compressor cooling}

CALL NH3H2O(234;P_HP;x_vap;h_4:T[4];P[4];x[4];h[4];s[4];u[4];v[4];q[4])

{---- 5 ----}

T_5=105+273,15

CALL NH3H2O(123;T[4];P_HP;x_vap:T[5];P[5];x[5];h[5];s[5];u[5];v[5];q[5])

{---- 6 ----}

$h_6 = ((h[5] \cdot m_{vr}) + (h[14] \cdot m_{lr})) / m_{ar}$

CALL NH3H2O(234;P_HP;ZZ;h_6:T[6];P[6];x[6];h[6];s[6];u[6];v[6];q[6])

{---- 7 ----}

CALL NH3H2O(238;P_HP;ZZ;0:T[7];P[7];x[7];h[7];s[7];u[7];v[7];q[7])

{---- 8 ----}

CALL ihx1(T[7];T[12];P_HP;P_HP;ZZ;x_liq;m_ar;m_lr;epsilon_ihx1:h_8;h_13) {Calling the ihx1 procedure to get return values for h[8], h[13]}

CALL NH3H2O(234;P_HP;ZZ;h_8:T[8];P[8];x[8];h[8];s[8];u[8];v[8];q[8])

{---- 9 ----}

CALL NH3H2O(234;P_LP;ZZ;h[8]:T[9];P[9];x[9];h[9];s[9];u[9];v[9];q[9])

{---- 10 ----}

CALL NH3H2O(123;T_1;P_LP;ZZ:T[10];P[10];x[10];h[10];s[10];u[10];v[10];q[10])
{---- 11 ----}

CALL NH3H2O(128;T_1;P_LP;0:T[11];P[11];x[11];h[11];s[11];u[11];v[11];q[11])
{---- 12 ----}

CALL NH3H2O(235;P_HP;x_liq;s[11]:T[12];P[12];x[12];h[12];s[12];u[12];v[12];q[12])
{---- 13 ----}

CALL NH3H2O(234;P_HP;x_liq;h_13:T[13];P[13];x[13];h[13];s[13];u[13];v[13];q[13])
{---- 14 ----}

CALL NH3H2O(234;P_HP;x_liq;h_14:T[14];P[14];x[14];h[14];s[14];u[14];v[14];q[14])

{DESORBER (Array [100]-[150])}

DELTAh_desorber = h[10] - h[9] {Specific enthalpy difference from state 9-10 }
 Q_desorber = DELTAh_desorber*m_dot_mix {Heat exchange in the desorber}
 T_dwater1 = T[10] + DELTAT_min {Heat source inlet temperature}
 T_dwater2 = T[9] + DELTAT_min {Heat source outlet temperature}
 h_dwater1 = enthalpy(F\$;T=T_dwater1;P=P_dwater) {Heat source inlet enthalpy}
 h_dwater2 = enthalpy(F\$;T=T_dwater2;P=P_dwater) {Heat source outlet enthalpy}
 m_dot_dwater = Q_desorber / (h_dwater1 - h_dwater2) {Heat source mass flow}

step_da = (h[10] - h[9]) / 50 {Specific enthalpy difference from state 9-10 in 50 steps}
 A[100] = h[9] {Enthalpy of mixed solution at state 9}
 duplicate i = 101;150 {Indexed enthalpy of mixed solution trough the desorber}
 A[i] = A[i-1] + step_da
 end
 duplicate i = 100;150
 CALL NH3H2O(234;P_LP;ZZ;A[i]:T[i];P[i];x[i];h[i];s[i];u[i];v[i];q[i]) {Indexed state properties of mixed solution trough the desorber}
 end
 step_dw = (T_dwater1 - T_dwater2) / 50 {Temperature difference between inlet and outlet of the heat source in 50 steps}
 T_water[150] = T_dwater1 - 273,15 {From K to C}
 duplicate i = 100;149
 T_water[i] = T_water[i+1] - step_dw {Heat source temperature in 50 steps}
 end
 Q_dot[100] = 0
 duplicate i = 100;150
 Q_dot[i] = Q_dot[i-1]+2 {Heat exchanged in % through the desorber}
 end

{ABSORBER (Array [200]-[250])}

```

DELTAh_absorber = h[6] - h[7]           {Specific enthalpy difference from state 6-7}
step_aa = (h[6] - h[7]) / 50           {Specific enthalpy difference from state 6-7 in 50 steps}

A[200] = h[7]                           {Enthalpy of mixed solution at state 7}
duplicate i = 201;250
  A[i] = A[i-1] + step_aa                 {Indexed enthalpy of mixed solution trough the absorber}
end
duplicate i =200;250
  CALL NH3H2O(234;P_HP;ZZ;A[i];T[i];P[i];x[i];h[i];s[i];u[i];v[i];q[i])
end

T_ewater1 = 323,15 [K]                   {Heat sink inlet temperature}
h_water1 = enthalpy(F$;T=T_ewater1;P=P_ewater) {Heat sink inlet enthalpy}
h_waterapprox2 = enthalpy(F$;T=T[250] - 5;P=P_ewater) {Guess value of heat sink outlet temperature}
m_waterapprox = Q_absorber / (h_waterapprox2 - h_water1) {Guess value of heat sink mass flow}

CALL absorber(T[200..250];h[200..250];P_ewater;m_dot_mix;m_waterapprox:m_dot_water;T_ewater2) {Call of the absorber procedure to get return values for heat sink water
flow and and outlet temperature}

T_water[40] = T_water[250]                {Putting the heat sink temperatures into Array [40-90] }
duplicate i = 41;90
  T_water[i] = T_water[290-i]
end

T_celsius[40] = T_celsius[250]            {Putting the mixed solution temperatures into Array [40-90] }
duplicate i = 41;90
  T_celsius[i] = T_celsius[290-i]         {Heat sink temperature in 50 steps}
end

Q_dot[40] = 0
duplicate i =41;90
  Q_dot[i] = Q_dot[i-1] +2                {Heat exchanged in % through the absorber}
end

T_water[200] = T_ewater1-273,15            {From K to C}
T_water[250] = T_ewater2-273,15
step_aw = (T_water[250] - T_water[200]) / 50
duplicate i = 201;249
  T_water[i] = T_water[i-1]+step_aw
end
T_water[6] = T_water[250]                 {Heat sink temp at the outlet of the the desorber, wa2}
T_water[7] = T_water[200]                 {Heat sink temp at the the inlet of the the desorber, wa1}

```

{DESUPERHEATER}**{Properties in the desuperheater are just like outlet properties of the absorber}**

$\Delta h_{\text{desuperheater}} = h[4] - h[5]$ **{Enthalpy difference through the dsh}**
 $Q_{\text{desuperheater}} = \Delta h_{\text{desuperheater}} \cdot m_{\text{dot_vap}}$
 $T_{\text{hid}} = T[5] - 273,15$
 $\text{CALL NH}_3\text{H}_2\text{O}(123; T_{\text{hid}} + 273,15; P_{\text{HP}}; x_{\text{vap}}; T[16]; P[16]; x[16]; h[16]; s[16]; u[16]; v[16]; q[16])$
 $T_{\text{hod}} = T[5]$ **{Ammonia vapor temp after the dsh}**
 $T_{\text{cid}} = T_{\text{water}}[6] + 273,15$ **{Heat sink temp before the dsh}**
 $\epsilon_{\text{dsh}} = \text{dsh}(T[16]; T[5]; T_{\text{cid}}; P_{\text{HP}}; x_{\text{vap}}; m_{\text{dot_vap}})$
 $h_{\text{cid}} = \text{enthalpy}(F\$; T = T_{\text{cid}}; P = P_{\text{awater}})$ **{Heat sink enthalpy before dsh}**
 $h_{\text{cod}} = h_{\text{cid}} + (Q_{\text{desuperheater}} / m_{\text{dot_water}})$ **{Heat sink enthalpy after the dsh}**
 $T_{\text{cod}} = \text{temperature}(F\$; P = P_{\text{awater}}; h = h_{\text{cod}})$ **{Heat sink temperature after the dsh}**

$T_{\text{celsius}}[30] = T_{\text{hid}}$ **{Hot stream inlet temperature}**
 $T_{\text{celsius}}[31] = T_{\text{hod}} - 273,15$ **{Hot stream outlet temperature}**
 $T_{\text{celsius}}[32] = T_{\text{water}}[6]$ **{Cold stream inlet temperature}**
 $T_{\text{celsius}}[33] = T_{\text{cod}} - 273,15$ **{Cold stream outlet temperature}**

$x[30] = 0$
 $x[31] = 1$
 $x[32] = 1$
 $x[33] = 0$

$T_{\text{water}}[5] = T_{\text{celsius}}[33]$

{IHX 1}

$T_{\text{celsius}}[20] = T_{\text{celsius}}[7]$ **{Hot stream inlet temperature}**
 $T_{\text{celsius}}[21] = T_{\text{celsius}}[8]$ **{Hot stream outlet temperature}**
 $T_{\text{celsius}}[22] = T_{\text{celsius}}[12]$ **{Cold stream inlet temperature}**
 $T_{\text{celsius}}[23] = T_{\text{celsius}}[13]$ **{Cold stream outlet temperature}**

$x[20] = 0$
 $x[21] = 1$
 $x[22] = 1$
 $x[23] = 0$

{IHX 1}

$T_{\text{celsius}}[25] = T_{\text{celsius}}[2]$ **{Hot stream inlet temperature}**
 $T_{\text{celsius}}[26] = T_{\text{celsius}}[3]$ **{Hot stream outlet temperature}**
 $T_{\text{celsius}}[27] = T_{\text{celsius}}[13]$ **{Cold stream inlet temperature}**
 $T_{\text{celsius}}[28] = T_{\text{celsius}}[14]$ **{Cold stream outlet temperature}**

$x[25] = 0$

```
x[26] = 1
x[27] = 1
x[28] = 0
```

{ENERGY}

```
W_comp1 = (h[2] - h[1]) * m_dot_vap
W_comp2 = (h[4] - h[3]) * m_dot_vap
W_pump = (h[12] - h[11]) * m_dot_liq
W_motor = (W_comp1+W_comp2)/eta_motor
COP = Q_sink / (W_motor + W_pump)
```

{MISCELLANEOUS}

```
m_ar = 1
m_vr = m_ar/(1+CR)
m_lr = m_ar - m_vr
```

```
duplicate i=1;14
  T_celsius[i] = tk(T[i])
end
```

```
duplicate i = 100;150
  T_celsius[i] = T[i]-273,15
end
```

```
duplicate i = 200;250
  T_celsius[i] = tk(T[i])
end
```

```
duplicate i = 1;5
  m_dot[i] = m_vr
end
```

```
duplicate i = 6;10
  m_dot[i] = m_ar
end
```

```
duplicate i = 11;14
  m_dot[i] = m_lr
end
```

EES Program Codes - Absorbers

\$UnitSystem SI MASS RAD PA K J
\$TabStops 0,1 0,4 0,6 0,8 cm

{FUNCTIONS}

"! Procedure with thermophysical properties for ammonia-water as outputs"

procedure thermophysical_properties(x;T:T_c_sol;P_c_sol;lambda_sol;mu_sol)

```

a_0:=647,14      "a_0-a_4: Constants for critical solution temperature from Conde-Petit"
a_1:= - 199,822371
a_2:=109,035522
a_3:= - 239,626217
a_4:=88,689691
b_0:=220,64      "b_0-b_4: Constants for critical solution pressure from Conde-Petit"
b_1:= - 37,923795
b_2:=36,424739
b_3:= - 41,851597
b_4:= - 65,805617
T_c_sol:=(a_0) + (a_1*x) + (a_2*x^2) + (a_3*x^3) + (a_4*x^4)      "Equation for critical solution temperature"
P_c_sol:=(b_0) + (b_1*x) + (b_2*x^2) + (b_3*x^3) + (b_4*x^4)      "Equation for critical solution pressure"
Theta:= T/T_c_sol      "Reduced temperature"
T_x_NH3:= Theta * 405,4      "Component specific temperature"
T_x_H2O:= Theta * 674,14

P_sat_NH3:=P_sat(Ammonia;T=T_x_NH3)
P_sat_H2O:=P_sat(Water;T=T_x_H2O)
lambda_NH3:=Conductivity(Ammonia;T=T_x_NH3-1;P=P_sat_NH3)      "Conductivity for the components"
lambda_H2O:=Conductivity(Ammonia;T=T_x_H2O-1;P=P_sat_H2O)
lambda_sol:=(x * lambda_NH3) + ((1 - x) * lambda_H2O)
mu_NH3:=Viscosity(Ammonia;T=T_x_NH3-1;P=P_sat_NH3)      "Viscosity for the components"
mu_H2O:=Viscosity(Water;T=T_x_H2O-1;P=P_sat_H2O)
F:= 6,38 * (1 - x)^(1,125 * x) * (1 - exp(- 0,585 * x * (1 - x)^(0,18))) * ln((mu_NH3)^0,5 * (mu_H2O)^0,5)      "required variable to find mu_sol"
DELTAmu_T_x:=(0,534 - 0,815 * (T / 674,14)) * F      "required variable to find mu_sol"
mu_sol := exp((x * ln(mu_NH3)) + ((1-x) * ln(mu_H2O)) + DELTAmu_T_x)      "Viscosity for the solution"
end

```

"! Procedure with heat transfer coefficient inside the tube as output"

procedure tube_flow(m_dot; mu; T_1; T_2; P; D_h; lambda; P_c; L; x; A; B; C; D)

```

CALL NH3H2O(128;T_1;P;0:T[1];P[1];x[1];h[1];s[1];u[1];v[1];q[1])
CALL NH3H2O(128;T_2;P;0:T[2];P[2];x[2];h[2];s[2];u[2];v[2];q[2])
CALL NH3H2O(128;T_1;P;1:T[3];P[3];x[3];h[3];s[3];u[3];v[3];q[3])
CALL NH3H2O(128;T_2;P;1:T[4];P[4];x[4];h[4];s[4];u[4];v[4];q[4])
CALL NH3H2O(123;T_1;P;x:T[5];P[5];x[5];h[5];s[5];u[5];v[5];q[5])
CALL NH3H2O(123;T_2;P;x:T[6];P[6];x[6];h[6];s[6];u[6];v[6];q[6])

```



```

v_l_avg:= (V[1] + V[2]) / 2           "average liquid volume"
rho_l_avg:= 1 / v_l_avg              "average liquid density"
v_g_avg:= (v[3]+v[4]) / 2           "average gas volume"
rho_g_avg:= 1 / v_g_avg              "average gas density"
q_avg:= (q[5] + q[6]) / 2           "average mixture vapor quality"
rho_avg:= (rho_l_avg * (1-q_avg)) + (rho_g_avg * q_avg) "average mixture density"
u_m:= (4 * m_dot) / (rho_avg * D_h^2) "mean liquid velocity"
Re_D:= (rho_l_avg * u_m * D_h) / (mu) "Reynolds number"
cp:= ((h[1] - h[2])*1000) / (T_1 - T_2) "specific heat capacity"
Pr:= (cp * mu) / lambda              "Prandtl number"
alpha:= 0,023 * (Re_D)^0,8 * Pr^0,4 * (lambda / D_h) "heat transfer coefficient"
R_in:= 1 / (alpha * pi * D_h * L)    "thermal resistance"
A:= alpha                            "heat transfer coefficient"
B:= R_in                             "thermal resistance"
C:= Re_d                             "Reynolds number"
D:= u_m                             "mean velocity"
end

"! Procedure for tube wall conductivity and conduction resistance as outputs"

procedure conduction_resistance(T_avg;th_plate;A_cont: A;B)
  A:= k_(Stainless_AISI304;T_avg)    "Conductivity for the specific material"
  B:= th_plate/(A*A_cont)
end

"! Procedure with air side resistance as output"

procedure air_flow(T_C_in ;T_C_out ;T_avg ;P ;m_dot_air ; th_plate;s_w_C;A_C ;L ;fin_thk ; L_fin ;k_m ; A_fin\A ;A_tot : A; B; C; D) "Defining all the procedure inputs and outputs"
  Call CHX_h_plate_fin('p_plate-fin_s1027T' ;th_plate;s_w_C; m_dot_air; A_C ; 'air'; T_C_in; P; h_out) "Function for the air heat transfer coefficient"
  Call CHX_DELTAP_plate_fin('p_plate-fin_s1027T'; th_plate;s_w_C; m_dot_air; A_C ;L ; 'air'; T_C_in;T_C_out; P : DELTAP) "Function for the pressure drop"
  eta_fin := eta_fin_straight_rect(fin_thk;L_fin;h_out;k_m) "Fin efficiency"
  eta_o := 1 - (A_fin\A)*(1-eta_fin) "Overall surface efficiency"
  R_out := 1 / (eta_o * h_out * A_tot) "Thermal resistance between air and air-side surface"
  A:= h_out "Air heat transfer coefficient"
  B:= R_out "Thermal resistance between air and air-side surface as output"
  C:= eta_o "Overall surface efficiency as output"
  D:= DELTAP "Pressure drop as output"
end

"!Procedure with capacitance of C,H,min,max and spec heat capacity as outputs"

procedure capacitance_rate(T_C_in ;T_C_out ;V_dot_C ;m_dot_H ;P ;c_H :A ;B ;C ;D ;E)
  rho_C:= density('air';T=(T_C_in + T_C_out) / 2; P=P) "Air density"
  m_dot_C:= rho_C * V_dot_C "Air mass flow rate"

```

```

A:= Cp(Air;T=(T_C_in + T_C_out) / 2)           "Air specific heat capacity"
B:= m_dot_C * A                               "capacitance rate of the air "
C:= m_dot_H * c_H                             "capacitance rate of the mxture"
D:= min(B;C)                                  "minimum capacitance rate"
E:= max(B;C)                                  "maximum capacitance rate"
end

"!INPUTS"

th_plate = 3 [mm]*convert(mm;m)               "plate channel divider thickness"
s_w_H = s_w_C / 4                             "width of the mixture channel"
H = 0,42 [m]                                  "Height of the absorber segment"
W = 0,8 [m]                                   "Width of the absorber"
L = 0,1 [m]                                   "Length of the absorber"
L_H_tot = H * N_ch_H * S                     "Total channel length of the mixture"
L_H_seg = H * N_ch_H                         "Channel length of mixture per segment"

u_m = 5,5                                     "frontal velocity for external flow calculation"
Call CHX_geom_plate_fin('p_plate-fin_s1027T' ;th_plate;s_w_H : s_w_C; D_o ; fin_pitch; D_h; fin_thk; sigma; A_avfrac; A_fin\A) "Function for different geometry for the HX"
A_C_fr = H * W                                "Frontal cross sectional area"
A_C = sigma * A_C_fr                          "Available area for air flow"
A_tot = A_avfrac * (H * W * L)               "Total heat transfer area"
A_cond = H * L * 2 * (N_ch_H - 1)           "Contact area for conduction"
eta_fan = 0,5                                 "Fan efficiency"
V_dot_C = u_m * A_C                           "Volumetric air flow"
N_ch_H = Round(W/(s_w_H+(2 * th_plate)+s_w_C)) "Integer number of mixture channel rows"
N_ch_C = Round(W/(s_w_H+(2 * th_plate)+s_w_C)) "Integer number of air channel columns"

P = 1 [atm]*convert(atm;Pa)                  "atmospheric pressure"
T_C_in = convertTemp(C;K;90 [C])             "inlet air temperature"
T_H_in = convertTemp(C;K;150 [C])            "inlet water temperature"

T_C_out = convertTemp(C;K;125 [C])           "guess value for the air outlet temperature"
T_H_out = convertTemp(C;K;100 [C])           "guess value for the mixture outlet temperature"

S = 10 [-]                                   "number of heat exchanger segments"

step_C = (T_C_out - T_C_in) / S               "initial temperature step per segment for air"
step_H = (T_H_in - T_H_out) / S              "initial temperature step per segment for mixture"

Q_dot_absorber = 50 [kW]                     "absorber duty"
P_H = 25 [bar]                               "mixture pressure"
CALL NH3H2O(128;T_H_out;P_H;0:T_x_out;P_out;x_out;h_out;s_out;u_out;v_out;q_out) "mixture outlet properties for guess value"
CALL NH3H2O(123;T_H_in;P_H;x_out:T_x_in;P_in;x_in;h_in;s_in;u_in;v_in;q_in) "mixture inlet properties"
m_dot_H_ch = m_dot_H_tot/N_ch_H              "mixture mass flow rate per channel"
m_dot_H_tot = Q_dot_absorber / (h_in - h_out) "total mixture mass flow rate"

```

```

h_air_in = Enthalpy('air';T=T_C_in)           "Air enthalpy at the inlet"
h_air_out = Enthalpy('air';T=T_C_out)        "Air enthalpy at the outlet"
m_dot_air_approximately = (Q_dot_absorber * 1000) / (h_air_out - h_air_in)           "Air density at the inlet"
rho_air_in = Density('air';T=T_C_in;P=P)     "Air density at the outlet"
rho_air_out = Density('air';T=T_C_out;P=P)   "Atmospheric air density"
rho_bar_air = (rho_air_in + rho_air_out) / 2 "Average air density"
V_dot_air_approximately = m_dot_air_approximately / rho_bar_air "Air volume flow rate"
m_dot_air = V_dot_C * rho_bar_air

```

"! -----"

```

T_C[1] = T_C_out           "Initial guessed air outlet temperature"
T_H[1] = T_H_in           "Mixture inlet temp"
DELTAT[1] = T_H[1] - T_C[1] "Temperature difference between air and mixture"
T_C_y[S+1] = T_C_in       "Air inlet temperature"
T_H_y[1] = T_H_in         "Mixture inlet temp for the use of corrected mixture temperatures"
h_H_y[1] = h_in           "Mixture inlet enthalpy for the use corrected mixture enthalpies"
DELTAT_C[1] = T_C[1] - T_C_in "Air temperature difference between two segments"
DELTAT_H[1] = T_H_in - T_H[S+1] "Mixture temperature change through the absorber"
CALL NH3H2O(123;T_H_in;P_H;x_out:T_x[1];P[1];x[1];h[1];s[1];u[1];v[1];q[1]) "Mixture inlet conditions"
L_x[1] = 1                 "Length of the entire absorber"

```

"! Initial absorber iteration"

```

duplicate i=2;(S+1)
  T_C[i] = T_C[i-1] - step_C "Stepwise temp change for the air"
  T_H[i] = T_H[i-1] - step_H "Stepwise temp change for the mixture"
  T_avg[i] = (T_H[i-1] + T_C[i]) / 2 "Approximated value used for average tube surface temperature"
  T_bar_H[i] = (T_H[i-1] + T_H[i]) / 2 "Avg mixture temp between current and previous segment"
  T_bar_C[i] = (T_C[i-1] + T_C[i]) / 2 "Avg air temp between current and previous segment"
  CALL NH3H2O(128;T_bar_H[i];P_H;0:T_x[i];P_x[i];x_x[i];h_x[i];s_x[i];u_x[i];v_x[i];q_x[i]) "Mixture liquid props"
  Call thermophysical_properties(x_l[i];T_bar_H[i];T_c_sol[i];P_c_sol[i];lambda_sol[i];mu_sol[i]) "Thermophysical properties with current segment inputs and outputs"
  Call tube_flow(m_dot_H_ch; mu_sol[i]; T_H[i-1]; T_H[i]; P_H; D_h; lambda_sol[i]; P_c_sol[i]; L_H_seg; x_out: alpha_in[i]; R_in[i]; Re_D[i]; u_m[i])
  Call conduction_resistance(T_avg[i]; th_plate; A_cond : k_m[i]; R_cond[i])
  Call air_flow(T_C[i]; T_C[i-1]; T_avg[i]; P; m_dot_air; th_plate ;s_w_C;A_C ;L ;fin_thk ; 2 * s_w_C; k_m[i]; A_fin\A ;A_tot : alpha_out[i]; R_out[i]; eta_o[i]; DELTAP[i])
  R_tot[i] = R_in[i] + R_cond[i] + R_out[i]
  UA[i] = 1 / R_tot[i]
  CALL NH3H2O(123;T_H[i];P_H;x_out:T_x[i];P[i];x[i];h[i];s[i];u[i];v[i];q[i])
  c_H[i] = ((h[i-1] - h[i]) / (T_x[i-1] - T_x[i])) * 1000 "specific mixture heat capacity"
  call capacitance_rate(T_C[i];T_C[i-1];V_dot_C;m_dot_H_ch;P;c_H[i];c_C[i];C_dot_C[i];C_dot_H[i];C_dot_min[i];C_dot_max[i])
  DELTAT[i] = T_H[i] - T_C[i]
  DELTAT_lm_cf[i] = (DELTAT[i]-DELTAT[i-1]) / ln(DELTAT[i] / DELTAT[i-1])
  P_HX[i] = (T_C[i-1] - T_C[i]) / (T_H[i-1] - T_C[i])
  R_HX[i] = (T_H[i-1] - T_H[i]) / (T_C[i-1] - T_C[i])
  F_HX[i] = LMTD_CF('crossflow_both_unmixed';P_HX[i];R_HX[i])

```

```

DELTAT_lm[i] = DELTAT_lm_cf[i] * F_HX[i]
q_dot[i] = UA[i] * DELTAT_lm[i]
T_C_y[i-1] = T_C_y[i] + (q_dot[i] / C_dot_C[i]) "Air temperature at the given segment in the absorber"
h_H_y[i] = h_H_y[i-1] - (q_dot[i] / (m_dot_H_tot * 1000)) "mixture enthalpy at the given segment in the absorber"
CALL NH3H2O(234;P_H;x_out;h_H_y[i];T_H_y[i];P_y[i];x_y[i];h_y[i];s_y[i];u_y[i];v_y[i];q_y[i])
L_x[i] = L_x[i-1] - (L_H_seg / L_H_tot) "Changing absorber length for each segment"
end

```

"! First absorber iteration"

```

S_2 = S+2
T_C[S_2] = (T_C[1] + T_C_y[1]) / 2
T_H[S_2] = (T_H[1] + T_H_y[1]) / 2
DELTAT[S_2] = T_H[S_2] - T_C[S_2]
T_C_y[S_2+S] = T_C_in
T_H_y[S_2] = T_H_in
h_H_y[S_2] = h_in
DELTAT_C[S_2] = T_C[S_2] - T_C_in
DELTAT_H[S_2] = T_H_in - T_H[S_2+S]
CALL NH3H2O(123;T_H_in;P_H;x_out:T_x[S_2];P[S_2];x[S_2];h[S_2];s[S_2];u[S_2];v[S_2];q[S_2]) "Mixture inlet conditions"
L_x[S_2] = 1

```

duplicate i=(S_2+1) ; (S_2+S)

```

T_C[i] = (T_C[i-1] + T_C_y[i-1]) / 2
T_H[i] = (T_H[i-1] + T_H_y[i-1]) / 2
T_avg[i] = (T_H[i-1] + T_C[i]) / 2
T_bar_H[i] = (T_H[i-1] + T_H[i]) / 2
T_bar_C[i] = (T_C[i-1] + T_C[i]) / 2
CALL NH3H2O(128;T_bar_H[i];P_H;0:T_l[i];P_l[i];x_l[i];h_l[i];s_l[i];u_l[i];v_l[i];q_l[i])
Call thermophysical_properties(x_l[i];T_bar_H[i];T_c_sol[i];P_c_sol[i];lambda_sol[i];mu_sol[i])
Call tube_flow(m_dot_H_ch; mu_sol[i]; T_H[i-1]; T_H[i]; P_H; D_h; lambda_sol[i]; P_c_sol[i]; L_H_seg; x_out: alpha_in[i]; R_in[i]; Re_D[i]; u_m[i])
Call conduction_resistance(T_avg[i]; th_plate; A_cond : k_m[i]; R_cond[i])
Call air_flow(T_C[i]; T_C[i-1]; T_avg[i]; P; m_dot_air; th_plate ; s_w_C; A_C ; L ; fin_thk ; 2 * s_w_C; k_m[i]; A_fin\A ; A_tot : alpha_out[i]; R_out[i]; eta_o[i]; DELTAP[i])
R_tot[i] = R_in[i] + R_cond[i] + R_out[i]
UA[i] = 1 / R_tot[i]
CALL NH3H2O(123;T_H[i];P_H;x_out:T_x[i];P[i];x[i];h[i];s[i];u[i];v[i];q[i])
c_H[i] = ((h[i-1] - h[i]) / (T_x[i-1] - T_x[i])) * 1000
call capacitance_rate(T_C[i];T_C[i-1];V_dot_C;m_dot_H_ch;P;c_H[i];c_C[i];C_dot_H[i];C_dot_min[i];C_dot_max[i])
DELTAT[i] = T_H[i] - T_C[i]
DELTAT_lm_cf[i] = (DELTAT[i]-DELTAT[i-1]) / ln(DELTAT[i] / DELTAT[i-1])
P_HX[i] = (T_C[i-1] - T_C[i]) / (T_H[i-1] - T_C[i])
R_HX[i] = (T_H[i-1] - T_H[i]) / (T_C[i-1] - T_C[i])
F_HX[i] = LMTD_CF('crossflow_both_unmixed';P_HX[i];R_HX[i])
DELTAT_lm[i] = DELTAT_lm_cf[i] * F_HX[i]
q_dot[i] = UA[i] * DELTAT_lm[i]

```

```

T_C_y[i-1] = T_C_y[i] + (q_dot[i] / C_dot_C[i])
h_H_y[i] = h_H_y[i-1] - (q_dot[i] / (m_dot_H_tot * 1000))
CALL NH3H2O(234;P_H;x_out;h_H_y[i];T_H_y[i];P_y[i];x_y[i];h_y[i];s_y[i];u_y[i];v_y[i];q_y[i])
L_x[i] = L_x[i-1] - (L_H_seg / L_H_tot)
end

```

"! Second absorber iteration"

```

S_3 = 2 * S + 3
T_C[S_3] = (T_C[S_2] + T_C_y[S_2]) / 2
T_H[S_3] = (T_H[S_2] + T_H_y[S_2]) / 2
DELTAT[S_3] = T_H[S_3] - T_C[S_3]
T_C_y[S_3+S] = T_C_in
T_H_y[S_3] = T_H_in
h_H_y[S_3] = h_in
DELTAT_C[S_3] = T_C[S_3] - T_C_in
DELTAT_H[S_3] = T_H_in - T_H[S_3+S]
CALL NH3H2O(123;T_H_in;P_H;x_out:T_x[S_3];P[S_3];x[S_3];h[S_3];s[S_3];u[S_3];v[S_3];q[S_3]) "Mixture inlet conditions"
L_x[S_3] = 1

```

```
duplicate i = (S_3 + 1) ; (S_3 + S)
```

```

T_C[i] = (T_C[i-1] + T_C_y[i-1]) / 2
T_H[i] = (T_H[i-1] + T_H_y[i-1]) / 2
T_avg[i] = (T_H[i-1] + T_C[i]) / 2
T_bar_H[i] = (T_H[i-1] + T_H[i]) / 2
T_bar_C[i] = (T_C[i-1] + T_C[i]) / 2
CALL NH3H2O(128;T_bar_H[i];P_H;0:T_l[i];P_l[i];x_l[i];h_l[i];s_l[i];u_l[i];v_l[i];q_l[i])
Call thermophysical_properties(x_l[i];T_bar_H[i];T_c_sol[i];P_c_sol[i];lambda_sol[i];mu_sol[i])
Call tube_flow(m_dot_H_ch; mu_sol[i]; T_H[i-1]; T_H[i]; P_H; D_h; lambda_sol[i]; P_c_sol[i]; L_H_seg; x_out: alpha_in[i]; R_in[i]; Re_D[i]; u_m[i])
Call conduction_resistance(T_avg[i]; th_plate; A_cond : k_m[i]; R_cond[i])
Call air_flow(T_C[i]; T_C[i-1]; T_avg[i]; P ; m_dot_air; th_plate ; s_w_C; A_C ; L ; fin_thk ; 2 * s_w_C; k_m[i]; A_fin\A ; A_tot : alpha_out[i]; R_out[i]; eta_o[i]; DELTAP[i])
R_tot[i] = R_in[i] + R_cond[i] + R_out[i]
UA[i] = 1 / R_tot[i]
CALL NH3H2O(123;T_H[i];P_H;x_out:T_x[i];P[i];x[i];h[i];s[i];u[i];v[i];q[i])
c_H[i] = ((h[i-1] - h[i]) / (T_x[i-1] - T_x[i])) * 1000
call capacitance_rate(T_C[i];T_C[i-1];V_dot_C;m_dot_H_ch;P;c_H[i];c_C[i];C_dot_C[i];C_dot_H[i];C_dot_min[i];C_dot_max[i])
DELTAT[i] = T_H[i] - T_C[i]
DELTAT_lm_cf[i] = (DELTAT[i]-DELTAT[i-1]) / ln(DELTAT[i] / DELTAT[i-1])
P_HX[i] = (T_C[i-1] - T_C[i]) / (T_H[i-1] - T_C[i])
R_HX[i] = (T_H[i-1] - T_H[i]) / (T_C[i-1] - T_C[i])
F_HX[i] = LMTD_CF('crossflow_both_unmixed';P_HX[i];R_HX[i])
DELTAT_lm[i] = DELTAT_lm_cf[i] * F_HX[i]
q_dot[i] = UA[i] * DELTAT_lm[i]
T_C_y[i-1] = T_C_y[i] + (q_dot[i] / C_dot_C[i])
h_H_y[i] = h_H_y[i-1] - (q_dot[i] / (m_dot_H_tot * 1000))
CALL NH3H2O(234;P_H;x_out;h_H_y[i];T_H_y[i];P_y[i];x_y[i];h_y[i];s_y[i];u_y[i];v_y[i];q_y[i])
L_x[i] = L_x[i-1] - (L_H_seg / L_H_tot)

```

end

"! Third absorber iteration"

```

S_4 = 3 * S + 4
T_C[S_4] = (T_C[S_3] + T_C_y[S_3]) / 2
T_H[S_4] = (T_H[S_3] + T_H_y[S_3]) / 2
DELTAT[S_4] = T_H[S_4] - T_C[S_4]
T_C_y[S_4+S] = T_C_in
T_H_y[S_4] = T_H_in
h_H_y[S_4] = h_in
DELTAT_C[S_4] = T_C[S_4] - T_C_in
DELTAT_H[S_4] = T_H_in - T_H[S_4+S]
CALL NH3H2O(123;T_H_in;P_H;x_out:T_x[S_4];P[S_4];x[S_4];h[S_4];s[S_4];u[S_4];v[S_4];q[S_4])    "Mixture inlet conditions"
L_x[S_4] = 1

```

duplicate i = (S_4 + 1) ; (S_4 + S)

```

T_C[i] = (T_C[i-1] + T_C_y[i-1]) / 2
T_H[i] = (T_H[i-1] + T_H_y[i-1]) / 2
T_avg[i] = (T_H[i-1] + T_C[i]) / 2
T_bar_H[i] = (T_H[i-1] + T_H[i]) / 2
T_bar_C[i] = (T_C[i-1] + T_C[i]) / 2
CALL NH3H2O(128;T_bar_H[i];P_H;0:T_l[i];P_l[i];x_l[i];h_l[i];s_l[i];u_l[i];v_l[i];q_l[i])
Call thermophysical_properties(x_l[i];T_bar_H[i];T_c_sol[i];P_c_sol[i];lambda_sol[i];mu_sol[i])
Call tube_flow(m_dot_H_ch; mu_sol[i]; T_H[i-1]; T_H[i]; P_H; D_h; lambda_sol[i]; P_c_sol[i]; L_H_seg; x_out: alpha_in[i]; R_in[i]; Re_D[i]; u_m[i])
Call conduction_resistance(T_avg[i]; th_plate; A_cond : k_m[i]; R_cond[i])
Call air_flow(T_C[i]; T_C[i-1]; T_avg[i]; P; m_dot_air; th_plate; s_w_C; A_C; L; fin_thk ; 2 * s_w_C; k_m[i]; A_fin^A; A_tot : alpha_out[i]; R_out[i]; eta_o[i]; DELTAP[i])
R_tot[i] = R_in[i] + R_cond[i] + R_out[i]
UA[i] = 1 / R_tot[i]
CALL NH3H2O(123;T_H[i];P_H;x_out:T_x[i];P[i];x[i];h[i];s[i];u[i];v[i];q[i])
c_H[i] = ((h[i-1] - h[i]) / (T_x[i-1] - T_x[i])) * 1000
call capacitance_rate(T_C[i];T_C[i-1];V_dot_C;m_dot_H_ch;P;c_H[i];c_C[i];C_dot_C[i];C_dot_H[i];C_dot_min[i];C_dot_max[i])
DELTAT[i] = T_H[i] - T_C[i]
DELTAT_lm_cf[i] = (DELTAT[i]-DELTAT[i-1]) / ln(DELTAT[i] / DELTAT[i-1])
P_HX[i] = (T_C[i-1] - T_C[i]) / (T_H[i-1] - T_C[i])
R_HX[i] = (T_H[i-1] - T_H[i]) / (T_C[i-1] - T_C[i])
F_HX[i] = LMTD_CF('crossflow_both_unmixed';P_HX[i];R_HX[i])
DELTAT_lm[i] = DELTAT_lm_cf[i] * F_HX[i]
q_dot[i] = UA[i] * DELTAT_lm[i]
T_C_y[i-1] = T_C_y[i] + (q_dot[i] / C_dot_C[i])
h_H_y[i] = h_H_y[i-1] - (q_dot[i] / (m_dot_H_tot * 1000))
CALL NH3H2O(234;P_H;x_out;h_H_y[i];T_H_y[i];P_y[i];x_y[i];h_y[i];s_y[i];u_y[i];v_y[i];q_y[i])
L_x[i] = L_x[i-1] - (L_H_seg / L_H_tot)

```

end

"! fourth absorber iteration"

S_5 = 4 * S + 5

```

T_C [S_5] = (T_C[S_4] + T_C_y[S_4]) / 2
T_H [S_5] = (T_H[S_4] + T_H_y[S_4]) / 2
DELTAT[S_5] = T_H[S_5] - T_C[S_5]
T_C_y[S_5+S] = T_C_in
T_H_y[S_5] = T_H_in
h_H_y[S_5] = h_in
DELTAT_C[S_5] = T_C[S_5] - T_C_in
DELTAT_H[S_5] = T_H_in - T_H[S_5+S]
CALL NH3H2O(123;T_H_in;P_H;x_out:T_x[S_5];P[S_5];x[S_5];h[S_5];s[S_5];u[S_5];v[S_5];q[S_5])      "Mixture inlet conditions"
L_x[S_5] = 1

duplicate i = (S_5 + 1) ; (S_5 + S)
  T_C[i] = (T_C[i-11] + T_C_y[i-11]) / 2
  T_H[i] = (T_H[i-11] + T_H_y[i-11]) / 2
  T_avg[i] = (T_H[i-1] + T_C[i]) / 2
  T_bar_H[i] = (T_H[i-1] + T_H[i]) / 2
  T_bar_C[i] = (T_C[i-1] + T_C[i]) / 2
  CALL NH3H2O(128;T_bar_H[i];P_H;0:T_l[i];P_l[i];x_l[i];h_l[i];s_l[i];u_l[i];v_l[i];q_l[i])
  Call thermophysical_properties(x_l[i];T_bar_H[i];T_c_sol[i];P_c_sol[i];lambda_sol[i];mu_sol[i])
  Call tube_flow(m_dot_H_ch; mu_sol[i]; T_H[i-1]; T_H[i]; P_H; D_h; lambda_sol[i]; P_c_sol[i]; L_H_seg; x_out: alpha_in[i]; R_in[i]; Re_D[i]; u_m[i])
  Call conduction_resistance(T_avg[i]; th_plate; A_cond : k_m[i]; R_cond[i])
  Call air_flow(T_C[i]; T_C[i-1]; T_avg[i]; P; m_dot_air; th_plate; s_w_C; A_C; L; fin_thk ; 2 * s_w_C; k_m[i]; A_fin/A; A_tot : alpha_out[i]; R_out[i]; eta_o[i]; DELTAP[i])
  R_tot[i] = R_in[i] + R_cond[i] + R_out[i]
  UA[i] = 1 / R_tot[i]
  CALL NH3H2O(123;T_H[i];P_H;x_out:T_x[i];P[i];x[i];h[i];s[i];u[i];v[i];q[i])
  c_H[i] = ((h[i-1] - h[i]) / (T_x[i-1] - T_x[i])) * 1000
  call capacitance_rate(T_C[i];T_C[i-1];V_dot_C;m_dot_H_ch;P;c_H[i];c_C[i];C_dot_C[i];C_dot_H[i];C_dot_min[i];C_dot_max[i])
  DELTAT[i] = T_H[i] - T_C[i]
  DELTAT_lm_cf[i] = (DELTAT[i]-DELTAT[i-1]) / ln(DELTAT[i] / DELTAT[i-1])
  P_HX[i] = (T_C[i-1] - T_C[i]) / (T_H[i-1] - T_C[i])
  R_HX[i] = (T_H[i-1] - T_H[i]) / (T_C[i-1] - T_C[i])
  F_HX[i] = LMTD_CF('crossflow_both_unmixed';P_HX[i];R_HX[i])
  DELTAT_lm[i] = DELTAT_lm_cf[i] * F_HX[i]
  q_dot[i] = UA[i] * DELTAT_lm[i]
  T_C_y[i-1] = T_C_y[i] + (q_dot[i] / C_dot_C[i])
  h_H_y[i] = h_H_y[i-1] - (q_dot[i] / (m_dot_H_tot * 1000))
  CALL NH3H2O(234;P_H;x_out:h_H_y[i];T_H_y[i];P_y[i];x_y[i];h_y[i];s_y[i];u_y[i];v_y[i];q_y[i])
  L_x[i] = L_x[i-1] - (L_H_seg / L_H_tot)
end

"! Fifth absorber iteration"
S_6 = 5 * S + 6
T_C [S_6] = (T_C[S_5] + T_C_y[S_5]) / 2
T_H [S_6] = (T_H[S_5] + T_H_y[S_5]) / 2
DELTAT[S_6] = T_H[S_6] - T_C[S_6]
T_C_y[S_6+S] = T_C_in

```

```

T_H_y[S_6] = T_H_in
h_H_y[S_6] = h_in
DELTAT_C[S_6] = T_C[S_6] - T_C_in
DELTAT_H[S_6] = T_H_in - T_H[S_6+S]
CALL NH3H2O(123;T_H_in;P_H;x_out:T_x[S_6];P[S_6];x[S_6];h[S_6];s[S_6];u[S_6];v[S_6];q[S_6])    "Mixture inlet conditions"
L_x[S_6] = 1

duplicate i = (S_6 + 1) ; (S_6 + S)
  T_C[i] = (T_C[i-11] + T_C_y[i-11]) / 2
  T_H[i] = (T_H[i-11] + T_H_y[i-11]) / 2
  T_avg[i] = (T_H[i-1] + T_C[i]) / 2
  T_bar_H[i] = (T_H[i-1] + T_H[i]) / 2
  T_bar_C[i] = (T_C[i-1] + T_C[i]) / 2
  CALL NH3H2O(128;T_bar_H[i];P_H;0:T_l[i];P_l[i];x_l[i];h_l[i];s_l[i];u_l[i];v_l[i];q_l[i])
  Call thermophysical_properties(x_l[i];T_bar_H[i];T_c_sol[i];P_c_sol[i];lambda_sol[i];mu_sol[i])
  Call tube_flow(m_dot_H_ch; mu_sol[i]; T_H[i-1]; T_H[i]; P_H; D_h; lambda_sol[i]; P_c_sol[i]; L_H_seg; x_out: alpha_in[i]; R_in[i]; Re_D[i]; u_m[i])
  Call conduction_resistance(T_avg[i]; th_plate; A_cond : k_m[i]; R_cond[i])
  Call air_flow(T_C[i]; T_C[i-1]; T_avg[i]; P; m_dot_air; th_plate; s_w_C; A_C; L; fin_thk ; 2 * s_w_C; k_m[i]; A_fin^A; A_tot : alpha_out[i]; R_out[i]; eta_o[i]; DELTAP[i])
  R_tot[i] = R_in[i] + R_cond[i] + R_out[i]
  UA[i] = 1 / R_tot[i]
  CALL NH3H2O(123;T_H[i];P_H;x_out:T_x[i];P[i];x[i];h[i];s[i];u[i];v[i];q[i])
  c_H[i] = ((h[i-1] - h[i]) / (T_x[i-1] - T_x[i])) * 1000
  call capacitance_rate(T_C[i];T_C[i-1];V_dot_C;m_dot_H_ch;P;c_H[i];c_C[i];C_dot_C[i];C_dot_H[i];C_dot_min[i];C_dot_max[i])
  DELTAT[i] = T_H[i] - T_C[i]
  DELTAT_lm_cf[i] = (DELTAT[i]-DELTAT[i-1]) / ln(DELTAT[i] / DELTAT[i-1])
  P_HX[i] = (T_C[i-1] - T_C[i]) / (T_H[i-1] - T_C[i])
  R_HX[i] = (T_H[i-1] - T_H[i]) / (T_C[i-1] - T_C[i])
  F_HX[i] = LMTD_CF('crossflow_both_unmixed';P_HX[i];R_HX[i])
  DELTAT_lm[i] = DELTAT_lm_cf[i] * F_HX[i]
  q_dot[i] = UA[i] * DELTAT_lm[i]
  T_C_y[i-1] = T_C_y[i] + (q_dot[i] / C_dot_C[i])
  h_H_y[i] = h_H_y[i-1] - (q_dot[i] / (m_dot_H_tot * 1000))
  CALL NH3H2O(234;P_H;x_out:h_H_y[i];T_H_y[i];P_y[i];x_y[i];h_y[i];s_y[i];u_y[i];v_y[i];q_y[i])
  L_x[i] = L_x[i-1] - (L_H_seg / L_H_tot)
end

"! Sixt absorber iteration"
S_7 = 6 * S + 7
T_C [S_7] = (T_C[S_6] + T_C_y[S_6]) / 2
T_H [S_7] = (T_H[S_6] + T_H_y[S_6]) / 2
DELTAT[S_7] = T_H[S_7] - T_C[S_7]
T_C_y[S_7+S] = T_C_in
T_H_y[S_7] = T_H_in
h_H_y[S_7] = h_in
DELTAT_C[S_7] = T_C[S_7] - T_C_in
DELTAT_H[S_7] = T_H_in - T_H[S_7+S]

```


CALL NH3H2O(123;T_H_in;P_H;x_out:T_x[S_7];P[S_7];x[S_7];h[S_7];s[S_7];u[S_7];v[S_7];q[S_7]) "Mixture inlet conditions"
L_x[S_7] = 1

```
duplicate i = (S_7 + 1) ; (S_7 + S)
  T_C[i] = (T_C[i-11] + T_C_y[i-11]) / 2
  T_H[i] = (T_H[i-11] + T_H_y[i-11]) / 2
  T_avg[i] = (T_H[i-1] + T_C[i]) / 2
  T_bar_H[i] = (T_H[i-1] + T_H[i]) / 2
  T_bar_C[i] = (T_C[i-1] + T_C[i]) / 2
  CALL NH3H2O(128;T_bar_H[i];P_H;0:T_l[i];P_l[i];x_l[i];h_l[i];s_l[i];u_l[i];v_l[i];q_l[i])
  Call thermophysical_properties(x_l[i];T_bar_H[i];T_c_sol[i];P_c_sol[i];lambda_sol[i];mu_sol[i])
  Call tube_flow(m_dot_H_ch; mu_sol[i]; T_H[i-1]; T_H[i]; P_H; D_h; lambda_sol[i]; P_c_sol[i]; L_H_seg; x_out: alpha_in[i]; R_in[i]; Re_D[i]; u_m[i])
  Call conduction_resistance(T_avg[i]; th_plate; A_cond : k_m[i]; R_cond[i])
  Call air_flow(T_C[i] ; T_C[i-1] ; T_avg[i] ; P ; m_dot_air; th_plate ; s_w_C; A_C ; L ; fin_thk ; 2 * s_w_C; k_m[i]; A_fin\A ; A_tot : alpha_out[i]; R_out[i]; eta_o[i]; DELTAP[i])
  R_tot[i] = R_in[i] + R_cond[i] + R_out[i]
  UA[i] = 1 / R_tot[i]
  CALL NH3H2O(123;T_H[i];P_H;x_out:T_x[i];P[i];x[i];h[i];s[i];u[i];v[i];q[i])
  c_H[i] = ((h[i-1] - h[i]) / (T_x[i-1] - T_x[i])) * 1000
  call capacitance_rate(T_C[i];T_C[i-1];V_dot_C;m_dot_H_ch;P;c_H[i];c_C[i];C_dot_C[i];C_dot_H[i];C_dot_min[i];C_dot_max[i])
  DELTAT[i] = T_H[i] - T_C[i]
  DELTAT_lm_cf[i] = (DELATAT[i]-DELATAT[i-1]) / ln(DELATAT[i] / DELATAT[i-1])
  P_HX[i] = (T_C[i-1] - T_C[i]) / (T_H[i-1] - T_C[i])
  R_HX[i] = (T_H[i-1] - T_H[i]) / (T_C[i-1] - T_C[i])
  F_HX[i] = LMTD_CF('crossflow_both_unmixed';P_HX[i];R_HX[i])
  DELTAT_lm[i] = DELTAT_lm_cf[i] * F_HX[i]
  q_dot[i] = UA[i] * DELTAT_lm[i]
  T_C_y[i-1] = T_C_y[i] + (q_dot[i] / C_dot_C[i])
  h_H_y[i] = h_H_y[i-1] - (q_dot[i] / (m_dot_H_tot * 1000))
  CALL NH3H2O(234;P_H;x_out:h_H_y[i];T_H_y[i];P_y[i];x_y[i];h_y[i];s_y[i];u_y[i];v_y[i];q_y[i])
  L_x[i] = L_x[i-1] - (L_H_seg / L_H_tot)
```

end

"! Seventh absorber iteration"

```
S_8 = 7 * S + 8
T_C [S_8] = (T_C[S_7] + T_C_y[S_7]) / 2
T_H [S_8] = (T_H[S_7] + T_H_y[S_7]) / 2
DELATAT[S_8] = T_H[S_8] - T_C[S_8]
T_C_y[S_8+S] = T_C_in
T_H_y[S_8] = T_H_in
h_H_y[S_8] = h_in
DELATAT_C[S_8] = T_C[S_8] - T_C_in
DELATAT_H[S_8] = T_H_in - T_H[S_8+S]
CALL NH3H2O(123;T_H_in;P_H;x_out:T_x[S_8];P[S_8];x[S_8];h[S_8];s[S_8];u[S_8];v[S_8];q[S_8]) "Mixture inlet conditions"  
L_x[S_8] = 1
```

duplicate i = (S_8 + 1) ; (S_8 + S)

```

T_C[i] = (T_C[i-11] + T_C_y[i-11]) / 2
T_H[i] = (T_H[i-11] + T_H_y[i-11]) / 2
T_avg[i] = (T_H[i-1] + T_C[i]) / 2
T_bar_H[i] = (T_H[i-1] + T_H[i]) / 2
T_bar_C[i] = (T_C[i-1] + T_C[i]) / 2
CALL NH3H2O(128;T_bar_H[i];P_H;0:T_l[i];P_l[i];x_l[i];h_l[i];s_l[i];u_l[i];v_l[i];q_l[i])
Call thermophysical_properties(x_l[i];T_bar_H[i];T_c_sol[i];P_c_sol[i];lambda_sol[i];mu_sol[i])
Call tube_flow(m_dot_H_ch; mu_sol[i]; T_H[i-1]; T_H[i]; P_H; D_h; lambda_sol[i]; P_c_sol[i]; L_H_seg; x_out: alpha_in[i]; R_in[i]; Re_D[i]; u_m[i])
Call conduction_resistance(T_avg[i]; th_plate; A_cond : k_m[i]; R_cond[i])
Call air_flow(T_C[i]; T_C[i-1]; T_avg[i]; P; m_dot_air; th_plate; s_w_C; A_C; L; fin_thk ; 2 * s_w_C; k_m[i]; A_fin\A ; A_tot : alpha_out[i]; R_out[i]; eta_o[i]; DELTAP[i])
R_tot[i] = R_in[i] + R_cond[i] + R_out[i]
UA[i] = 1 / R_tot[i]
CALL NH3H2O(123;T_H[i];P_H;x_out:T_x[i];P[i];x[i];h[i];s[i];u[i];v[i];q[i])
c_H[i] = ((h[i-1] - h[i]) / (T_x[i-1] - T_x[i])) * 1000
call capacitance_rate(T_C[i];T_C[i-1];V_dot_C;m_dot_H_ch;P;c_H[i];c_C[i];C_dot_C[i];C_dot_H[i];C_dot_min[i];C_dot_max[i])
DELTAT[i] = T_H[i] - T_C[i]
DELTAT_lm_cf[i] = (DELTAT[i]-DELTAT[i-1]) / ln(DELTAT[i] / DELTAT[i-1])
P_HX[i] = (T_C[i-1] - T_C[i]) / (T_H[i-1] - T_C[i])
R_HX[i] = (T_H[i-1] - T_H[i]) / (T_C[i-1] - T_C[i])
F_HX[i] = LMTD_CF('crossflow_both_unmixed';P_HX[i];R_HX[i])
DELTAT_lm[i] = DELTAT_lm_cf[i] * F_HX[i]
q_dot[i] = UA[i] * DELTAT_lm[i]
T_C_y[i-1] = T_C_y[i] + (q_dot[i] / C_dot_C[i])
h_H_y[i] = h_H_y[i-1] - (q_dot[i] / (m_dot_H_tot * 1000))
CALL NH3H2O(234;P_H;x_out:h_H_y[i];T_H_y[i];P_y[i];x_y[i];h_y[i];s_y[i];u_y[i];v_y[i];q_y[i])
L_x[i] = L_x[i-1] - (L_H_seg / L_H_tot)

```

end

"! Eighth absorber iteration"

```

S_9 = 8 * S + 9
T_C[S_9] = (T_C[S_8] + T_C_y[S_8]) / 2
T_H[S_9] = (T_H[S_8] + T_H_y[S_8]) / 2
DELTAT[S_9] = T_H[S_9] - T_C[S_9]
T_C_y[S_9+S] = T_C_in
T_H_y[S_9] = T_H_in
h_H_y[S_9] = h_in
DELTAT_C[S_9] = T_C[S_9] - T_C_in
DELTAT_H[S_9] = T_H_in - T_H[S_9+S]
CALL NH3H2O(123;T_H_in;P_H;x_out:T_x[S_9];P[S_9];x[S_9];h[S_9];s[S_9];u[S_9];v[S_9];q[S_9])
L_x[S_9] = 1

```

"Mixture inlet conditions"

duplicate i = (S_9 + 1) ; (S_9 + S)

```

T_C[i] = (T_C[i-11] + T_C_y[i-11]) / 2
T_H[i] = (T_H[i-11] + T_H_y[i-11]) / 2
T_avg[i] = (T_H[i-1] + T_C[i]) / 2
T_bar_H[i] = (T_H[i-1] + T_H[i]) / 2

```

```

T_bar_C[i] = (T_C[i-1] + T_C[i]) / 2
CALL NH3H2O(128;T_bar_H[i];P_H;0:T_l[i];P_l[i];x_l[i];h_l[i];s_l[i];u_l[i];v_l[i];q_l[i])
Call thermophysical_properties(x_l[i];T_bar_H[i];T_c_sol[i];P_c_sol[i];lambda_sol[i];mu_sol[i])
Call tube_flow(m_dot_H_ch; mu_sol[i]; T_H[i-1]; T_H[i]; P_H; D_h; lambda_sol[i]; P_c_sol[i]; L_H_seg; x_out: alpha_in[i]; R_in[i]; Re_D[i]; u_m[i])
Call conduction_resistance(T_avg[i]; th_plate; A_cond : k_m[i]; R_cond[i])
Call air_flow(T_C[i]; T_C[i-1]; T_avg[i]; P; m_dot_air; th_plate; s_w_C; A_C; L; fin_thk ; 2 * s_w_C; k_m[i]; A_fin\A ; A_tot : alpha_out[i]; R_out[i]; eta_o[i]; DELTAP[i])
R_tot[i] = R_in[i] + R_cond[i] + R_out[i]
UA[i] = 1 / R_tot[i]
CALL NH3H2O(123;T_H[i];P_H;x_out:T_x[i];P[i];x[i];h[i];s[i];u[i];v[i];q[i])
c_H[i] = ((h[i-1] - h[i]) / (T_x[i-1] - T_x[i])) * 1000
call capacitance_rate(T_C[i];T_C[i-1];V_dot_C;m_dot_H_ch;P;c_H[i];c_C[i];C_dot_C[i];C_dot_H[i];C_dot_min[i];C_dot_max[i])
DELTAT[i] = T_H[i] - T_C[i]
DELTAT_lm_cf[i] = (DELTAT[i]-DELTAT[i-1]) / ln(DELTAT[i] / DELTAT[i-1])
P_HX[i] = (T_C[i-1] - T_C[i]) / (T_H[i-1] - T_C[i])
R_HX[i] = (T_H[i-1] - T_H[i]) / (T_C[i-1] - T_C[i])
F_HX[i] = LMTD_CF('crossflow_both_unmixed';P_HX[i];R_HX[i])
DELTAT_lm[i] = DELTAT_lm_cf[i] * F_HX[i]
q_dot[i] = UA[i] * DELTAT_lm[i]
T_C_y[i-1] = T_C_y[i] + (q_dot[i] / C_dot_C[i])
h_H_y[i] = h_H_y[i-1] - (q_dot[i] / (m_dot_H_tot * 1000))
CALL NH3H2O(234;P_H;x_out;h_H_y[i];T_H_y[i];P_y[i];x_y[i];h_y[i];s_y[i];u_y[i];v_y[i];q_y[i])
L_x[i] = L_x[i-1] - (L_H_seg / L_H_tot)
end

```

"! Ninth absorber iteration"

```

S_10 = 9 * S + 10
T_C[S_10] = (T_C[S_9] + T_C_y[S_9]) / 2
T_H[S_10] = (T_H[S_9] + T_H_y[S_9]) / 2
DELTAT[S_10] = T_H[S_10] - T_C[S_10]
T_C_y[S_10+S] = T_C_in
T_H_y[S_10] = T_H_in
h_H_y[S_10] = h_in
DELTAT_C[S_10] = T_C[S_10] - T_C_in
DELTAT_H[S_10] = T_H_in - T_H[S_10+S]
CALL NH3H2O(123;T_H_in;P_H;x_out:T_x[S_10];P[S_10];x[S_10];h[S_10];s[S_10];u[S_10];v[S_10];q[S_10])
L_x[S_10] = 1

```

"Mixture inlet conditions"

duplicate i = (S_10 + 1) ; (S_10 + S)

```

T_C[i] = (T_C[i-11] + T_C_y[i-11]) / 2
T_H[i] = (T_H[i-11] + T_H_y[i-11]) / 2
T_avg[i] = (T_H[i-1] + T_C[i]) / 2
T_bar_H[i] = (T_H[i-1] + T_H[i]) / 2
T_bar_C[i] = (T_C[i-1] + T_C[i]) / 2
CALL NH3H2O(128;T_bar_H[i];P_H;0:T_l[i];P_l[i];x_l[i];h_l[i];s_l[i];u_l[i];v_l[i];q_l[i])
Call thermophysical_properties(x_l[i];T_bar_H[i];T_c_sol[i];P_c_sol[i];lambda_sol[i];mu_sol[i])
Call tube_flow(m_dot_H_ch; mu_sol[i]; T_H[i-1]; T_H[i]; P_H; D_h; lambda_sol[i]; P_c_sol[i]; L_H_seg; x_out: alpha_in[i]; R_in[i]; Re_D[i]; u_m[i])

```

```

Call conduction_resistance(T_avg[i]; th_plate; A_cond : k_m[i]; R_cond[i])
Call air_flow(T_C[i]; T_C[i-1]; T_avg[i]; P; m_dot_air; th_plate; s_w_C; A_C ; L ; fin_thk ; 2 * s_w_C; k_m[i]; A_fin\A ; A_tot : alpha_out[i]; R_out[i]; eta_o[i]; DELTAP[i])
R_tot[i] = R_in[i] + R_cond[i] + R_out[i]
UA[i] = 1 / R_tot[i]
CALL NH3H2O(123;T_H[i];P_H;x_out:T_x[i];P[i];x[i];h[i];s[i];u[i];v[i];q[i])
c_H[i] = ((h[i-1] - h[i]) / (T_x[i-1] - T_x[i])) * 1000
call capacitance_rate(T_C[i];T_C[i-1];V_dot_C;m_dot_H_ch;P;c_H[i];c_C[i];C_dot_C[i];C_dot_H[i];C_dot_min[i];C_dot_max[i])
DELTAT[i] = T_H[i] - T_C[i]
DELTAT_lm_cf[i] = (DELTAT[i]-DELTAT[i-1]) / ln(DELTAT[i] / DELTAT[i-1])
P_HX[i] = (T_C[i-1] - T_C[i]) / (T_H[i-1] - T_C[i])
R_HX[i] = (T_H[i-1] - T_H[i]) / (T_C[i-1] - T_C[i])
F_HX[i] = LMTD_CF('crossflow_both_unmixed';P_HX[i];R_HX[i])
DELTAT_lm[i] = DELTAT_lm_cf[i] * F_HX[i]
q_dot[i] = UA[i] * DELTAT_lm[i]
T_C_y[i-1] = T_C_y[i] + (q_dot[i] / C_dot_C[i])
h_H_y[i] = h_H_y[i-1] - (q_dot[i] / (m_dot_H_tot * 1000))
CALL NH3H2O(234;P_H;x_out:h_H_y[i];T_H_y[i];P_y[i];x_y[i];h_y[i];s_y[i];u_y[i];v_y[i];q_y[i])
L_x[i] = L_x[i-1] - (L_H_seg / L_H_tot)

```

end

"! Tenth absorber iteration"

```

S_11 = 10 * S + 11
T_C[S_11] = (T_C[S_10] + T_C_y[S_10]) / 2
T_H[S_11] = (T_H[S_10] + T_H_y[S_10]) / 2
DELTAT[S_11] = T_H[S_11] - T_C[S_11]
T_C_y[S_11+S] = T_C_in
T_H_y[S_11] = T_H_in
h_H_y[S_11] = h_in
DELTAT_C[S_11] = T_C[S_11] - T_C_in
DELTAT_H[S_11] = T_H_in - T_H[S_11+S]
CALL NH3H2O(123;T_H_in;P_H;x_out:T_x[S_11];P[S_11];x[S_11];h[S_11];s[S_11];u[S_11];v[S_11];q[S_11])
L_x[S_11] = 1

```

"Mixture inlet conditions"

duplicate i = (S_11 + 1) ; (S_11 + S)

```

T_C[i] = (T_C[i-11] + T_C_y[i-11]) / 2
T_H[i] = (T_H[i-11] + T_H_y[i-11]) / 2
T_avg[i] = (T_H[i-1] + T_C[i]) / 2
T_bar_H[i] = (T_H[i-1] + T_H[i]) / 2
T_bar_C[i] = (T_C[i-1] + T_C[i]) / 2
CALL NH3H2O(128;T_bar_H[i];P_H;0:T_l[i];P_l[i];x_l[i];h_l[i];s_l[i];u_l[i];v_l[i];q_l[i])
Call thermophysical_properties(x_l[i];T_bar_H[i];T_c_sol[i];P_c_sol[i];lambda_sol[i];mu_sol[i])
Call tube_flow(m_dot_H_ch; mu_sol[i]; T_H[i-1]; T_H[i]; P_H; D_h; lambda_sol[i]; P_c_sol[i]; L_H_seg; x_out: alpha_in[i]; R_in[i]; Re_D[i]; u_m[i])
Call conduction_resistance(T_avg[i]; th_plate; A_cond : k_m[i]; R_cond[i])
Call air_flow(T_C[i]; T_C[i-1]; T_avg[i]; P; m_dot_air; th_plate; s_w_C; A_C ; L ; fin_thk ; 2 * s_w_C; k_m[i]; A_fin\A ; A_tot : alpha_out[i]; R_out[i]; eta_o[i]; DELTAP[i])
R_tot[i] = R_in[i] + R_cond[i] + R_out[i]
UA[i] = 1 / R_tot[i]

```

```

CALL NH3H2O(123;T_H[i];P_H;x_out:T_x[i];P[i];x[i];h[i];s[i];u[i];v[i];q[i])
c_H[i] = ((h[i-1] - h[i]) / (T_x[i-1] - T_x[i])) * 1000
call capacitance_rate(T_C[i];T_C[i-1];V_dot_C;m_dot_H_ch;P;c_H[i];c_C[i];C_dot_C[i];C_dot_H[i];C_dot_min[i];C_dot_max[i])
DELTAT[i] = T_H[i] - T_C[i]
DELTAT_lm_cf[i] = (DELTAT[i]-DELTAT[i-1]) / ln(DELTAT[i] / DELTAT[i-1])
P_HX[i] = (T_C[i-1] - T_C[i]) / (T_H[i-1] - T_C[i])
R_HX[i] = (T_H[i-1] - T_H[i]) / (T_C[i-1] - T_C[i])
F_HX[i] = LMTD_CF('crossflow_both_unmixed';P_HX[i];R_HX[i])
DELTAT_lm[i] = DELTAT_lm_cf[i] * F_HX[i]
q_dot[i] = UA[i] * DELTAT_lm[i]
T_C_y[i-1] = T_C_y[i] + (q_dot[i] / C_dot_C[i])
h_H_y[i] = h_H_y[i-1] - (q_dot[i] / (m_dot_H_tot * 1000))
CALL NH3H2O(234;P_H;x_out;h_H_y[i];T_H_y[i];P_y[i];x_y[i];h_y[i];s_y[i];u_y[i];v_y[i];q_y[i])
L_x[i] = L_x[i-1] - (L_H_seg / L_H_tot)
end

duplicate i = 1; (S+1) "from Kelvin to Celcius conversion "
  T_H_celsius[i] = T_H_y[i] - 273,15
  T_C_celsius[i] = T_C_y[i] - 273,15
end

duplicate i = (S_11); (S_11+S) "from Kelvin to Celcius conversion "
  T_H_celsius[i] = T_H_y[i] - 273,15
  T_C_celsius[i] = T_C_y[i] - 273,15
end

Q_11 = (h_H_y[S_11] - h_H_y[S_11 + S]) * m_dot_H_tot "calculated heat transfer"

R_cond_avg = (sum(R_cond[i]; i=(S_11+1); (S_11+S)))/10 "average conduction resistance"
R_in_avg = (sum(R_in[i]; i=(S_11+1); (S_11+S)))/10 "avg inner thermal resistance"
R_out_avg = (sum(R_out[i]; i=(S_11+1); (S_11+S)))/10 "avg outer thermal resistance"
R_tot_avg = (sum(R_tot[i]; i=(S_11+1); (S_11+S)))/10 "total avg thermal resistance"
alpha_in_avg = (sum(alpha_in[i]; i=(S_11+1); (S_11+S)))/10 "avg mixture heat transfer coefficient"
alpha_out_avg = (sum(alpha_out[i]; i=(S_11+1); (S_11+S)))/10 "avg air heat transfer coefficient"
u_m_avg = (sum(u_m[i]; i=(S_11+1); (S_11+S)))/10 "avg mean velocity through the absorber"

q_dot_10 = sum(q_dot[i] ; i = (S_11 + 1) ; (S_11+S))
theta_H = (T_H[S_11] - T_C[S_11]) "tempeature difference to calculate LMTD"
theta_C = (T_H[S_11 + S] - T_C[S_11 + S]) "tempeature difference to calculate LMTD"
DELTAT_LMTD = (theta_H - theta_c) / ln(theta_H / theta_C)
DELTAP = sum(DELTAP[i] ; i = (S_11 + 1) ; (S_11 + S)) "total pressure drop throught the absorber"
W_dot_fan = ((2 * DELTAP * V_dot_C) / eta_fan) / 1000 "required fan power input"

```

Scientific Paper

Optimizing the Compression/Absorption Heat Pump System at High Temperatures

Martin BERGLAND^(*)

^(*) Norwegian University of Science and Technology, Kolbjorn Hejes vei 1D, Trondheim, 7049, Norway
martberg@stud.ntnu.no

ABSTRACT

Two separate simulation models were developed comprising a two-stage CAHP system and an absorber model using ammonia-water. The two-stage CAHP system was simulated at four different compressor discharge temperature limitations. The absorber model compared five different compact heat exchangers heating air in a cross-flow. The two-stage process investigated the benefits of the desuperheater, where the supply temperatures with and without the desuperheater were nearly the same. Maximum supply temperatures were obtained at 171.8°C with a COP of 2.08, when the maximum discharge temperature was set to 250°C. Simulations from the absorber model yielded much larger mass flow rate for the air than for the mixture. The heat exchange between the air and the mixture was sensitive to the absorber height and the air mass flow rate, which resulted in large fan work. Finned flat tube heat exchangers gave the best results with respect to the absorber height and fan work.

1. INTRODUCTION

Large amounts of low grade waste heat are not exploited, due to lack of waste heat utilization. Available waste heat has a temperature range suited as heat sources for heat pumps in industrial processes at higher temperatures (Chan et al., 2013). Simultaneously, the demands for environmentally benign working fluids become more dominant. Therefore, compression-absorption heat pumps (CAHP) could be more useful in high temperature processes. The CAHP is based on the Osenbrück cycle, comprising a vapour compression heat pump with a solution circuit (Osenbrück, 1895). Working fluids used in the CAHP are zeotropic, where the heat exchanges occur at gliding temperatures. Ammonia-water is a typical working fluid used in the compression-absorption heat pumps. Hultén and Berntsson (1999) compared the CAHP to a relevant compression heat pump at high temperature operations. Characteristics as small swept compressor volume, high heat transfer coefficients, environmentally friendly working fluids, good capacity control and high achievable working temperatures were advantages listed by Hultén and Berntsson (1999). Their results concluded that the CAHP was favourable for heat sink and heat source temperature glides larger than 10 K.

The absorber which is the heat exchanger delivering heat in CAHP process has a significant impact on the process performance. Fernández – Seara (2007) et al. carried out an investigation of vertical tubular absorbers cooled by air using ammonia-water as working fluid. Results from the paper showed that the fin spacing should be reduced as much as possible, in order to reduce the absorber length. Optimal tube diameter could also reduce the absorber length. Another variable that could increase the absorber length was decreased air velocities.

One design constraint that is dominant for heat pumping processes is the compressor discharge temperature. Jensen et al. (2014) investigated the set of feasible combinations of ammonia concentration and liquid circulation ratio for supply temperatures up to 175°C. At supply temperatures of 150°C and up to 175°C were feasible using transcritical CO₂ components modified to operate at compressor discharge temperatures up to 250°C. The goal in this research is to develop simulation models to optimize a two-stage CAHP process and compare the suitability for different types of ammonia-water absorbers used for heating air.

2. SETUP AND ASSUMPTIONS

Calculation of the two simulation models are computed in Engineering Equation Solver (EES) (Klein, 2014). An external procedure is used for the thermodynamic properties of the ammonia-water mixture developed by Ibrahim and Klein (1993).

2.1. The Two-Stage CAHP Model

The main objectives of the two-stage CAHP simulations are to obtain maximum all maximum supply temperatures at different constraints of maximum allowable discharge temperatures. In order to achieve this goal, optimal levels for intermediate pressure, absorber pressure, circulation ratio and the suitability of the desuperheater are evaluated. Two different approaches were used for the desuperheater. In the first method, the vapour was cooled to weak solution temperature and down to saturated vapour by the other approach. Simulations are carried out in four different scenarios with maximum discharge temperatures of 150, 175, 200 and 250°C. The process use waste heat water with inlet heat sink and heat source temperatures of 50°C.

Figure 1 shows a schematic of the two-stage CAHP. In order to calculate the thermodynamic parameters of the two-stage system some general assumptions are carried out. Heat losses to the surroundings and frictional pressure drops are considered as negligible. The vapour at the compressor inlet is in thermodynamic equilibrium with the liquid in the liquid/vapour separator. All of the heat exchangers have a counter-current flow direction. The mixing of the vapour and the weak solution before the absorber is adiabatic. The strong solution leaving the absorber is assumed to be saturated liquid. At the expansion valve outlet, the liquid is in thermodynamic equilibrium with the vapour created in the isenthalpic expansion process. The pressure lift from the solution pump is assumed to be isentropic.

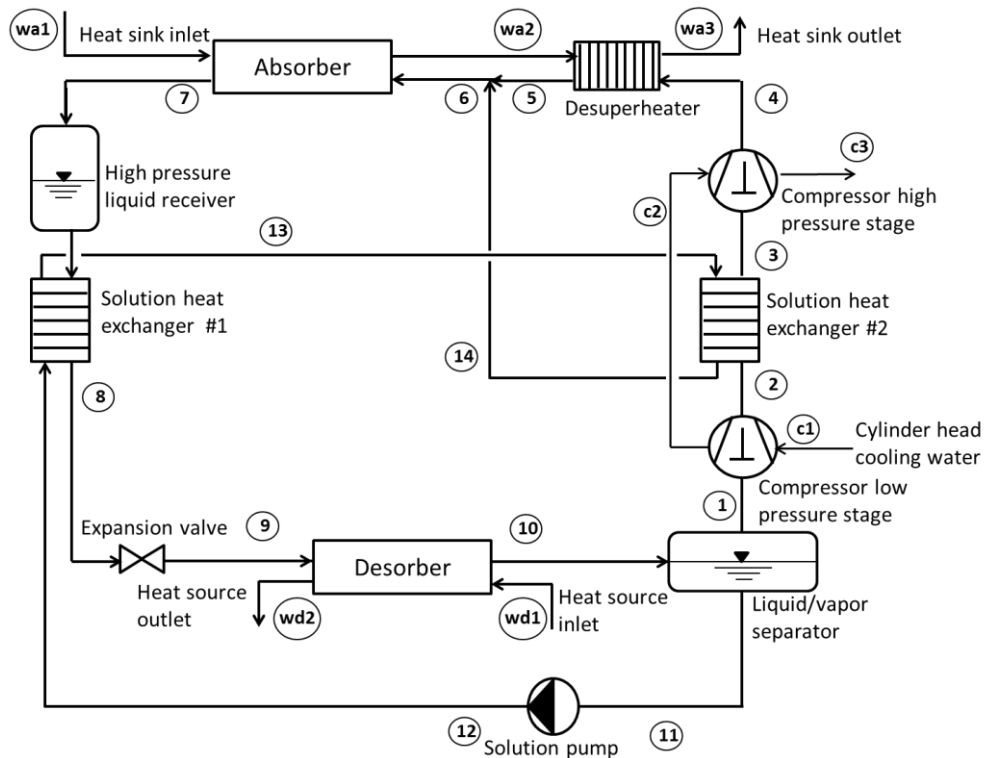


Figure 1. Schematic of the two-stage CAHP.

The isentropic and volumetric compressor efficiencies are taken from some data fitted polynomial functions Nordtvedt (2005) made in a previous investigation. Equation (1) and (2) shows the functions for the isentropic and volumetric efficiencies correlated to the pressure ratio across the compressor, while the compressor motor efficiency is set to a constant of 0.9. Those equations are used for both of the compressor stages. Intermediate pressure is determined with respect to the maximum allowable discharge temperature. In order to find the optimum intermediate pressure at the given operating conditions, P_{MP} is expressed with a

correction factor K (K-factor) in equation (3). Water cooling of the cylinder heads is assumed to be 5% of the shaft power. Input parameters used for scenarios of the two-stage CAHP are listed in Table 1.

$$\eta_{is} = 0.9051 - 0.0422 \cdot PR \quad [-] \quad (1)$$

$$\eta_{vol} = 1.0539 - 0.0788 \cdot PR \quad [-] \quad (2)$$

$$P_{MP} = K \cdot \sqrt{P_{LP} \cdot P_{HP}} \quad [\text{bar}] \quad (3)$$

Table 1. Input parameters used for all scenarios.

Parameter	Value
Q_{sink} [kW]	100
η_{motor} [-]	0.90
$\varepsilon_{\text{IHX}\#1}$ [-]	0.80
$\varepsilon_{\text{IHX}\#2}$ [-]	0.75
$T_{\text{sink},in}$ [°C]	50
$T_{\text{source},in}$ [°C]	50
P_{LP} [bar]	2.6

2.2. The Absorber Model

The main goal of the absorber simulations is to find the most suited heat exchanger design with respect to minimum absorber length and required fan power input. The process treats a cross-flow absorber heating air from 90°C to a guessed temperature of 125°C, while cooling ammonia-water from 150°C to a guessed temperature of 100°C. In order to achieve more accurate thermodynamic properties, the absorbers are divided into 10 segments. Mixture and air outlet parameters are the inlet parameters for the next segment. Five different compact heat exchangers from the EES heat exchanger library comprise the simulation scenarios for the absorbers. Geometry for all the heat exchangers is constrained by the EES design. The heat exchanger types in the simulations are a finned circular tube, finned flat tube, louvered plate-fin and plain plate-fin, where the finned tube and plate-fin comprise the main categories of the heat exchangers. Length and width are equal for all the heat exchangers, while air velocity and absorber height are adjusted, in order to carry out the simulations. Figure 2 shows a schematic of the two segments main heat exchanger categories with corresponding design parameters.

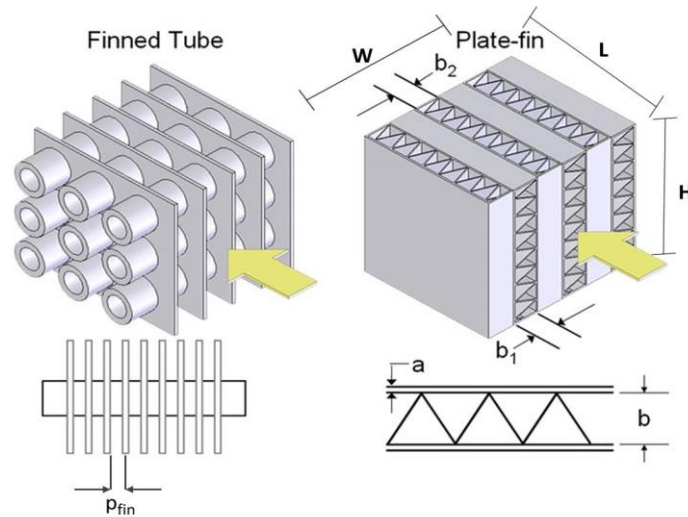


Figure 2. Schematic of a finned tube and plate-fin heat exchanger segment. The yellow arrows indicate the flow direction for air. H, L and W stand for height, length and width. The fin pitch is p_{fin} . Plate thickness is indicated by a, while b_1 and b_2 stand for air and mixture channel width, respectively (Klein, 2014).

Thermophysical properties for the ammonia-water mixture are calculated from the correlations of Conde-Petit (2004). Heat exchanger geometry, pressure drop and air heat transfer coefficient (α_{air}) are given from EES functions. Fin efficiencies for the finned tube heat exchanger are found with an approach that the fins acted like annular fins connected to the tubes, while the fins for the plate-fin heat exchangers acted like straight-base fins connected to the plates. The total thermal resistance, conductance and the absorber heat duty is calculated according to equation (4), (5) and (6), respectively.

$$R_{tot} = R_{in} + R_{cond} + R_{out} \quad [K/kW] \quad (4)$$

$$UA = \frac{1}{R_{tot}} \quad [kW/K] \quad (5)$$

$$\dot{Q} = UA \cdot \Delta T_{lm} \quad [kW] \quad (6)$$

EES has a function that calculates the correction factor for the cross-flow LMTD (F_{HX}), where the LMTD effectiveness (P_{HX}) and the LMTD capacitance ratio (R_{HX}) in equation (7) and (8) are the input variables. Hence, the corrected LMTD is given by equation (9).

$$P_{HX} = \frac{T_{C,out} - T_{C,in}}{T_{H,in} - T_{C,in}} \quad [-] \quad (7)$$

$$R_{HX} = \frac{T_{H,in} - T_{H,out}}{T_{C,out} - T_{C,in}} \quad [-] \quad (8)$$

$$\Delta T_{lm} = F_{HX} \cdot \Delta T_{lm,cf} \quad [K] \quad (9)$$

The average mixture density is calculated using equation (10) as a function of the given temperature and pressure. Assuming constant mixture flow rate, the mean ammonia-water velocity is given from equation (11). In order to simplify the ammonia-water calculations, the Prandtl and Reynolds number are calculated using the mixture liquid properties as in equation (12) and (13), respectively.

$$\rho_{avg} = \rho_{liq} \cdot (1 - q) + \rho_{vap} \cdot q \quad [kg/m^3] \quad (10)$$

$$u_m = \frac{4 \cdot \dot{m}}{\rho_{avg} \cdot \pi D_h^2} \quad [m/s] \quad (11)$$

$$Re_D = \frac{\rho_{liq} \cdot u_m \cdot D_h}{\mu_{liq}} \quad [-] \quad (12)$$

$$Pr = \frac{c_p \cdot \mu_{liq}}{\lambda_{liq}} \quad [-] \quad (13)$$

Dittus-Boelter equation is applied for the mixture heat transfer coefficient in equation (14), while the thermal resistance between mixture and the channel/tube wall is computed according to equation (15) (Incropera et al., 2007). The overall surface efficiency ($\eta_{overall}$), air heat transfer coefficient and total surface area are found from EES functions. Hence, the thermal resistance between the air and the air-side surface is calculated is equation (16).

$$\alpha_{mix} = 0.023 \cdot Re_D^{0.8} \cdot Pr^{0.4} \cdot \frac{\lambda_{liq}}{D_h} \quad [W/m^2 \cdot K] \quad (14)$$

$$R_{in} = \frac{1}{\alpha_{mix} \cdot \pi \cdot D_h \cdot L} \quad [K/W] \quad (15)$$

$$R_{out} = \frac{1}{\eta_{overall} \cdot \alpha_{air} \cdot A_{tot}} \quad [K/W] \quad (16)$$

The conduction resistance for the finned tube and plate-fin heat exchangers are calculated from equation (17) and (18).

$$R_{cond,ft} = \frac{\ln(\frac{D_{out}}{D_h})}{\lambda_{mat}} \text{ [K/W]} \quad (17)$$

$$R_{cond,pf} = \frac{th_{plate}}{\lambda_{mat} \cdot A_{cond}} \text{ [K/W]} \quad (18)$$

3. RESULTS

3.1. The Two-Stage Model

Table 2 comprises some of the most important variables from six of the simulations made for the two-stage CAHP. Simulations #1 to #3 have a maximum allowable discharge temperature of 150°C, while the other simulations are limited to 250°C. Figure 3 shows the behaviour the compressor discharge temperature as a function of the intermediate pressure correction factor for both the low pressure and high pressure stages with a maximum allowable discharge temperature of 175°C.

Table 2. Simulation results from the two-stage CAHP.

Simulation #	#1	#2	#3	#4	#5	#6
P _{HP} [bar]	17	17	17	47.5	47.5	47.5
PR _{LP} [-]	2.97	2.97	2.97	5.77	5.77	5.77
PR _{HP} [-]	2.20	2.20	2.20	3.17	3.17	3.17
K [-]	1.16	1.16	1.16	1.35	1.35	1.35
CR [-]	1.2	1.2	1.2	0.20	0.20	0.20
Q _{abs} [kW]	100	91.4	90.5	100	96.1	76.7
Q _{dsh} [kW]	0	8.6	9.5	0	3.9	23.3
COP [-]	3.85	3.85	3.85	2.08	2.08	2.08
η _{is,LP} [-]	0.78	0.78	0.78	0.66	0.66	0.66
η _{is,HP} [-]	0.81	0.81	0.81	0.77	0.77	0.77
η _{vol,LP} [-]	0.82	0.82	0.82	0.60	0.60	0.60
η _{vol,HP} [-]	0.88	0.88	0.88	0.80	0.80	0.80
v ₃ [m ³ /kg]	0.209	0.209	0.209	0.121	0.121	0.121
T ₂ [°C]	149.4	149.4	149.4	248.7	248.7	248.7
T ₄ [°C]	149.8	149.8	149.8	249.5	249.5	249.5
T _{sink,abs,out} [°C]	103.3	98.5	98.0	169.1	165.1	144
T _{sink,dsh,out} [°C]	-	103.0	103.0	-	169.6	171.8

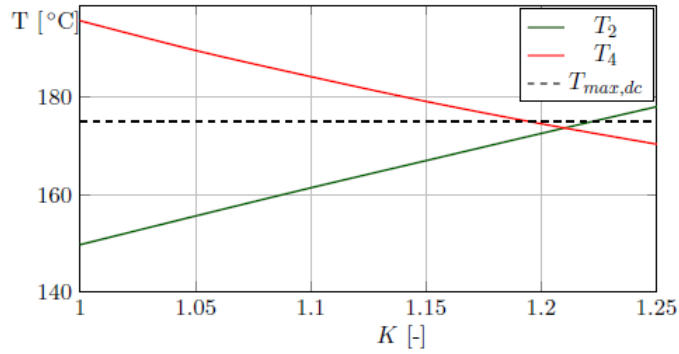


Figure 3. Discharge temperatures of the high and low compressor stage as a function of the K-factor.

3.2. The absorber model

Table 3 shows the simulation results from the absorber model with an absorber duty of 50kW. The heat exchangers are numbered where the finned circular tube, finned flat tube, louvered plate-fin, wavy plate-fin and plain plate-fin heat exchangers corresponds to heat exchanger #1, #2, #3, #4 and #5, respectively.

Table 3. Simulation results from the absorber model

HX number	#1	#2	#3	#4	#5
Minimum free flow area/frontal area [-]	0.534	0.697	0.426	0.511	0.541
Hydraulic diameter[m]	0.0062	0.0036	0.0045	0.0032	0.0038
Total absorber height [m]	2.0	2.5	1.8	1.6	4.2
Pressure drop [kPa]	4.28	1.56	35.8	41.4	1.32
Fan work [kW]	14.6	8.7	140	162	5.3
Mean air velocity [m/s]	10	10	16	15	5.5
Mean mixture velocity [m/s]	0.093	0.105	0.421	1.09	0.928
Air heat transfer coefficient [$W/m^2 \cdot K$]	1017	1129	3479	8065	6877
Mixture heat transfer coefficient [$W/m^2 \cdot K$]	155	71	335	402	71.4
Air mass flow rate[kg/s]	0.794	1.30	0.91	0.90	0.93
Air mass flow/mixture mass flow rate [-]	12.4	20.3	14.3	14.0	14.5
R_{cond} [K/kW]	$1.94 \cdot 10^{-4}$	$1.86 \cdot 10^{-4}$	$1.73 \cdot 10^{-4}$	$1.42 \cdot 10^{-4}$	$6.56 \cdot 10^{-5}$
R_{in} [K/kW]	$2.04 \cdot 10^{-3}$	$1.75 \cdot 10^{-3}$	$2.00 \cdot 10^{-3}$	$1.86 \cdot 10^{-3}$	$8.45 \cdot 10^{-4}$
R_{out} [K/kW]	$1.80 \cdot 10^{-3}$	$1.19 \cdot 10^{-3}$	$1.18 \cdot 10^{-3}$	$1.37 \cdot 10^{-3}$	$2.42 \cdot 10^{-3}$
R_{tot} [K/kW]	$4.04 \cdot 10^{-3}$	$3.13 \cdot 10^{-3}$	$3.36 \cdot 10^{-3}$	$3.38 \cdot 10^{-3}$	$3.3 \cdot 10^{-3}$
Number of mixture channels[-]	-	-	57	41	34
Number of mixture tubes[-]	124	108	-	-	-

4. DISCUSSION

In order to achieve maximum supply temperature for the two-stage CAHP, the absorber pressure, circulation ratio and the K-factor were optimized for each scenario. By making those variables deviate from the optimum results, the outcome would either end with lower supply temperatures or exceed the maximum allowable discharge temperature. Figure 3 shows that elevating K-factor decreases the low pressure stage discharge temperature, simultaneously as it reduces the high pressure discharge temperature, due to higher intermediate pressure. The vapour mass flow rate was approximately constant for all the scenarios. However, the volumetric efficiency resulted in a variation of the required swept volume in the low pressure stage from 154 m³/h in simulation #1 to 203 m³/h in simulation #4. At the higher compressor stage, the specific volume decreased at increasing pressure. Therefore, the increasing intermediate pressure entailed a lower swept volume. An intermediate pressure at 15 bar required a swept volume of 42 m³/h, compared to a P_{MP} of 7.71 bar and a required swept volume of 55 m³/h. Both of the cooling methods for the desuperheater application yielded approximately the same supply temperatures compared to the simulations without the

desuperheater at the lower discharge temperature constraints. On the hand, there was a difference in the cooling methods in the scenario with a discharge temperature limitation of 250°C. In that scenario, supply temperatures were simulated to 169.6 and 171.8°C for cooling approach #1 and #2, respectively. The desuperheater heat duty were then at 3.9 kW for method #1 and 23.3 kW for method #2. In comparison, the largest heat supply temperature without desuperheater was found at 169.1°C.

At increasing absorber pressure, the heat sink outlet temperatures increased as well. The optimum circulation ratio decreased at elevated absorber pressure. This can be explained from the decreasing mixture mass flow rate and nearly constant vapour mass flow rate. Since the vapour mass flow rate remains approximately the constant, liquid mixture flow rate decreases simultaneously with the total mixture mass flow rate, hence a decrease in the optimum CR. The required compressor input power increased at higher absorber for two reasons. First reason is due to increased compressor work at higher pressure lifts. Second reason is the decreasing isentropic efficiency at increasing pressure ratios.

According to the simulations, there is a large difference between the air and the mixture mass flow rate, due to a corresponding difference in the specific heat capacity. The air mass demand is between 12 to 20 times higher than the mixture mass flow rate. The heat exchange between the mixture and the air is very sensitive to the absorber height and the air mass flow rate. If the absorber height is too large, the mixture becomes subcooled and the mixture outlet temperature would be lower than the inlet air temperature and thus infeasible heat exchange. In addition, the heat exchange is depending on a certain air mass flow rate, which required a high mean air velocity. This is why some of the heat exchangers required a high mean air velocity.

The finned tube heat exchangers had a large number of tubes, which resulted in a lower heat transfer coefficient, compared to the plate-fin heat exchangers. A smaller frontal area provided a smaller air heat transfer coefficient for type #2 than #1. The pressure drop for type #2 was significantly lower than for the circular finned tube heat exchanger. An advantage of using type #1 over #2 was the shorter absorber height, but still the flat finned tube heat exchanger had a substantially lower required fan power, which made it preferable over the finned circular tube heat exchanger. Compared to the finned tube heat exchangers, the plate-fin heat exchangers had a smaller number of mixture channels, which yielded higher mixture heat transfer coefficients. Low minimum free flow area – frontal area ratio (σ) were low for the heat exchanger type #3 and #4, which entailed large air velocity demands and thus pressure drop and fan work. On the other hand plain plate-fin heat exchangers required low fan work, but the height was too large. Finned flat tube heat exchangers gave the best results with respect to absorber height and fan work. The high air velocity demands are not fully realistic and there might be some errors somewhere in the simulation model.

5. CONCLUSIONS

At a maximum discharge temperature of 250°C resulted in a COP of 2.08, absorber pressure of 47.5 bar, supply temperatures of 171.8°C and a K-factor of 1.35. The K-factor increased at elevating absorber pressures. Volumetric efficiency entailed higher swept compressor volume at increasing pressure ratio at the low pressure stage. On the hand, the swept volume at the high pressure stage decreased at increasing pressure due to a decreasing specific volume of the compressor inlet gas. Cooling the discharge gas down to saturated vapour yielded a slightly higher supply temperature than cooling down to weak solution temperature by the use of a desuperheater. The supply temperatures with the use of a desuperheater were approximately the same as the supply temperatures without the desuperheater. Optimum circulation ratio decreased at elevated absorber pressure, due to a decrease in the mixture mass flow rate and nearly constant vapour mass flow rate.

The heat exchange between the air and the mixture was very sensitive to the absorber height and the air mass flow rate. A too large absorber height could cause subcooled mixture outlet temperatures below the air inlet temperature and thus infeasible heat exchange. Required fan power input had a large impact on the process. Demands for high air velocities resulted in large pressure drops and fan work, due to the sensitivity to the absorber height or if there were any errors in the simulation model. Finned flat tube heat exchangers were found to be the most preferable of the simulated heat exchangers, due to its low drops and the absorber height. An absorber duty of 50 kW yielded an absorber height of 2.5 m and a required fan power input of 8.7 kW.

NOMENCLATURE

Latin letters			Subscripts	
A	Area	[m ²]	abs	Average Absorber
CAHP	Compression-absorption heat pump	[-]	avg	Average
COP	Coefficient of performance	[-]	C	Cold
c _p	Specific heat capacity	[kJ/kg·K]	cf	Cross-flow
D	Diameter	[m]	cond	Conduction
F _{HX}	Cross-flow correction factor	[-]	D	Diameter
H	Height	[m]	dc	Discharge
K	Intermediate pressure correction factor	[-]	dsh	Desuperheater
L	Length	[m]	ft	Finned tube
LMTD	Log mean temperature difference	[K]	H	Hot
P	Pressure	[bar]	h	Hydraulic
P _{HX}	LMTD effectiveness	[-]	HP	High pressure
PR	Pressure ratio	[-]	is	Isentropic
Pr	Prandtl number	[-]	IHX	Internal heat exchanger
Q	Heat Duty	[kW]	liq	Liquid
q	Vapour quality	[-]	lm	Log mean
R	Thermal resistance	[K/W]	LP	Low pressure
Re	Reynolds number	[-]	mat	Material
R _{HX}	LMTD capacitance ratio	[-]	MP	Intermediate pressure
T	Temperature	[°C or K]	pf	Plate-fin
th	Wall thickness	[m]	tot	Total
UA	Conductance	[kW/K]	vol	Volumetric
u _m	Mean velocity	[m/s]	wa	Water absorber
v	Specific volume	[m ³ /kg]	wd	Water desorber
W	Width	[m]		
Greek Letters				
α	Heat transfer coefficient	[W/m ² ·K]		
ε	Thermal efficiency	[-]		
λ	Conductivity	[W/m·K]		
η	Efficiency	[-]		
ρ	Density	[m ³ /kg]		

REFERENCES

- Chan, C.W. et al. 2013, Reprint of “A review of chemical heat pumps thermodynamic cycles and thermal energy storage technologies for low grade heat utilization”, *Appl. Therm. Eng.* 53:160-176.
- Conde-Petit, D.M.R. 200, Thermophysical properties of NH₃+H₂O solution for the industrial design of absorption refrigeration equipment. Zürich: M. Conde Engineering.
- Fernández – Seara, J. 2007, Analysis of an air cooled ammonia-water vertical tubular absorber, *Int. J. Therm. Sci.* :93-103.
- Hultén, M. and Berntsson T. 1999, The compression/absorption cycle – influence of some major parameters on COP and a comparison with the compression cycle, *Int. J. Refrig.* 22: 91-106.
- Ibrahim, C.M. and Klein, S.A. 1993, Thermodynamic Properties of Ammonia-Water Mixtures, *ASHRAE Trans.* 21(2): 1495.
- Incropera, F.P. et al. 2007, *Heat and Mass Transfer*, 6th ed., Wiley, Hoboken, 997 p.
- Klein, S.A. 2014, Engineering Equation Solver, Professional version 9.605, F-Chart Software.
- Jensen, J. K. 2014, Investigation of ammonia/water hybrid absorption/compression heat pumps for heat supply temperatures above 100°C, *Proc. International Sorption Heat Pump Conference*, CEEE: 311-321.
- Nordtvedt, S.R. 2005, Experimental and theoretical study of a compression/absorption heat pump with ammonia/water as working fluid, Ph.D. dissertation
- Osenbrück, A.1895. Verfahren kalteerzeugung bei Absorptions- Maschinen.

